DEVELOPMENT AND CHARACTERIZATION OF A BIOHYBRID SCAFFOLD FOR REGENERATIVE MEDICINE APPLICATIONS

by

Donald O. Freytes

Bachelor of Science in Mechanical Engineering, Purdue University, 2000

Master of Science in Biomedical Engineering, Purdue University, 2002

Submitted to the Graduate Faculty of the

Swanson School of Engineering in partial fulfillment

of the requirements for the degree of

Doctor of Philosophy

University of Pittsburgh

2008

UNIVERSITY OF PITTSBURGH

SWANSON SCHOOL OF ENGINEERING

This dissertation was presented

by

Donald O. Freytes

It was defended on

March 19rd, 2008

and approved by

David A. Vorp, PhD, Associate Professor, Department of Bioengineering

William R. Wagner, PhD, Associate Professor, Department of Bioengineering

Peter D. Wearden, PhD, MD, Assistant Professor, Department of Surgery

Dissertation Director: Stephen F. Badylak, DVM, MD, PhD, Research Professor, Department of Surgery

DEVELOPMENT AND CHARACTERIZATION OF A BIOHYBRID SCAFFOLD FOR REGENERATIVE MEDICINE APPLICATIONS

Donald O. Freytes, Ph.D.

University of Pittsburgh, 2008

Most approaches to tissue engineering and regenerative medicine include a scaffold component. The scaffold material could be synthetic or natural and may be intended simply as a delivery vehicle for cells or growth factors or as an integral component of an engineered tissue or organ. Regardless of the type of material used, the scaffold must be "cell friendly" and promote host cell attachment, proliferation, migration, differentiation, and eventual three-dimensional tissue organization. Biologic scaffolds composed of extracellular matrix have shown minimal scar tissue formation with constructive remodeling of the damaged or missing tissue structures in a variety of clinical and pre-clinical applications. However, ECM scaffolds are typically characterized by a two-dimensional sheet and are limited to the mechanical and material properties inherent to the tissue from which it was derived.

A soluble form of ECM scaffold would expand the clinical utility of ECM by allowing the delivery of the scaffold via minimally invasive methods to the site of interest. The present work describes the enzymatic digestion of an ECM scaffold derived from the porcine urinary bladder (urinary bladder matrix or UBM). UBM was successfully digested with pepsin and papain under different conditions. The enzymatically digested UBM showed chemotactic and mitogenic properties towards progenitor cells while inhibition was found toward endothelial cells. In addition, pepsin digested UBM was able to self-assemble into a gel form. The present

study investigated the *in vitro* cell growth of different cell types on the surface of the gels and measured the rheological properties of the UBM gel.

Synthetic scaffold materials are an alternative to naturally derived ECM scaffolds. However, synthetic materials lack the bioactivity and beneficial host tissue response characteristic of ECM-derived scaffolds and often result in fibrous encapsulation when implanted *in vivo*. Poly(ester-urethane)urea (PEUU) is a biodegradable polymer that can be manufactured into an elastomeric scaffold by electro-spinning techniques with an ultrastructural morphology similar to the ECM. The present work successfully combined the soluble form of the UBM with the PEUU to create hybrid scaffolds. The *in vitro* characterization of the scaffolds and the *in vivo* response are described. Hybrid scaffolds showed a change in the host tissue response and higher degradation rates *in vivo* in a subcutaneous location when compared to the polymer alone. Finally, the potential use of the PEUU and a PEUU/UBM hybrid scaffold as a left ventricular patch in a canine model is discussed.

TABLE OF CONTENTS

LIST OF TABLES

LIST OF FIGURES

ACKNOWLEDGEMENTS

Where should I begin? The work presented in this dissertation is the culmination of long hours and hard work and was conducted with the help and guidance of an amazing and talented group of people. It has been a great experience and one that I will cherish for the rest of my research career. I would like to thank Dr. Harvey Borovetz, the University of Pittsburgh, the McGowan Institute for Regenerative Medicine, and the Department of Bioengineering for their support and for allowing me to pursue a doctoral degree in such a fine institution. I have yet to find a place that fosters collaboration and interdisciplinary research as the University of Pittsburgh and the McGowan Institute for Regenerative Medicine.

I would like to thank my graduate committee: Drs. Stephen Badylak, William Wagner, David Vorp, and Peter Wearden. Thank you for your guidance and support throughout the entire process. It was an invaluable experience filled with great challenges. Your input and opinions helped me shape my doctoral work and has had a great impact on my professional development.

I would like to thank Dr. Stephen Badylak for his tutelage and mentorship. Dr. Badylak took me in as a young mechanical engineering student and introduced me to the world of regenerative medicine (not an easy task in a traditional engineering environment). He believed in me and my abilities early on and allowed me to explore possibilities that I would not have been able to explore otherwise. As a doctoral student, Dr. Badylak gave me an incredible

amount of freedom and flexibility permitting me to grow as an independent researcher. It has been a great honor and privilege working with him and with such a talented lab.

During my time in Pittsburgh, I had the opportunity to work with many talented individuals. I would like to thank the entire Badylak's Lab. Everyone is "awesome!" I would like to thank Dr. Ann Stewart-Akers for her early tutelage and help. I would also like to thank Drs. Annie Lee and Li Zhang for their help with assays in every step of the way. I would like to thank the graduate students (and former graduate students) Jolene Valentin, Bryan Brown, John Wainwright, Scot Zundel, Vineet Agrawal, and Tiffany Sellaro. All of you have been very supportive and always represented a healthy competition that drove me to excel. I would also like to thank Janet Reign, Dr. Julie Myers-Irvin, Dr. Hongbin Jiang, Dr. Thomas Gilbert (who helped me move to Pittsburgh), Jennifer Debarr, Dr. Allison Beatie, John Freund, Dr. Alan Boruch, Dr. Neil Turner, and Scot Johnson for all of their help and encouragements. Finally, I would like to thank the undergraduate students: Jon Grasman, Sam Kolman, and Urvi Patel. Your help has been tremendous and you have played an important role in this dissertation.

I would like to extend a special thanks to Renee Atkinson, Alison Earhart, Erin Menzies, Brooke Marchetti, and Jessica Lewis. Without your help most of my work would have not been possible. Your work "behind the scenes" was extremely vital and invaluable.

I also had the opportunity to collaborate with many different laboratories during my time in Pittsburgh. I would like to thank Wagner's Laboratory for their help and support in creating the hybrid scaffolds. Specifically, I thank Drs. William Wagner, John Stankus, Jianjun Guan, and Yi Hong. I would like to acknowledge Drs. Jorge Genovese, Amit Patel, and Cristiano Spadaccio for their help and support. I thank Keller's Laboratory and Dr. Kimimasa Tobita, Joseph Tinney, and Dr. Bradley Keller for their help and support with the chick cardiomyocytes.

I would also like to thank Dr. Sachin Velankar and Dr. Jeffrey Martin for their help with the rheological testing.

As part of my doctoral training I had the privilege of working with an remarkable surgical team and I would like to express my appreciation to Drs Peter Wearden, Irfan Quireshi, and Pietro Bajona for their time and dedication to my project. In addition, I would also like to express my gratitude to the entire staff at the animal facility and everyone involved in the surgical implantation of the cardiac patch. More specifically, I would like to thank Buffie Kerstetter, Joseph Hanke, Shawn Bengston, Dr. Stijn Vandenberghe, and Donald Koch for their help and assistance. Your dedication and support for the animal work will always be tremendously appreciated.

I cannot thank enough my family and friends. Without you, all the sacrifices would have been pointless and grueling. Thank you for your motivation in such hectic times and for serving as an inspiration during graduate school. I thank my mom (Sandra Caldwell) for understanding and supporting my dreams and my aspirations to pursue this type of work even if it meant having me miles away. A special thanks to my sister (Dr. Sandra Freytes) for serving as an inspiration in every facet of my life. Finally, I would like to thank my wife (Dr. Saly Romero). If there was anyone that could have deterred me from pursuing my doctoral training at Pittsburgh it would have been you. Instead you were an absolute facilitator and a fountain of understanding and patience. For five years we lived apart and commuted between IN, NJ, and PA supporting each other in every way. For that I will always be in debt. I would have never been able to imagine a better friend, wife, and companion than you.

ACRONYMS

ADP	Adenosine diphosphate
ANOVA	Analysis of variance
ATP	Adenosine triphosphate
BDI	1,4-butanediisocyanatobutane
BDO	1,4-butanediol
bFGF	Basic fibroblast growth factor
CEC	Chick embryonic cardiomyocytes
CL	ε-caprolactone
Col	Collagen
DSC	Differential scanning calorimetry
DMEM	Dulbecco's Modified Eagle Medium
DMF	N,N-dimethyl formamide
DMSO	Dimethyl sulfoxide
EBM-2	Endothelial Basal Medium
ECM	Extracellular matrix
EGM-2	Endothelial Growth Medium
ETO	Ethylene oxide
EVCPP	Endoventricular circular patch plasty
ePTFE	Expanded polytetrafluoroethlyene
FBS	Fetal bovine serum
GAG	Glycosaminoglycans
HA	Hyaluronic acid
H&E	Hematoxylin and Eosin
HF	Heart Failure

HFC-LV	Human fetal cardiomyocytes from the left ventricle
HFC-RV	Human fetal cardiomyocytes from the right ventricle
HFIP	Hexafluoroisopropanol
HGF	Hepatocyte growth factor
HAECs	Human aortic endothelial cells
kV	Kilovolt
LV	Left ventricle
MI	Myocardial Infarction
MPa	Megapascal
PBS	Phosphate-buffered saline
PCL	Poly(ε-caprolactone)
PCNA	Proliferating cell nuclear antigen
PDGF	Platelet derived growth factor
PG	Proteoglycan
PGA	Polyglycolide
PGCL	Poly(glycolide-*co*-ε-caprolactone)
PGS	Poly(glycerol sebacate)
PLA	Polylactide
PLCL	Poly(lactide-*co*-ε-caprolactone)
PLGA	Poly(lactide-*co*-glycolide)
PEG	Poly(ethylene glycol)
PEUU	Poly(ester urethane)urea
PS	Phosphatidylserine
PTMC	Polytrimethylene carbonate
P(TMC-LA)	Poly(trimethylene carbonate-*co*-lactide)
PU	Polyurethane
RV	Right ventricle
RVOT	Right ventricular outflow tract
SEM	Scanning electron microscopy
SIS	Small intestinal submucosa
SMC	Smooth muscle cell

T_g	Glass transition temperature
T_m	Melting temperature
TCPS	Tissue culture polystyrene
TGF-β	Transforming growth factor beta
TIPS	Thermally induced phase separation
UBM	Urinary bladder matrix
UV	Ultraviolet
VEGF	Vascular endothelial growth factor
wt%	Weight percent

1.0 INTRODUCTION AND SPECIFIC AIMS

Biologic Scaffolds composed of extracellular matrix (ECM) have been used for the repair of a variety of tissues including the lower urinary tract [1, 2], esophagus [3, 4], myocardium [5-7], and musculotendinous [8-10] tissues, often leading to tissue-specific constructive remodeling with minimal or no scar tissue formation. These biologic scaffolds are typically prepared by decellularization of intact tissues or organs [11]. The resulting ECM scaffold materials are composed of the structural and functional molecules that characterize the native tissue ECM such as collagen, laminin, fibronectin, growth factors, glycosaminoglycans, glycoproteins, and proteoglycans [4, 12, 13]. The ECM scaffolds prepared from most tissues have a two-dimensional sheet form with limited ability to conform to irregular three-dimensional shapes and sizes. Therefore, the clinical utility of an ECM biologic scaffold for many clinical applications is typically restricted to topical administration or to invasive surgical procedures that can accommodate variations of the two dimensional sheet forms. The ECM biologic scaffold is also limited to the mechanical and material properties inherent to the tissue from which it was derived [14].

A soluble form of the ECM biologic scaffold would expand its clinical utility by providing a form that could potentially be delivered via minimally invasive methods to the site of interest. The solubilization of the ECM would ideally retain the bioactivity that characterizes the two dimensional sheet form of the ECM scaffold and would avoid harsh purifications steps to

preserve large and low molecular weight peptides/proteins. Degradation products of ECM scaffolds have been shown to possess antimicrobial and chemotactic properties which could favorably affect the host tissue response when used for tissue reconstruction [13, 15, 16]. Furthermore, if the soluble form could be self assembled into a gel, the resulting scaffold could be used to fill defects, used as a topical solution, as an injectable scaffold, or could be used as a cell delivery vehicle.

Synthetic scaffold materials are an alternative to naturally derived ECM scaffolds and are used in a variety of clinical applications. Polymeric materials can be manufactured to produce biodegradable scaffolds with a wide range of mechanical properties and ultrastructural morphology. Biodegradable polymers are often constructed from polyesters which allow for the hydrolytic degradation of the ester bonds. Examples of commonly used biodegradable polyesters include polylactide (PLA), polyglycolide (PGA), or the combination of both into copoly(lactic-glycolic acid) (PLGA) [17]. These materials are sometimes characterized by low compliance when compared to most soft tissues and the degradation products (lactic acid and glycolic acid) might have detrimental effects within the microenvironment of the wound bed during the healing response [17]. Poly(ester-urethane)urea (PEUU) described by Guan et al. is another type of polyester combined with a urethane that can be manufactured into an elastomeric biodegradable scaffolds by thermally induced phase separation (TIPS) or by electro-spinning techniques [18-22]. The degradation of PEUU is faster than other polyurethanes with cytocompatible degradation products such as putrescine, a polyamine needed for cell growth and differentiation [20, 22, 23]. The elastomeric properties of the PEUU may be better suited for soft tissue applications and represent one of the new synthetic scaffolds researched for tissue engineering applications [18-28]. However, synthetic materials such as these polyurethanes lack

the bioactivity and beneficial host tissue response characteristic of ECM derived scaffolds and often result in fibrous encapsulation [29].

The studies presented in this dissertation describe and characterize a soluble form of an ECM scaffold, one of which can be induced to self-assemble into an ECM gel. In addition, the present work combines the constructive remodeling characteristic of the ECM and the favorable biomechanical properties of a biodegradable polyurethane material into an engineered polymer-ECM hybrid scaffold. The polymer-ECM hybrid is composed of an electrospun mixture of an ECM derived from the porcine urinary bladder (UBM-ECM) and a synthetic component composed of PEUU. Both materials have been previously shown to be good candidates for tissue reconstruction and hold great promise as scaffolds for regenerative medicine applications.

1.1 THE SCAFFOLD COMPONENT OF TISSUE ENGINEERING AND REGENERATIVE MEDICINE

Most approaches to tissue engineering and regenerative medicine include a scaffold component. The scaffold may be intended simply as a delivery vehicle for cells or growth factors or as an integral component of an engineered tissue or organ. Scaffolding materials can be assembled from either synthetic sources (e.g., poly-(L)-lactic co-glycolic acid) or biological sources (e.g., purified type I collagen) utilizing engineering principles. These scaffold materials can be designed to be biodegradable and can be chemically modified to contain surface ligands for cell-scaffold interactions. The choice of the ideal scaffold for selected tissue reconstructive purposes depends upon the mechanical and material properties of the material and the ability of the

scaffold to be repopulated by the appropriate cells within a given environment leading to a functional tissue.

Regardless of the type of scaffold material used, there are important issues that must be addressed if clinical success is to be expected. The scaffold material must be "cell friendly" and promote host cell attachment, proliferation, migration, differentiation, and eventual three-dimensional tissue organization. The scaffold material must have physical and material properties that will support clinical utility (e.g., surgical manipulation, suture retention strength, and local tissue mechanical forces) and ideally would degrade at an appropriate rate while new matrix is deposited and tissue remodeling occurs [17].

Cells that participate in tissue repair require the appropriate signals for proliferation, differentiation, and three-dimensional morphogenesis. The source of this instruction can come from the surrounding environment and from stressors including oxygen tension, blood flow, and mechanical forces. Another source for these signals can come from the scaffold in which the cells reside. The extracellular matrix is the natural substrate through which signals are communicated to the cell surface and has the potential to direct cell and tissue responses during the initial phases of the remodeling process [4, 12, 30, 31]. These combine roles of structure and function make the ECM an attractive material for regenerative medicine application and worthy of further study.

1.2 THE EXTRACELLULAR MATRIX

The ECM is the natural scaffolding material composed of proteinaceous and non- proteinaceous components found in nearly all tissues and organs and it is secreted, assembled and maintained

by resident and neighboring cells [32]. The ECM is tissue specific and serves as a temporary scaffold for tissue development, or as a permanent but dynamic scaffold in mature tissues providing a bioactive substrate for cell recruitment, attachment, maintenance, maturation, and proliferation. Among the different functions of the ECM is maintenance of mechanical integrity via structural proteins, mechanical adhesion to cells via cell-matrix interactions, support of cell proliferation and renewal, transmission of mechanical forces to the resident cells, and the storage and release of bioactive molecules [30, 33].

ECM varies from tissue to tissue and can even vary spatially within the same tissue or organ [34]. There are also differences in the constituents and the ultrastructural composition of the ECM within the same organ. ECM can be interstitial/stromal matrix or can be found as a specialized matrix called the basement membrane or basal lamina which serves as the matrix for epithelial cells. The ECM can also be dynamic by constantly adapting to external stressors such as mechanical stimulation. An example of the dynamic nature of the ECM can be seen in the matrix of bone where it is constantly adapting to changes in stresses[32, 34].

Traditionally, the ECM has been divided into structural and functional components. Structural components include molecules such as collagens, elastin, proteoglycans, and glycosaminoglycans while functional components include growth factors and cytokines present within the ECM. Our current understanding of the ECM suggest that structural components may also have functional roles in many circumstances and may possess matricryptic sites that act as bioactive signals when released or revealed from a parent molecule [35, 36]. This notion challenges the traditional distinction between structural and functional components of the ECM and perhaps suggests that all of the constituents of the ECM have a bioactive component. For simplicity, the components traditionally regarded as structural (the components that carry the

mechanical loads normally present in the tissue) will be described first. The ECM will be described in the subsequent section followed by a description of the functionality inherent in all ECM components and a description of the ECM as a scaffold material.

1.2.1 Structural Components of ECM

The major structural components responsible for the mechanical integrity of the ECM are collagens, elastin, proteoglycans, and glycosaminoglycans [17, 32]. These components are responsible for the tissues' mechanical and material properties such as strength, distensibility, resilience, and viscoelasticity and have great impact upon the tissues' function in both healthy and disease states [37]. Mutations in genes encoding ECM components can give rise to many diseases characterized by improper formation of the ECM such as osteogenesis imperfect, marfan syndrome, and Ehlers-Danlos syndrome. The following sections briefly describe the major structural components of the ECM found in soft tissues[32, 34].

1.2.1.1 Collagen

Collagen is the primary constituent of all tissues and represents the most abundant protein in mammals by comprising about 30% of the total protein weight [32]. Collagen is highly conserved across species and there are over 20 types of collagen with different functions and properties throughout mammalian tissues. Collagen type I, II, III, and V have a rod-like shape due to the unique assembly of three helical structures and normally serve as structural molecule providing strength and the basic scaffolding for cells. Other collagen types are less abundant but play important roles in tissue health and the maintenance of tissue structure. For example,

collagen type VI and IX are fibril-associated collagens that form connections between structural collagens such as type I and II and can bind glycosaminoglycans (important for tissue hydration). In addition, collagen IV, VII, and XV are sheet-forming collagens that can be found in a specialized ECM called the basal lamina or the basement membrane that support epithelial cells in tissues such as blood vessels and myocardium [17, 32, 38].

Collagens' unique structural properties are in part a result of its unique amino acid sequence of $(\text{-Gly-X-Y})_n$ where X is typically proline (Pro) and Y is hydroxyproline (Hyp). This sequence gives rise to a symmetrical pattern of three left-handed helical chains. Two of the chains are identical and are termed α1(I) and the third chain is termed α2(I). There are non-helical structures at the N- and C-terminal ends about 9-26 residues in length called telopeptides. Collagen molecules are typically found staggered with respect to each other forming microfibrils and then aggregate in and end-to-end fashion forming collagen fiber. This staggering effect gives rise to the "striated" appearance of collagen fibers when observed under an electron microscope. A diagrammatic representation of collagen molecules is shown in Figure 1-1. Further stabilization of collagen fibers can occur enzymatically by lysyl oxidase. Collagen can be degraded by matrix metalloproteinases (MMPs) [32, 34, 38]. In summary, collagen is the major structural component of the ECM and is responsible for the mechanical strength and structural integrity of tissues.

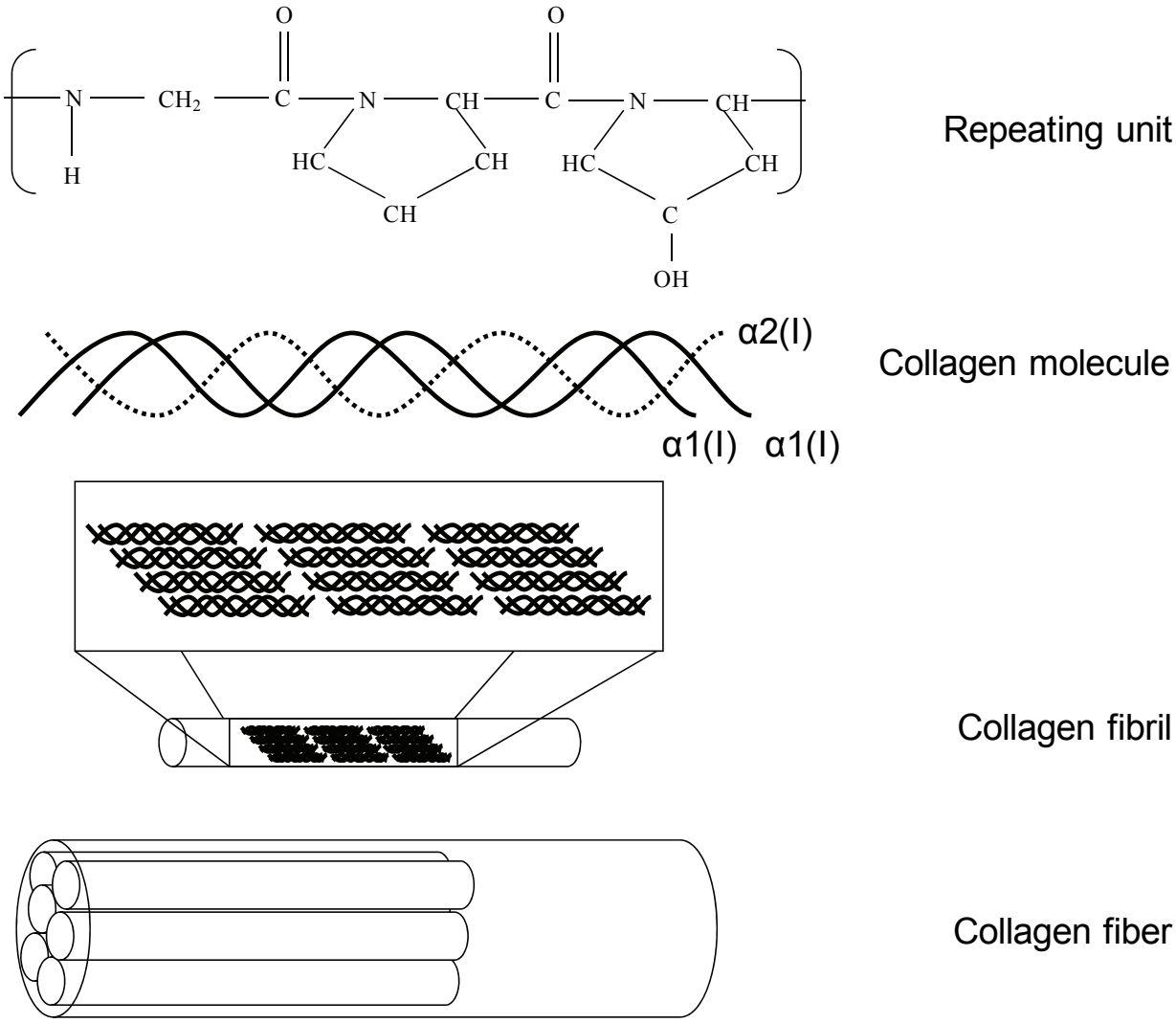

Figure 1-1: Diagrammatic representation of the assembly of collagen type I. The polypeptide chain with the repeating Gly-Pro-Hyp sequence gives rise to the helical structure of the collagen molecule with two α1(I) chains and one α2(I) chain. The collagen molecules are then staggered with respect to each other forming microfibrils. The microfibrils then are stacked on top of each other or end-to-end forming collagen fibers.

1.2.1.2 Elastin

Many tissues such as blood vessels, lungs, and the myocardium exhibit the ability to undergo high deformations, are compliant, and have a high degree of resilience. These characteristics are a result of many factors one of which is the presence of the elastic protein elastin within the ECM. Elastin is a non-glycosylated protein formed by a cross-linked (between desmosine and isodesmosine) network of amino acids. It is mostly composed of glycine, alanine, valine, proline, and lysine and is cross-linked by lysyl oxidase. Elastin can be found surrounded by a sheath of microfibrils formed by fibrillin which helps bind elastin to the surrounding matrix. Mutations in the fibrillin-1 gene results in Marfan Syndrome. Removal of elastin from blood vessels markedly reduces the compliance of the tissue attesting to the importance of elastin for tissue elasticity and resilience [32, 34]. In summary, elastin is responsible for the elasticity and resilience of tissues.

1.2.1.3 GAGs and Proteoglycans

Glycosaminoglycans (GAG) are naturally occurring polysaccharides in the 5-60 kDa range and are typically found as an alternating copolymer of hexosamine (i.e. N-acetyl glucosamine or N-acetyl galactosamine) and other sugars (i.e. galactose). Among the different GAGs found in the ECM are heparin, hyaluronate, keratin sulfate, dermatan sulfate, and chondroitin sulfate (both chondroitin-6-sulfate and chondroitin-4-sulfate). The structures of common GAGs are shown in Figure 1-2. Most GAGs are sulfated with the exception of hyaluronic acid which is not sulfated and has a higher molecular weight (50-500 kDa). The sugar backbone of GAG is linked by glycosidic bonds with the exception of keratin sulfate. Hyaluronate is a component of the synovial fluid that helps lubricate joints and chondroitin and

keratin sulfate are found in tendons and cartilage and modulate the hydration and the viscoelasticity of tissues [17, 32, 38].

For the most part, GAGs are covalently bonded to a protein backbone forming a glycoprotein termed proteoglycans (PGs). PGs are found both on the cell membrane and on the extracellular matrix. Secreted or extracellular PGs include large aggregating cartilage proteoglycans, versican, perlecan, and decorin. Syndecan is a membrane-intercalated proteoglycan that interacts with fibronectin playing an important role in cell-matrix interactions. Perlecan is a heparin sulfate PG found in the base basement membrane of vascular tissues [32, 34, 38, 39]. Proteoglycans and glycosaminoglycans are responsible for tissue hydration and in part responsible for the viscoelasticity found in certain tissues.

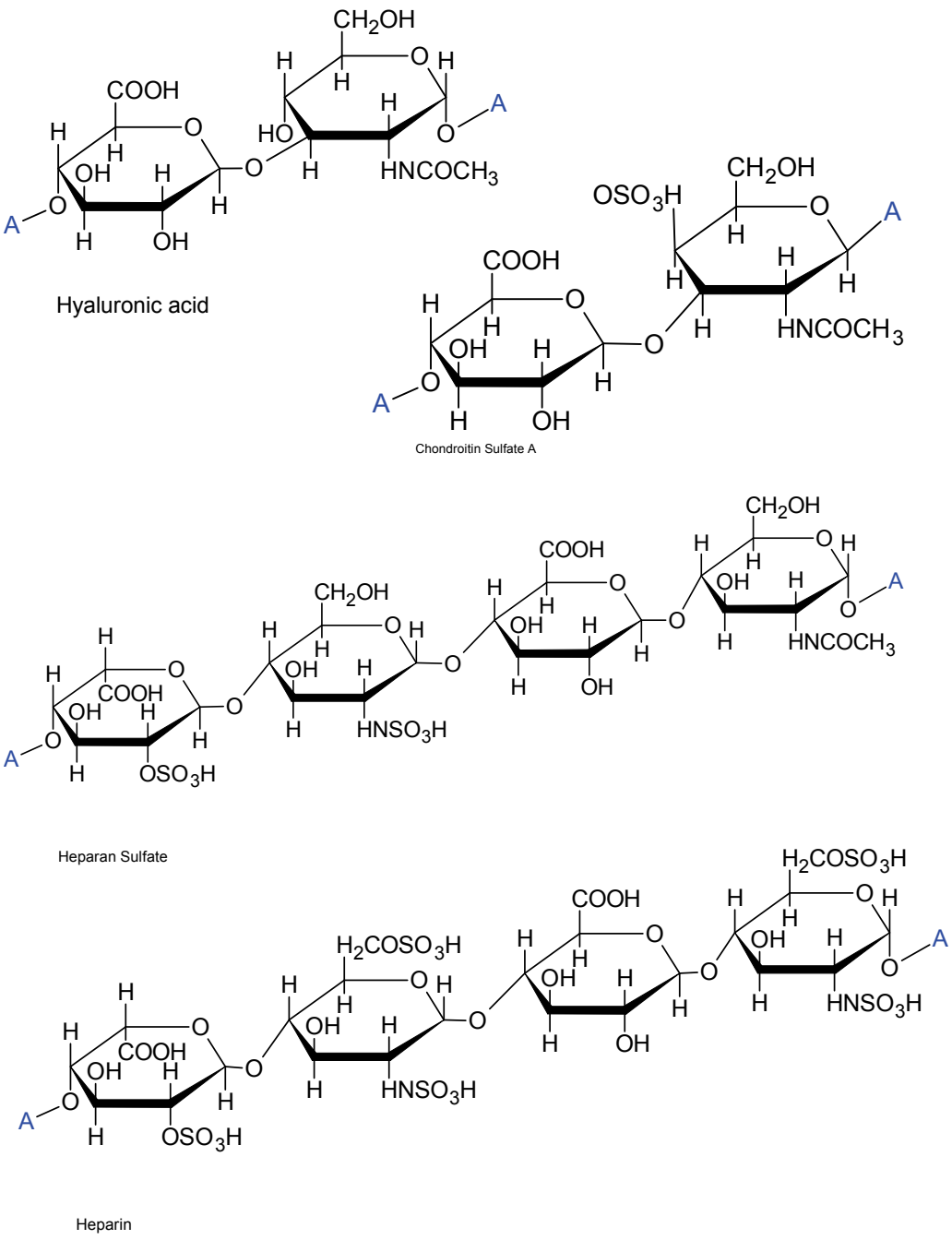

Figure 1-2: Structures of glycosaminoglycans found in the extracellular matrix.

1.2.2 Functional Components of ECM

There are many functional components in the ECM and they may vary according to the tissue and/or organ and may also vary with health, age, and species. The following section describes the most abundant and commonly found functional components within the ECM as well as the functionality found in degradation products of the ECM.

1.2.2.1 Fibronectin

Fibronectin is 250 kDa molecule part of a family of glycoproteins secreted by the resident cells involved in the formation of the extracellular matrix and is an important molecule for cell adhesion, spreading, and migration. Due to its adhesive properties, the role of fibronectin in wound healing has been closely examined. The amino acid sequence Arg-Gly-Asp or RGD was first found in fibronectin and later associated with cell-matrix binding via the $\alpha_5\beta_1$ integrin. Within the ECM, fibronectin can be found as a large insoluble multimeric molecule or found as a soluble dimer. Fibronectin also contains a heparin binding domain that can interact with proteoglycans in the cell membrane (i.e. syndecan) to increase cell-matrix binding strength or with other proteoglycans within the matrix. Fibronectin can also bind tenascin, an extracellular matrix glycoprotein, blocking the interaction with syndecan and effectively reducing cell-matrix binding strength. Fibronectin can be found in the ECM of basement membranes and interstitial tissues and is the second most abundant protein in the ECM [32, 34, 38-40]. Fibronectin serves as a major adhesion molecules for cells within the ECM.

1.2.2.2 Laminin

Laminin is another glycoprotein mostly found in the basement membrane of tissues and has been associated with cell binding and migration. It is composed of three polypeptide chains (α, β, and γ chains) linked by disulfide bonds forming a cross-like shape. There have been 11 isoforms of laminin described. As in the case of fibronectin, laminin contains cell-binding amino acid sequences. Laminin contains the RGD sequence as well as a YIGSR and IKVAV sequence that have been shown to have cell binding and chemotactic properties. Laminin can bind with entactin, type IV collagen, and heparin sulfate [32, 34, 38-40]. Laminin is a major adhesion molecule typically found in the basement membrane of tissues.

1.2.2.3 Entactins (Nidogens)

Entactins are sulfated glycoproteins (~150 kDa) commonly found in basement membranes associated with collagen type IV, proteoglycans, laminin, and fibronectin. By connecting laminin with collagen type IV, entactins provide mechanical stability to basement membranes and they are essential for the differentiation of adult tissues [34, 41].

1.2.2.4 Growth Factors and Cytokines

Growth factors and cytokines are present in small quantities throughout the ECM and help modulate cell behavior during normal tissue maintenance or after injury. The presence of growth factors and cytokines is tissue dependent and tissue specific. Growth factors that have been identified within the ECM include vascular endothelial cell growth factor (VEGF), fibroblast growth factor family (FGF), stromal-derived growth factor (SDF-1), epithelial cell growth factor (EGF), transforming growth factor beta (TGF-β), keratinocyte growth factor

(KGF), hepatocyte growth factor (HGF), platelet derived growth factor (PDGF), and bone morphogenetic protein (BMP) [4, 12, 32-35, 38, 40, 42].

1.2.2.5 Matricryptic Sites and Degradation Products

Davis et al. defined matricryptic sites as "biologically active sites that are not exposed in the mature, secreted form of the ECM molecules (including both proteins and carbohydrates such as glycosaminoglcyans), but which become exposed after structural and conformational alterations [35]." The presence of such sites opens the door for an entirely new interpretation of bioactivity within the ECM. Current research suggests that matricryptic sites within the ECM may modulate ECM assembly, the wound healing response, and signal transduction following cell-matrix interactions. Examples of matricryptic sites include 120-kD cell biding domain in fibronectin which after enzymatic degradation has been shown to stimulate cell migration. Similar matricryptic sites have been found in vitronectin, collagens, laminins, fibrin, hyaluronic acid, tenascin, and elastin [35].

Digested ECM from a variety of tissues such as the small intestine, urinary bladder, and liver has also been shown to possess anti-microbial activity against *Escherichia Coli* (Gram-negative) or *Staphylococcus aureus* (Gram-positive) for up to 13 hours [15, 16]. A recent study which showed that bacteria grow on the intact ECM also suggested that degradation of the ECM is required for the antimicrobial activity to be manifested [43]. The antimicrobial effect of degraded ECM is also evident in pre-clinical and clinical studies where infection was inhibited after deliberate contamination of the graft or with prior contamination at the implant site [44-47]. Acid digested ECM has also been shown to have chemoattractant properties to primary murine adult liver, heart, and kidney endothelial cells *in vitro* using the Boyden chamber [13]. The chemotactic property was confirmed by loading Matrigel with the ECM digest and implanting it

in a subcutaneous pocket in mice. The ECM loaded Matrigel showed grater angiogenesis when compared to the Matrigel implant alone [13]. Others have described proteolytic degradation products released during ECM digestion with anti-angiogenic affects. Examples include endostatin, laminin fragments, nidogen fragments, and perlecan fragments [36]. The presence of bioactive fragments within ECM molecules suggests that the inherent bioactivity found within the ECM could be result of an abundance of bio-signals, both stimulatory and inhibitory. These signals can be working in concert and arise from intact bioactive proteins and from degradation products produced during the breakdown of the ECM following injury or implantation.

1.2.3 Biologic scaffolds Composed of ECM

As discussed in the previous sections, the ECM consists of immobilized molecules, both structural and functional in design, which are potent modulators of resident cells within the ECM and those cells that migrate to the ECM in response to tissue injury. The native composition and structure of the ECM represents the optimal scaffold material and consists of functional and structural components in ideal amounts and spatial distribution to support cell and tissue function. Individual components of the matrix can be degraded with specific enzymes (i.e. collagenase, hyaluronase, elastase, etc) secreted by the cells repopulating the matrix during the host tissue response, thus subjecting the scaffold to degradation after implantation. The combination of inherent bioactivity, “cell friendliness”, and biodegradable properties make the ECM the ideal scaffold for tissue repair [4, 12, 33].

1.2.3.1 Clinical Application

Biologic scaffolds composed of naturally occurring ECM for soft tissue applications have been investigated for a wide range of preclinical animal studies [3, 9, 12, 48-54] and human clinical applications [55-57]. Among the potential applications are the repair of vascular [54, 58, 59], lower urinary tract [52, 53, 60, 61], musculotendinous [9, 48, 50, 51], skin [62, 63], larynx [64-67], and esophageal [3, 56, 68] tissues. ECM scaffolds are typically derived from mammalian tissue sources and are subjected to a variety of processing steps including mechanical manipulation, chemical-mediated decellularization, dehydration, sterilization, and storage at different environmental conditions [11, 69-72]. Such processing and manufacturing steps, which are necessary to prepare a device composed of ECM with a reasonable shelf life, may affect material properties and ultimately the host tissue response. ECM mammalian sources can be allogeneic or xenogeneic and include human, porcine, bovine, and equine sources. A list of biologic scaffolds used clinically, their name, and their source is shown in Table1-1. ECM scaffolds derived from the small intestine have been used in over 1 million human patients and their use is increasing.

Table 1-1: Commercially available ECM scaffold.

Product	*Company*	*Material*
AlloDerm	Lifecell	Human skin
AlloPatch®	Musculoskeletal Transplant Foundation	Human fascia lata
Axis™ dermis	Mentor	Human dermis
Bard® Dermal Allograft	Bard	Cadaveric human dermis
CuffPatch™	Arthrotek	Porcine small intestinal submucosa (SIS)
DurADAPT™	Pegasus Biologicals	Horse pericardium
Dura-Guard®	Synovis Surgical	Bovine pericardium
Durasis®	Cook SIS	Porcine small intestinal submucosa (SIS)
Durepair®	TEI Biosciences	Fetal bovine skin
FasLata®	Bard	Cadaveric fascia lata
Graft Jacket®	Wright Medical Tech	Human skin
Oasis®	Healthpoint	Porcine small intestinal submucosa (SIS)
OrthADAPT™	Pegasus Biologicals	Horse pericardium
Pelvicol®	Bard	Porcine dermis
Peri-Guard®	Synovis Surgical	Bovine pericardium
Permacol™	Tissue Science Laboratories	Porcine skin
PriMatrix™	TEI Biosciences	Fetal bovine skin
Restore™	DePuy	Porcine small intestinal submucosa (SIS)
Stratasis®	Cook SIS	Porcine small intestinal submucosa (SIS)
SurgiMend™	TEI Biosciences	Fetal bovine skin
Surgisis®	Cook SIS	Porcine small intestinal submucosa (SIS)
Suspend™	Mentor	Human fascia lata
TissueMend®	TEI Biosciences	Fetal bovine skin
Vascu-Guard®	Synovis Surgical	Bovine pericardium
Veritas®	Synovis Surgical	Bovine pericardium
Xelma™	Molnlycke	ECM protein, PGA, water
Xenform™	TEI Biosciences	Fetal bovine skin
Zimmer Collagen Patch ®	Tissue Science Laboratories	Porcine dermis

1.2.3.2 Effects of Manufacturing upon Material Properties

The first step in the manufacture of an ECM scaffold is the harvest and decellularization of the tissue. The decellularization process will depend on the tissue and may include physical, chemical, and enzymatic methods. Physical methods include freezing, direct pressure, sonication, and agitation. Tissues can be chemically decellularized with acid/alkaline solutions,

detergents (ionic, non-ionic, sodium deoxycholate, etc), hypotonic and hypertonic solutions, and enzymatic solutions. Each method exerts its effect in different ways and has different effect upon the ECM. The most common detrimental effects of decellularization upon the material properties of ECM include disruption of the collagen matrix, removal of the glycosaminoglycans, and changes in structural and material properties [11].

Currently marketed biologic devices are packaged and stored under different conditions including: hydrated (Pelvicol™, Bard, Inc.), laminated and vacuum dried (Restore™, Depuy Orthopedics, Inc.), and freeze-dried (Bard® Dermal Allografts, Bard, Inc.). Storage of biologic devices in a hydrated state may help to maintain some of the native structure by avoiding extra processing steps but may lead to leaching and/or hydrolysis of structural and non-structural components of the device. Dehydration of biologic devices minimizes hydrolytic degradation during storage but may permanently alter the structure, material properties, and the ability to support cell growth. The final step in manufacturing an ECM scaffold is terminal sterilization. Sterilization methods commonly used include ethylene oxide (ETO), gamma irradiation, and electron beam irradiation [73-81]. Each method exerts its effect by modifying the structure and/or function of critical components of the target microorganism (e.g. proteins and nucleic acids), however, these methods also change the material and mechanical properties of the ECM scaffold itself.

The ECM is a major structural component of most tissues and is responsible in part for their mechanical and material properties. The material properties of biological scaffold devices composed of ECM will depend on the tissue from which the ECM is harvested as well as any manufacturing and processing steps used to create the final device. Two methods of dehydration are commonly used for ECM based medical devices. Vacuum pressing dehydrates the ECM by

applying pressure under a vacuum and can be used to create multilaminate devices with varying degrees of isotropy and mechanical properties [69]. Lyophilization, also known as freeze-drying, is a process by which a sample is dehydrated under low temperatures and high vacuum. Lyophilization is commonly used to preserve biological tissues such as bone [82-84] and tendon grafts [85, 86], as well as commercially available biologic materials (i.e. Bard® Dermal Allografts, Bard, Inc.) and biological molecules (i.e. purified collagen, fibronectin, and enzymes). During the lyophilization process, ice crystal formation and changes to protein structures may affect structural proteins and may have an effect upon the material properties. A summary of the effects of manufacturing upon ECM scaffold is summarized in Table 1-2.

Table 1-2: Effects of manufacturing upon minimally processed ECM scaffolds.

Manufacture Process	***Effects upon Structural Properties of the ECM scaffold***	
	Hydration	
Keep Hydrated	Maintains native structure but prone to leaching and hydrolytic degradation	[72]
Lyophilization	Changes ultra-structure and rehydration capability but no significant effects upon structural properties	[72]
Vacuum Press	Increases strength of scaffold but significantly alters the ultra-structure	[69, 87]
	Storage	
Refrigerated	Increases maximum elongation of lyophilized scaffolds 1year of storage	[71]
Room Temperature	Increases strength of lyophilized scaffold after 1 year or storage	[71]
	Terminal Sterilization	
e-beam	Decreases strength of lyophilized ECM scaffolds	[70]
Gamma	Decreases strength of lyophilized ECM scaffolds	[70]
ETO	Minimal effects upon structural properties of lyophilized ECM scaffolds	[70]

1.2.3.3 Inherent Limitations of ECM Derived Biologic Scaffolds

ECM scaffolds, are constrained by their inherent shape and their mechanical and material properties. There are limited ways in which the material and mechanical properties of ECM scaffolds can be manipulated. For example, the maximum strength of ECM scaffolds can be increased by creating multilaminated ECM devices of varying number of layers [16, 17]. Mechanical strength can also be increased by cross-linking the scaffold with chemicals such as gluteraldehyde, carbodiimide, and hexamethylene-diisocyanate [17]. However, cross-linking ECM scaffold reduces the degradation *in vivo* and renders the material almost inert by significantly altering the host tissue response [88]. The material properties of ECM scaffolds can also be affected by the manufacturing process (i.e. mechanical decellularization versus chemical decellularization) and by the age and health status of the animal from which the ECM is harvested.

1.3 ALTERNATIVES TO ECM SCAFFOLDS

Synthetic scaffold materials and purified biopolymers are alternatives to naturally derived ECM scaffolds. Synthetic materials such as polyesters are typically characterized by uniform and reproducible mechanical and material properties [17]. However, they lack the bioactivity characteristic of ECM derived scaffolds. Individual components of the ECM such as collagen and other naturally occurring biopolymers such as alginate and fibrin have also been investigated as biodegradable scaffolds with limited success. These types of biopolymers are biocompatible and with some degree of bioactivity but lack the complexity found in the native ECM. The

following sections will briefly summarize the current state of biodegradable synthetics and natural polymer used as scaffold materials for regenerative medicine applications.

1.3.1 Synthetic Polymers

Synthetic polymers have been used as biomaterials for more than 30 years with varying degrees of success depending on the intended application. As our understanding of wound healing and tissue reconstruction progressed, the idea of a scaffold material that could be degraded by the host and replaced with functional tissue became more attractive. Prior to the 1960's, collagen was one of the few biodegradable scaffold materials known. The lack of biodegradable scaffolds led to the investigation of polyesters as bioresorbable materials for the repair of damaged tissues and as an alternative to collagen matrices [89]. Common polyesters in regenerative medicine include polyglycolide, polylactide, poly-ε-caprolactone, polytrimethylene carbonate, and poly(glycerol sebacate) [17]. Common polyesters are shown in Figure 1-3.

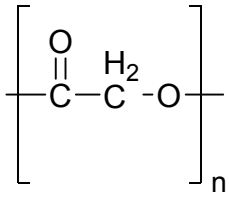

Polyglycolide (PGA)

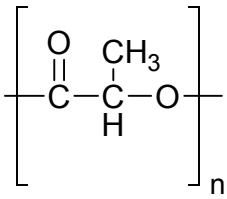

Polylactide (PLA)

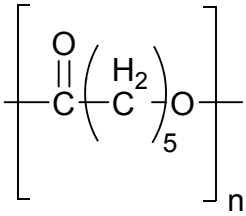

Poly(ε-caprolactone) (PCL)

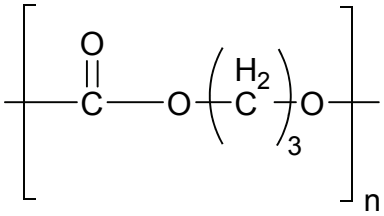

Polytrimethylene carbonate (PTMC)

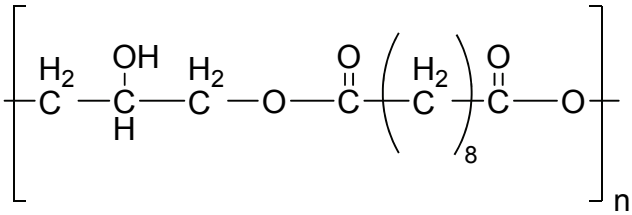

Poly(glycerol sebacate) (PGS)

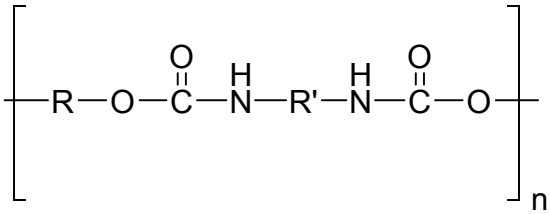

Polyurethane (PU)

Figure 1-3: Chemical structures of commonly used polyesters as scaffold materials.

Polyesters are the most researched synthetic biomaterials for tissue engineering and regenerative medicine applications. Among the most commonly used polyesters are polyglycolide (PGA), polylactide (PLA), and poly-ε-caprolactone. PGA is a hydrolytically unstable polymer with high crystallintity. PLA is more hydrophobic than PGA due to the extra methyl group and has a lower rate of hydrolytic degradation. PLA can be found in two stereoisomeric forms (poly(D-lactide) or poly(L-lactide)). As a result of the similarity in the synthesis of PGA and PLA, a combination of both polymers can be synthesized with differing degradation rate [17]. However the acidic degradation product may lead to an unfavorable inflammatory response when used as an implantable material [17, 89]. Poly-ε-caprolactone is a semicrystalline polymer that degrades slower than PLGA and has been used to create co-polymers with different mechanical properties. There are other examples of polyesters used as scaffold materials such as poly(trimethylene carbonate) (PTMC) and Poly(glycerol sebacate). PTMC degrades slowly *in vivo* and *in vitro* with high tensile strength and elongation. Copolymerization of trimethylene carbonate with ε-caprolactone or lactic acid yields scaffold materials with elastomeric properties and high tensile strength but a slow degradation rate. Poly(glycerol sebacate) (PGS) is a relatively hydrophilic elastomer formed after the polycondensation of glycerol and sebacic acid. PGS has lower tensile strength than the polymers mentioned above [17, 38, 89].

Polyurethanes are elastomers with a great range of commercial uses. They are typically formed by the reaction of a monomer with at least two isocyanate functional groups, another monomer containing at least two alcohol groups, and a catalyst [17, 89]. The elastomeric properties present in polyurethanes elastomer arise from the presence of a soft segment and a

hard segment. The soft segment is formed by longer chains of polyesters or polyethers while the hard segment is formed by the diisocyante and the chain extender [17, 89]. The elastomeric properties of the polyurethane scaffold materials is attractive for tissue engineering purposes since they more closely match the mechanical properties of soft tissues and can be subjected to cyclic mechanical conditioning *in vitro* [17, 20-23, 28, 89] . Polyurethanes such as poly(ester-urethane)urea have been shown to have reproducible mechanical properties, non-toxic degradation products, and excellent biocompatibility [18-23, 28, 90].

1.3.2 Naturally Occurring Biopolymers

Among the naturally occurring biopolymers used as scaffolds for tissue engineering applications are polysaccharide such as hyaluronic acid, alginate, and chitosan and fibrous proteins such as purified collagen (native and cross-linked), gelatin, and fibrin [17]. These materials are generally biocompatible, biodegradable, and are relatively easy to purify and obtain although there might be variations between batches due to harvesting procedures and health and status of the tissue of origin.

Hyaluronic acid (HA) is a high molecular weight polysaccharide of great importance during embryonic development, extracellular matrix homeostasis, would healing, inflammation, angiogenesis, and tissue regeneration. HA is a non-sulfated GAG formed by the polymerization of D-glucuronic acid and D-N-acetylglucosamine. HA can be degraded by cell secreted enzymes. It has received attention as a biologic scaffold material and has found clinical utility in osteoarthritis, ophthalmology, and wound healing [17, 39] .

Alginate is a polysaccharide derived from algae that has received great attention as scaffold material for the delivery of cell, proteins, and genes. Alginate polymerizes into a

hydrogel in the presence of divalent cations such as calcium or multivalent polymers such as polylysine. It is composed of blocks of β-D-mannuronate (M) and α-L-guluronate (G). The inability of proteins or cells to bind to alginate gel makes it an interesting biomaterial for the delivery of cell, growth factors, and genes without eliciting an intense immunological response [39, 89, 91].

Fibrin is the major component of blood clots and its function is to provide a temporary matrix during tissue injury and to control homeostasis. Fibrin is formed by the conversion of the glycoprotein fibrinogen to fibrin by the protease thrombin and then cross-linked by factor XIII of the coagulation cascade. As a scaffold material, fibrin polymerizes rapidly when placed in the presence of thrombin and factor XIII and has been shown to adhere to tissues with good biocompatibility. Fibrin can be degraded by plasmin into fibrin degradation products [39, 89, 91].

Acid solubilized collagen, the most abundant being collagen type I, can self-assemble into a gel by raising the pH and ionic strength to physiological levels driving the self assembly of the collagen molecules. Collagen is the most abundant protein in mammalian tissues and represents a biocompatible scaffold for tissue reconstruction. Manipulation of self-assembled collagen has led to the manufacture of fibrous or porous meshes although chemical cross-linking is necessary to obtain appropriate mechanical properties. Thermal degradation of collagen molecules yields another form called gelatin. Gelatin also possesses cell adhesion properties and is an excellent cell substrate. Collagen and gelatin can be degraded by matrix metalloproteinases [39, 89, 91].

1.4 SCAFFOLDS FOR CARDIAC TISSUE REGENERATION

Heart failure (HF), the inability of the heart to pump blood at an appropriate rate in order to maintain adequate tissue perfusion, is one of the major causes of death within the Western population with a five-year survival of 50% [92]. HF can be caused by slow deterioration of myocardial contraction or can be brought on by acute events. For patients with heart failure, the current treatment is heart transplantation or the use of left ventricular assist devices (LVADs). With the high number of patients in need of a heart transplant and the short list of available hearts, it is evident that alternative therapies are needed [92]. One of the most common causes of heart failure is myocardial infarction (MI) where one or more blood vessels supplying the heart are occluded inhibiting the transfer of oxygen and nutrients to regions of the myocardium. This ischemic assault leads to irreversible cell death within the myocardium and the eventual formation of scar tissue. Other events that can cause heart failure, specifically left-sided heart failure, are hypertension, aortic and mitral valvular diseases, and non-ischemic myocardial diseases. Failure of the left side of the heart can lead to poor quality of life or death. The loss of LV contractility due to an MI leads to a decrease in the stroke volume and changes in the geometry and structure of the ventricular wall. The heart compensates by dilating the ventricular wall leading to an increase in wall stresses and increased energy consumption [93, 94].

Cardiac tissue engineering and cellular therapies are currently being investigated as possible treatments for HF and for the restoration of ventricular tissue function. The goal of cardiac tissue engineering is to repair cardiac tissue by the formation of an implantable device manufactured from a scaffold component alone or from a combination of a scaffold component and a cellular component [95-97]. Ideally, cardiac-like tissue can be grown in a bioreactor prior to implantation and then used to regenerate diseased myocardium. Cellular therapies, such as

cellular cardiomyoplasty, attempt to deliver cells derived from bone marrow (mesenchymal or haematopoietic), embryonic stem cells, adult stem cells, or progenitor cells to the site of interest with the hope that the injected cells will engraft and repopulate the damaged myocardium and differentiate into functioning cardiomyocytes. However, both approaches have their limitations. Both approaches are limited by poor cell survival and engraftment after the removal from laboratory conditions, the choice of cells that are required for optimum results, the isolation of sufficient quantities of cells, and, depending on the cell source, the immunological response to the implanted cells [95-97].

Current surgical treatments attempt to correct the problem of decreased ventricular function by restoring the ventricular geometry via the removal and/or replacement of non-viable tissue. The most common surgical techniques used are endoventricular circular patch plasty (EVCPP), partial left ventriculectomy (Batista operation), or the use of cardiac support devices (such as the Apicorn CorpCap mesh) [92]. In the EVCPP procedure, the non-viable tissue is removed and replaced by a synthetic patch resulting in improved systolic and diastolic functions due to the reshaping of the ventricle. However, the use of a synthetic patch leads to fibrous encapsulation without the integration of the surrounding tissue or the infiltration of myocardiocytes to the scaffold. An ideal scaffold would allow the reshaping of the ventricle and would degrade at an appropriate rate while attracting resident and circulating stem cells and progenitor cells to the remodeling site culminating in the formation of functioning myocardium [92, 98, 99].

1.4.1 Synthetic Scaffolds

The current treatment to prevent left ventricular dilation include EVCPP or restraint devices such as poly(propylene) meshes (Marlex), polyethylene terepthalate (Dacron), expanded polytetrafluoroethylene (Gore-Tex), and knitted polyester devices. These polymers are non-degradable and are characterized by the typical host tissue response to a foreign material (i.e. fibrous encapsulation and no functional tissue growth) [92, 98, 99].

Synthetic scaffolds can also be used as a template to grow myocardial tissue either *in vitro* or *in vivo*. The most common biodegradable material researched as potential cardiac patches include PGA, PCLA, PLLA, PGS, and PEUU [25, 95, 96, 100]. The synthetic patches can be placed on the myocardial surface of akinetic or dyskinetic regions after MI or be used to replace a defect in the myocardial tissue. PEUU scaffold manufactured using thermally induced phase separation (TIPS) have been investigated as a myocardial patch in LV infarcted myocardium or in a surgical defect in the right ventricular outflow tract (RVOT) [25, 100]. Six millimeter defects created in the right ventricular outflow tract of rats repaired with PEUU showed cellular integration with endothelialization. The same patch placed on the surface of infarcted myocardium showed the in-growth of contractile smooth muscle tissue formation and improvement in long-term contractile function [25, 100]. The use of PCLA, gelatin, and PGA seeded with smooth muscle cells (SMCs) have also been investigated for the repair of a defect created in the RVOT [101]. Defects repaired with the PCLA-SMCs combination showed no dilation or thinning *in vivo* without a pronounced inflammatory response [101]. A biodegradable and porous scaffold composed of 1,3-trimethylene carbonate (TMC) and D,L-lactide (DLLA) as well as TMC and ε-caprolactone (CL) have been also reported as potential scaffold material for cardiac tissue engineering with relatively slow degradation rates [102, 103]. TMC and DLLA

copolymers showed no adverse tissue reaction and were degraded after 10 months *in vivo* in a subcutaneous pocket. Other groups have studied effects of the implantation of commercial polyurethane seeded with skeletal myoblasts on rat hearts post-infarction. Although myoblasts could be found inside the scaffold four weeks after implantation, there were no signs of differentiation [104, 105]. Dermagraft, a combination of human dermal fibroblasts on a knitted Vycryl mesh, has been placed in the epicardial surface of infarcted LV of severe combined immunodeficient mice. The implant reduced the loss of LV function after acute myocardial infarction 14 days post-op [106]. In addition, neonatal rat cardiomyocytes cultured on electrospun polycaprolactone and a combination of fibroblasts, endothelial and cardiomyocytes cells on poly(ethylene glycol) discs have also been investigated as possible cardiac tissue engineered devices [107]. A short list of scaffolds and the scaffolds and cell combinations used for cardiac tissue engineering is summarized in Table 1-3. However, the approach of using a synthetic scaffold and a cellular component together is still limited and the optimum scaffold and/or cell choice remains unknown.

Table 1-3: Synthetic polymers used for cardiac tissue engineering.

Polymer	*Cell component*	*Ref*
poly(ester-urethane)urea	No	[25, 100]
Poly-L-lactide fabric	Rat smooth muscle cells	[101]
Polyglycolic acid	Rat smooth muscle cells	[101]
1,3-Trimethylene Carbonate & D,L-lactide co polymer	No	[102]
1,3-Trimethylene Carbonate & ε-caprolactone	No	[102]
Polyurethane	Rat skeletal myoblasts	[104, 105]
Knitted Vycryl	Human dermal fibroblasts	[106]
Polycaprolactone	Rat cardiomyocytes	[107]
ePoly(lactide-co-glycolide)	Rat cardiomyocytes	[108]

1.4.2 ECM Scaffolds

Approaches to cardiac tissue engineering include the use of intact ECM scaffolds or scaffolds composed of purified ECM proteins such as collagen and glycosaminoglycans. As in the case of polymeric scaffolds, ECM scaffolds can be used alone or as a combination of cells, growth factors, and/or the ECM material. For example, Zimmermann et al. have used a combination of collagen type I, Matrigel, and rat neonatal cardiomyocytes to create engineered heart tissues (EHT) [109, 110]. Li et al. used fetal rat ventricular cells in combination with a gelatin mesh (Gelafoam) [111]. Both methods failed to show improvements in cardiac function after implantation in infarcted myocardium.

ECM scaffolds have found encouraging success for the repair of cardiac tissue by avoiding scar tissue formation and by inducing constructive remodeling. Scaffolds investigated for cardiac repair include small intestinal submucosa (SIS) and urinary bladder matrix (UBM) [5-7, 112, 113]. SIS and UBM were used to repair a 2.5 cm in diameter created in the right ventricular wall of a porcine and canine model [5]. The scaffold was degraded, the defect size decreased by approximately 20%, and cardiomyocytes were found within the defect area after 24 weeks. The remodeled site showed spontaneous contraction with peak force at 70% of adjacent myocardium. Other studies have investigated different configurations of UBM in different animal models. Kochupura et al. repaired a full thickness defect in the right ventricle in a canine model with a single sheet of UBM [113]. After 8 weeks, the UBM patch improved regional mechanical function and cardiomyocytes were found within the remodeling tissue. Badylak et al. used a single sheet of UBM to repair a 2 cm^2 full thickness defect in a canine model and showed improvements in regional systolic contraction when compared to defects repaired with Dacron after 8 weeks [6]. The scaffold was degraded and cardiomyocytes were found randomly distributed within the remodeling site. A similar study found cardiomyocytes-like cells within the remodeling site and moderate electrical activity using the NOGA system [114]. Robinson et al. repaired a full-thickness defect in infarcted left ventricular wall using a 4 layers multilamintated UBM scaffold in a porcine model [7]. The UBM was degraded and repopulated by cells normally found in the myocardium (by flow cytometry analysis) and better tissue remodeling when compared to ePTFE repaired defects was observed. Other groups have investigated the use of acellular bovine pericardium (AGP) cross-linked with genipin to repair a right ventricular defect in rats [115]. Tissue regeneration was observed after 12 weeks with the

presence of new capillary, neoglycosaminoglycans, and the presence of smooth muscle cells. AGP has been loaded with basic fibroblast growth factors and mesenchymal stem cells [116].

1.4.3 Injectable Scaffolds

Injectable scaffolds are attractive for the delivery of cells via minimally invasive methods. The advantages of injectable scaffolds are: the possibility of delivery using minimally invasive methods and the ability to use the scaffold in irregularly shaped locations. Cellular cadiomyoplasty approaches have been limited by cellular engraftment and survival after injection and with the use of injectable scaffolds better cell retention can be achieved. Among the most common injectable scaffolds are fibrin, collagen, alginate, Matrigel, gelatin and self-assembling peptides [95-97]. A list of commonly used ECM based scaffolds for cardiac tissue engineering is shown in Table 1-4.

Table 1-4: ECM based scaffolds used for cardiac tissue engineering.

Scaffold	*Cell component*	*Ref*
Fibrin	Skeletal myoblasts	[117]
Fibrin	Bone marrow mononuclear cells	[118]
Fibrin	Mesenchymal stem cells	[119]
Matrigel	--	[120]
Collagen	--	[120]
Collagen	Neonatal rat cardiomyocytes	[121]
Collagen	Mouse embryonic stem cells	[122]
Collagen	Bone marrow derived cells	[123]
Collagen + GAG	Mesenchymal stem cells	[124]
Collagen + GAG	Bone-marrow derived mesenchymal cells	[124]
Collagen + Matrigel	Neonatal cardiomyocytes	[110]
Alginate	--	[97]
Alginate	Rat fetal cardiac cells	[60]
Matrigel	Embryonic stem cells	[122]
Gelfoam	Rat ventricular cells	[111]
Gelatin + FGF		[125]
Small intestinal submucosa	--	[5]
Urinary bladder matrix	--	[6]
Acellular bovine pericardium	--	[126]
Acellular bovine pericardim + bFGF	Mesenchymal stem cells	[116]

1.5 SPECIFIC AIMS

The previous section described the importance of a scaffold component for tissue engineering and tissue reconstruction. The choice of the scaffold component in any tissue engineering strategy will most likely have great impact on its success and thus the search for the ideal scaffold material continues. Biologic scaffolds derived from the extracellular matrix (ECM) have been successfully used for tissue reconstruction in both preclinical animal studies and in human clinical applications and are characterized by the ability to support the adhesion, proliferation, and differentiation of a variety of cells both *in vitro* and *in vivo*. Biologic scaffolds are also characterized by the ability to induce constructive remodeling of tissues [12, 30]. However, biologic scaffolds composed of ECM are limited by the inherent geometrical and mechanical properties of the tissue from which they are derived. In addition, the mechanical and material properties of ECM derived scaffolds are subject to biologic variations dependent upon the age of the host and the specific methods of processing [69, 87, 127].

Synthetic scaffold materials are an alternative to naturally derived ECM scaffolds. Synthetic materials such as poly(ester-urethane)urea (PEUU) are typically characterized by uniform and reproducible mechanical and material properties. Synthetic polymers have been used to treat ischemic cardiomyopathies, correct congenital defects, and treat traumatic ventricular perforations and aneurysms [98, 99, 128]. However, synthetic materials lack the bioactivity and functional host tissue response characteristic of ECM derived scaffolds and often result in fibrous encapsulation and does not grow and change in size in the case of congenital defects. Different forms of the UBM-ECM scaffold have been investigated in preclinical studies as cardiac patches in both the left and right ventricular wall with encouraging results [5, 7, 113]. However, UBM-ECM is typically restricted to topical administration or to invasive surgical

procedures that can accommodate variations of the two dimensional sheet forms and to the mechanical properties inherent to the tissue from which it was derived. Therefore the goals of the proposed studies are to develop a soluble form of the ECM scaffold that could be combined with a synthetic component to create a hybrid scaffold and to develop a gel form of the ECM scaffold that can be delivered via minimally invasive methods to the site of injury.

SPECIFIC AIM No. 1: To compare the mitogenic and chemoattractant properties of enzymatically solubilized UBM-ECM.

Overall Rationale: Combination of UBM with PEUU will require solubilization of the UBM-ECM followed by the re-polymerization in a hybrid form. The bioactivity present in the UBM-ECM is most likely a result of the specific three-dimensional ultrastructure and the composition of structural and non-structural components. Low-molecular weight peptides, growth factors, and cytokines naturally present in the ECM scaffolds have been shown to have chemotactic and bioactive properties [12, 30]. In addition, acid-hydrolyzed ECM has also been shown to have small molecular weight peptides with chemoattractant activity for primary murine adult liver, heart, and kidney endothelial cells *in vitro* [13]. Therefore, it is plausible that UBM-ECM can be solubilized and that its bioactivity can be retained depending on the chemical environment used even though the solubilization process will most likely disrupt the three dimensional ultrastructure and spatial distribution of proteins.

Hypothesis$_1$: A solubilized form of UBM-ECM can be created by enzymatic digestion and the digested UBM-ECM will show chemoattractant and mitogenic properties.

SPECIFIC AIM No. 2: To create a gel form of an ECM scaffold that can support the in vitro growth of endothelial cells, myoblasts, cardiomyocytes, and smooth muscle cells.

Overall Rationale: A soluble form that can be induced to polymerize into a gel form could expand the clinical utility of ECM biologic scaffolds. ECM gels with appropriate viscosities could be delivered via minimally invasive surgical techniques with the ability to conform to three-dimensional spaces after injection. Previous studies have described a gel form of an ECM derived from the small intestine but the preparation required an aggressive purification process that may have resulted in the loss of bioactive molecules, and the rheological properties of the gel were not determined [129]. A gel form of the UBM scaffold can expand its clinical utility and used in different applications for tissue reconstruction.

Hypothesis$_2$: A UBM-ECM gel can be created and the gel will support the in vitro growth of endothelial cells, myoblasts, cardiomyocytes, and smooth muscle cells.

SPECIFIC AIM No. 3: To create a hybrid scaffold composed of UBM-ECM and poly(ester-urethane)urea.

Overall Rationale: Electrospinning is a technique that can create fibrous scaffolds with the morphology typically observed in the native ECM. Electrospun scaffolds have been previously created using individual components of the ECM such as collagen and elastin or using biodegradable polymers such as polyethylene oxide (PEO) and poly(ester-urethane)urea (PEUU)

[23, 130-135]. However, electrospinning the entire composition of solubilized UBM-ECM protein with a synthetic polymer has not been attempted. We believe it is possible to combine the more favorable properties of each scaffold material (polymer and ECM) resulting in a hybrid scaffold with appropriate mechanical, material, and bioactive properties.

Hypothesis$_3$: Hybrid scaffolds can be constructed from solubilized UBM-ECM and PEUU. Hybrid scaffold will enhance the growth of endothelial cells in vitro and will change the host tissue response when compared to the PEUU alone.

SPECIFIC AIM 4: To create a polymer-ECM hybrid scaffold with appropriate strength and material properties to function as a surgical patch for repair of a left ventricular wall defect and to characterize the in vivo response to the polymer-ECM hybrid scaffold when used as a left ventricular patch in a dog model.

Hypothesis$_4$: Solubilized UBM-ECM and PEUU can be used to create hybrid scaffold that effectively function as a left ventricular patch.

Rationale: Synthetic materials have been previously investigated as cardiac patches with limited success due to the foreign body reaction and fibrous encapsulation of the scaffold [98, 99, 128]. Preclinical studies have shown that the UBM-ECM scaffold can be successfully used as a cardiac patch in the left and right ventricle [7, 113]. However, the compliance and the mechanical properties of the scaffolds do not match the compliance and anisotropy of the ventricular wall. PEUU scaffolds can be electrospun to have appropriate elastomeric properties

but lack the bioactivity present in the UBM-ECM scaffolds [23, 27]. We believe that the combination of UBM-ECM and PEUU will result in a bioactive hybrid scaffold that results in the constructive remodeling of the left ventricular wall.

2.0 ENZYMATIC SOLUBILIZATION OF UBM

2.1 BACKGROUND

Extracellular matrix scaffolds are derived from a variety of tissues and/or organs typically by the decellularization of a tissue followed by disinfection and terminal sterilization. ECM scaffold have found success in pre-clinical and clinical applications but remain limited by the mechanical and material properties inherent to the tissue from which they were derived. Solubilization of the ECM could expand the clinical utility of ECM scaffolds and could also allow for the combination of ECM with synthetics to create hybrid scaffold materials.

Degradation products from the ECM have been shown to possess anti-microbial and chemotactic properties. Previous studies have shown that acid digested ECM from the small intestine, urinary bladder, and liver possess anti-microbial activity against *Escherichia Coli* (Gram-negative) or *Staphylococcus aureus* (Gram-positive) for up to 13 hours [15, 16]. Li et al. showed that acid digested ECM has chemoattractant properties to primary murine adult liver, heart, and kidney endothelial cells *in vitro* using the Boyden chamber [13]. The chemotactic property was confirmed by loading Matrigel with the ECM digest and implanting it in a subcutaneous pocket in mice. The ECM loaded Matrigel showed grater angiogenesis when compared to the Matrigel implant alone. These studies show some of the inherent bioactivity found within the ECM. If the outcome after implantation (i.e. constructive remodeling versus

scar tissue formation) is dependent upon degradation products of ECM scaffolds, clearly the method used to degrade the ECM may affect the types of molecules present and ultimately its bioactivity and clinical utility.

A goal of this dissertation was to combine UBM-ECM with a synthetic component such as PEUU to create a hybrid scaffold. Combination of UBM-ECM with PEUU will require solubilization of the UBM-ECM followed by the re-polymerization in a hybrid form. It is plausible that UBM-ECM can be solubilized and that its bioactivity can be retained depending on the methodology used even though the solubilization process will most likely disrupt the three dimensional ultrastructure and spatial distribution of proteins. If bioactivity can be retained after digestion, the soluble form of the ECM can be used alone or with other components to create new scaffold materials. The solubilization of UBM using pepsin or papain and the effect of the solubilized UBM upon the mitogenicity and chemotaxis of various cell types *in vitro* will be described in this chapter.

2.2 METHODS

2.2.1 UBM Preparation

The preparation of UBM has been previously described [69]. In brief, porcine urinary bladders were harvested from 6-month-old 108-118 kg pigs (Thoma Meats, PA) immediately following euthanasia. The excess connective tissue and residual urine were removed. The tunica serosa, tunica muscularis externa, the tunica submucosa, and majority of the tunica muscularis

mucosa were mechanically removed. The urothelial cells of the tunica mucosa were dissociated from the luminal surface by soaking the tissue in 1.0 N saline solution. The resulting biomaterial, which was composed of the basement membrane of the urothelial cells plus the subjacent lamina propria, was referred to as urinary bladder matrix (UBM). UBM sheets were placed in a solution containing 0.1% (v/v) peracetic acid (Sigma), 4% (v/v) ethanol (Sigma), and 95.9% (v/v) sterile water for two hours. Peracetic acid residue was then removed with two 15 minute phosphate-buffered saline (pH=7.4) washes, followed by two washes with sterile water for 15 minutes each. The decellularized UBM sheets were then lyophilized using a FTS Systems Bulk Freeze Dryer Model 8-54 and comminuted to a particulate form using a Wiley Mini Mill.

2.2.2 Pepsin Digestion

UBM was digested with pepsin by mixing 1 g of lyophilized and powdered UBM with 100 mg of pepsin (~2,000-2,300 Units/mg, Sigma-Aldrich, St. Louis, MO) in sterile 100 mL 0.01 N HCl. This solution was stirred constantly at room temperature (25°) for 48 hours. The resultant viscous solution of digested UBM had a pH of approximately 3.0-4.0. A control solution was made in parallel by keeping a portion of the pepsin-HCl solution used to digest the UBM under similar conditions but without the addition of the UBM powder.

2.2.3 Papain Digestion

One gram of lyophilized, powdered UBM was mixed with 100 mL of phosphate buffered saline (PBS) containing 1 U/mL of papain (Sigma-Aldrich, St. Louis, MO). The flask was covered to minimize evaporation, placed inside an incubator at 37°C or on hot plate at 60°C, and kept under

constant stir for a total of 24 hours. After the 24 hour digestion period, the solution was brought to room temperature, spun at 1000 RPM for 6 minutes, and the supernatant collected. For each milliliter of solution, one milliliter of 1 mM E-64 protease inhibitor (Sigma-Aldrich, St. Louis, MO) was added to inactivate the papain. The unused portion of the solution containing 1 U/mL of Papain in PBS, with no UBM, was incubated, centrifuged and inactivated with 1mM E-64 in parallel.

2.2.4 Biochemical Characterization

Enzymatically digested UBM solutions were electrophoresed on 7.5% polyacrylamide gels under reducing conditions (5% 2-Mercaptoethanol). The proteins were visualized with a silver stain and images recorded by a Kodak imaging station. Collagen and sulfated glycosaminoglycan (S-GAG) content of the UBM gel were determined using the Syrcol™ assay kit and the Blyscan™ assay kit (Biocolor, Northern Ireland). The Blyscan™ assay and the Sircol™ assay were performed according to the manufacturer's instructions. Standard curves were generated using collagen and chondroitin-4-sulfate and used to calculate the total amount of collagen and sGAG present in the digested UBM solutions. Total protein concentrations were determined using the BCA™ Protein Assay (Pierce) by following the manufacturer's instructions. The colorimetric change was measured by the absorbance at 550 nm using a SpectraMax spectrophotometer (Molecular Devices).

2.2.5 Cell Culture

2.2.5.1 Human Aortic Endothelial Cells

HAECs were purchased from Cambrex (CC-2535). HAEC were cultured in EGM-2 medium (Lonza, Walkersville, MD) under a humidified atmosphere in 95% air/5% CO_2.

2.2.5.2 Mouse C2C12 Myoblasts

C2C12 mouse myoblasts were purchased from the American Tissue Culture Collection (ATCC). The C2C12 population was expanded in Dulbecco's modified Eagle medium (DMEM) (Invitrogen Corporation, Grand Island, NY), low bicarbonate, supplemented with 10% calf serum (Hyclone, Logan, UT), and 100 U/ml Penicillin/100 μg/ml Streptomycin (Invitrogen Corporation, Grand Island, NY). C2C12 were culture under a humidified atmosphere in 95% air/5% CO_2.

2.2.5.3 MRL Blastema Cells

MRL blastema cells (MRL) were isolated from the ears of MRL/MpJ mice (Jackson Laboratories, Bar Harbor, Maine). A 2.0 mm hole was punched through the ear of each mouse. The MRL/MpJ mice have been described as having unusual healing/regenerative properties [136]. At the site of the ear hole punch in the MRL/MpJ mice a blastema-like structure forms, and if the cells are allowed to accumulate, differentiate and organize, then the result is ear hole closure and tissue regeneration [137]. At eleven days after creating the ear hole, there was evidence of partial closure and cells were isolated from the healing edge of the defect. Cells were grown in DMEM (Cat. No. D6429, Sigma-Aldrich, St. Louis, MO) supplemented with 10%

FCS, 2 mM glutamine, 100 U/mL penicillin and 100 ug/mL streptomycin. MRL cells express MSX1, THBS, TnC, Thy1, Dlk, TBX5, and Pref-1[138].

2.2.5.4 Human Fetal Cardiomyocytes

Human fetal cardiomyocytes were provided by Dr. Amit Patel and Dr. Jorge Genovese at the University of Pittsburgh. Human hearts were collected from fetuses ranging between 14 – 22 weeks in gestational age, within 1 hour of medically induced termination. Hearts were dissected out and washed 3X in DPBS(-) at 4°C. Hearts were dissected to separate left (LV), right ventricles (RV) and each section (LV, RV) was finely minced in a solution of DPBS(-)/0.01% EDTA and incubated at 4°C for 10 minutes. This was followed by enzymatic digestion in a solution of DPBS(-)/0.01% EDTA containing 1mg/m collagenase 1A and 20units/ml of DNase 1 at 37°C for 30 minutes. After digestion, collagenase activity was neutralized with fetal bovine serum (FBS) at the final concentration of 10%. Undigested tissues and cell clumps were separated by passing the cell suspension through a 100 μm cell strainer and were discarded. Dissociated cells were washed 3X by centrifugation at 400 g for 10 min. Cells were re-suspended in plating medium and plated onto tissue culture dishes. HFCs were cultured in DMEM/F-12 supplemented with 10% FBS and 1% P/S 100 U/ml Penicillin/100 μg/ml Streptomycin under a humidified atmosphere in 95% air/5% CO_2.

2.2.6 Mitogenic Assay

The mitogenic assay was performed on 96-well plates each well receiving $1x10^4$ (C2C12 and HFCs) or $2x10^4$ cells (HAECs). The cells of interest were cultured in the appropriate medium, detached from the culture flask, counted and placed on the 96-well plate. Each well received 200

µl of the stock cell solution at a concentration of 5 x 10^4 cells/ml or 10 x 10^4 cells/ml. The cells were placed at 37ºC in a humidified 95% air/5% CO_2 incubator for 24 hours. After the 24 hour period, the culture medium was aspirated and 200 µl of the appropriate culture medium without growth factors or serum (referred to as base media) was added to each well and the plate was placed in the incubator for 24 hours. The base medium was aspirated and 200 µl of the base media with the enzymatically digested UBM or base media with control solution were added to each well and the plate placed in the incubator for 24 hours. The control solution is the neutralized solution used to digest the ECM but without the ECM powder. After the 24 hours of incubation period, the media was aspirated and 100 µl of base media was added to each well and the ViaLight® Bioassay Kit (Lonza, Allendale, NJ) or the ApoGlow® Rapid Apoptosis Screening Kit (Lonza, Allendale, NJ) were used to determine cell proliferation or apoptosis by following the manufacturer's instruction. The Apopercentage™ (Biocolour, Norther Ireland) assay was used to quantify changes in levels of floppase, an enzyme that modulates externalization of phosphatidylserine (PS). Increases in externalization of PS may be due to apoptosis or differentiation of myoblast into myotubes. Images were taken of representative wells using an inverted microscope.

2.2.7 Chemotactic Assay

Migration of cells towards the UBM degradation products were quantitatively evaluated utilizing the Neuro Probe 48-well micro chemotaxis chamber (Neuro Probe Inc., Gaithersburg, MD). Cells were starved for 14 to 17 hours in base media (media with no added growth factors and 0.5% heat-inactivated fetal calf serum) prior to use. The starved cells were trypsinized, re-suspended in serum free media at a concentration of 6x10^5 cells/mL, and incubated for 1 hour

while in suspension in a humidified 95% air/5% CO_2 37ºC incubator. Polycarbonate PFB chemotaxis filters (Neuro Probe, Gaithersburg, MD) (8 μm pore size for HAECs and HFCs and 12 μm pore size for MRL cells) were coated with 0.05 mg/mL collagen I (BD Biosciences, San Jose, CA). The enzymatically digested UBM was added to the bottom chamber wells, the filter was placed over the bottom chamber, and the apparatus was assembled by following the manufacturer's instructions. Approximately 30,000 cells were then added to each upper chamber well of the apparatus and the chamber was incubated for 3 hours at 37ºC under a humidified atmosphere in 95% air/5% CO_2. Non-migrating cells remaining on the top side of the membrane were removed and migrating cells on the bottom side of the membrane were stained with Diff Quik (Dade AG Liederbach, Germany). Three pre-determined fields were counted from each well at 20X magnification. Fields were pre-determined by location in the well: cells in the top left, top right, and bottom center fields in each well were counted. Each experimental condition was tested in quadruplicate wells and the average number of migrated cells was determined for each condition.

2.2.8 Statistical Analysis

The Student's t-test was used to test the null hypothesis that there was no difference between cell migration toward the enzymatically digested ECM when compared to the corresponding control of 10% FBS. P values ≤ 0.05 were considered significant**.**

2.3 RESULTS

2.3.1 Enzymatic Digestion of UBM

UBM was successfully digested using both pepsin at room temperature (~25°C) and papain at 60°C and 37°C. Each condition yielded a solubilized form of UBM with a different macroscopic appearance and fluidity. Pepsin digested UBM yielded a viscous solution while papain digested UBM (60°C and 37°C) yielded a more "suspension-like" solution. Papain digested UBM at 37°C had a white appearance while papain digested UBM at 60°C and pepsin digested UBM had a "green" color. The visual differences between UBM digests are shown in Figure 2-1. Initial attempts at solubilizing UBM using pepsin showed that lyophilized UBM was more readily digested by pepsin than air dried UBM or hydrated UBM. A successful digestion or solubilization of UBM using pepsin was defined as the presence of a viscous solution with no floating UBM particulate visible by macroscopic inspection. The size of the UBM particle/pieces affected the speed with which pepsin could digest UBM. Air dried UBM cut into small ~1 cm^2 pieces took longer to digest than lyophilized powder and sometimes was not completely solubilized after 48 hours of digestion. Stirring also played a big role in digesting UBM using pepsin. Slow stir was found to digest UBM but particulates were visible by macroscopic inspection after 48 hours. Similar outcomes were found with papain digested UBM although the end product had a different appearance. Even after 72 hours undigested particles were still visible by macroscopic examination and no changes were observed with prolonged digestion times. Papain digested UBM resulted in a "suspension" where large particles precipitated to the bottom of the container if left unstirred. In the case of papain digested UBM, the protocol that used the least amount of papain in the least amount of time (24hours) was used.

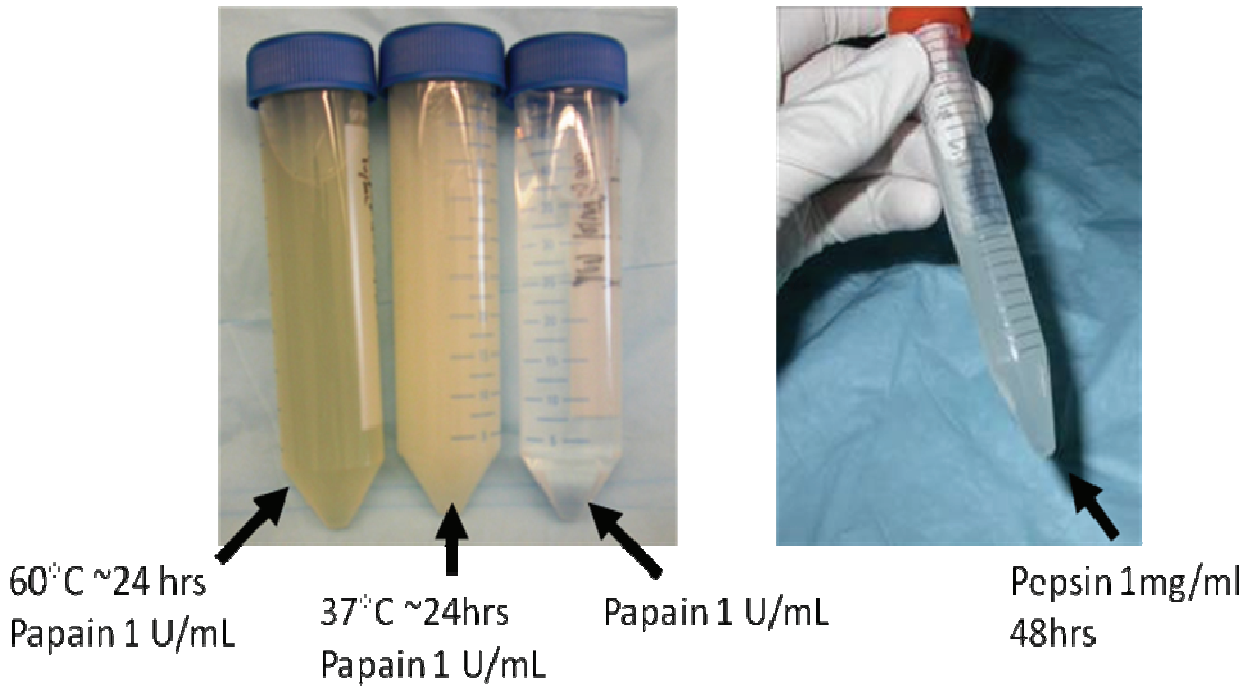

Figure 2-1: Enzymatically digested UBM using papain and pepsin. Macroscopical appearance is markedly different for all methods of digestion. Papain digested UBM at 60°C has a more transparent appearance while UBM digested at 37°C has an off-white color. Pepsin digested UBM is less transparent than papain digested UBM and is more viscous.

2.3.2 Biochemical Characterization

The results for the total protein concentration, collagen content, and sulfated glycosaminoglycans content are summarized in Tables 2-1 and 2-2. The total protein concentration of pepsin digested UBM was based on the initial weight by volume concentration used during the preparation process. Solubilizing UBM using pepsin has a 100% yield since there are no purification steps during its preparation. Digesting UBM using papain requires the separation by centrifugation to

remove large particles of undigested UBM. The centrifugation step greatly reduces the yield of UBM digest obtained using papain (based on total protein content). The total protein yield also varies with the temperature at which the digestion took place. Papain digested UBM at 60°C yields approximately 31% total protein content while UBM digested at 37°C has a yield of 20%. The difference in yield between both papain digests was evident by macroscopical examination during the digestion process.

Pepsin digested UBM showed the greater amount of collagen per initial dry weight of UBM. Papain digested UBM showed significantly lower collagen content when compared to pepsin digested UBM. The opposite finding was true for sGAG. Papain digested UBM showed the highest content of sGAG while pepsin had lower amounts of sGAG per initial weight of UBM. The differences between pepsin and papain digested UBM can also be seen on Figure 2-2. Different protein profiles were observed an all three methods.

Table 2-1: Results from the BCA™, Syrcol™, and Byglascan™ assays measuring the total protein, collagen, and sulfated glycosaminoglycan (sGAG) content in UBM digested with pepsin and papain. Data represent s mean ± SD of three different digestion for each condition (n=3).

Digest	Protein (mg/ml)		Collagen (mg/ml)		sGAG (mg/ml)	
	Mean	± SD	Mean	± SD	Mean	± SD
Upep	10	--	9.184	3.830	0.020	0.016
Upap37	2.031	0.167	0.148	0.048	0.054	0.012
Upap60	3.144	0.109	0.158	0.061	0.046	0.019

Table 2-2: Results from Syrcol® and Byglascan® assays collagen and sulfated glycosaminoglycan content in UBM digested with pepsin and papain. Data represents mean ± SD of three different digestion for each condition (n=3).

	Collagen (mg/mg)		sGAG (µg/mg)	
	Mean	± SD	Mean	± SD
Upep	0.92	0.38	2.00	1.55
Upap37	0.07	0.02	27.20	7.42
Upap60	0.05	0.02	14.76	6.28

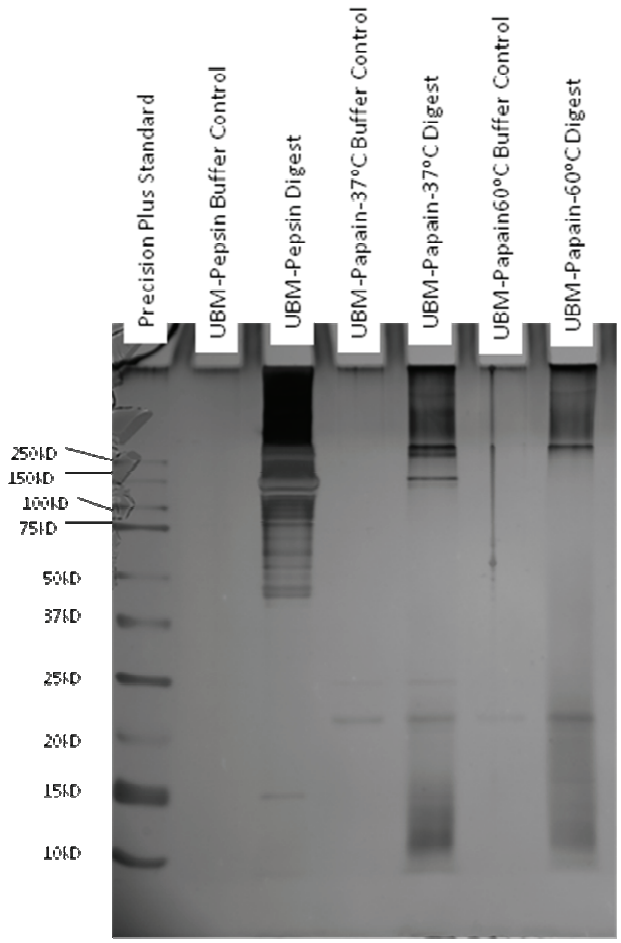

Figure 2-2: Protein gel showing the different profiles between pepsin and papain digested UBM (Courtesy of Janet Reing).

2.3.3 Mitogenic Assay

Results from the mitogenic assay using human aortic endothelial cells (HEACs), C2C12 myoblasts, and human fetal cardiomyocytes (HFCs) are summarized in Figure 2-3. ***Pepsin digested UBM was not included in this set of experiments due to its ability to form a gel under physiological conditions. Formation of a gel on the top surface of the plated cells could affect***

the results due to adhesion of cells to the gel (which is later aspirated) as well as problems with diffusion of nutrients and oxygen. The gel form will be further explored in Chapter 3. All cell types recovered as judged by the increase in cell number when compared to controls after the addition of 10% FBS following the starvation period and showed a 100-200% improvement when compared to cells receiving base media alone. All cell types showed less proliferation of UBM treated groups when compared to 10% FBS. Papain digested UBM at 60°C (Upap60) had no effect upon HAECs and HFCs but showed an increase (~20%) in the number of C2C12 cells. Papain digested UBM at 37°C (Upap37) showed a slight inhibition of HAECs when compared to Upap60. Upap37 also showed an increase in C2C12 and no change in HFCs under the conditions studied.

To further study the effect of starving conditions upon the stimulation of papain digested UBM upon C2C12 cells, cells were starved with either DMEM or DMEM supplemented with 0.5% FBS. The results are shown in Figure 2-4. Only the higher concentrations yielded a significant increase from control (data not shown) and there was a slight increase in cell number if the cells are starved in 0.5% FBS instead of 0% FBS. However, the same trend was observed under both conditions.

The cells undergo a starvation period to arrest cell proliferation. This may lead to undesirable conditions and may drive the cells to undergo apoptosis or to arrested proliferation. To address this question, the levels of ATP and ADP were quantified and the results are shown in Figure 2-5. C2C12 myoblasts were tested using this assay due to their high level of ATP at the concentration of cells used. HAECs yield lower ATP levels when compared to C2C12 cells and due to the low sensitivity to ATP of the ApoGlow™ assay (when compared to the ViaLightT(M) assay) C2C12 were chosen. There was difference in increase of ATP when

compared to controls between UBM digested at 60°C (Upap60) and 37°C (Upap37). There was a change in ADP concentration from controls between Upap60 and Upap37. The ratio of ADP and ATP are shown on the bottom graph on Figure 2-5. There was no change in ADP/ATP ratio between Upap60 and its control. However there was a change in ADP/ATP ratio between Upap37 and its control. The following guidelines are provided by the manufacturer of the ApoGlow™ kit:

1. **Apoptosis:** Lower levels of ATP when compared to controls with an increase in ADP:ATP ratios over control.
2. **Necrosis:** Considerably lower ATP levels than control but increased ADP and ADP:ATP ratios over controls.
3. **Arrested proliferation:** Lower levels of ATP than controls with little or no change in ADP:ATP ratio.
4. **No effect:** Similar or slightly higher levels of ATP without a change in ADP when compared to controls.
5. **Proliferation:** Markedly elevated ATP levels when compared to controls with no significant increase in ADP levels.

The Apopercentage™ assay stains cells with increased floppase activity. The asymmetry of phospholipid composition of the extracellular membrane is maintained by enzymes termed "flippase". Flippase maintains phosphatidyl ethanolamine on the outer leaflet and phosphotidylcholine, sphingomyelin, and phosphatydylserine on the inner leaflet of the extracellular membrane in healthy cells. In apoptotic committed cells, the enzyme floppase (scramblase) overwhelms or inactivates flippase allowing for the expression of phosphatydylserine on the outer leaflet of the extracellular membrane. The switch in position of phosphatydylserine allows for the internalization of the Apopoercentage™ dye. In myoblasts, floppase activity may be related to apoptosis or differentiation into myotubes. After the 24 hours incubation in the presence of FBS, digested UBM, or controls, nearly all C2C12 cells stained

positive regardless of the treatment. The greater cell number on the FBS, UPap60, and Upap37 wells is evident on the images taken from representative wells. Results for C2C12 are summarized in Figure 2-6. HAECs showed greater number of cells on the FBS and media control wells when compared to the UBM treated groups in agreement with the results from the ATP assay. Even though more cells can be found on the FBS treated group based on the ATP assay, a greater number of cells were stained as apoptotic. There was no different after visual inspection of stained cells between digested UBM and the appropriate controls. There was a difference in the absorbance between Upap37 and its control. The greater number of apoptotic cells on the control groups could be due to greater number of cells consistently found on the ATP assay. The results are summarized in Figure 2-7.

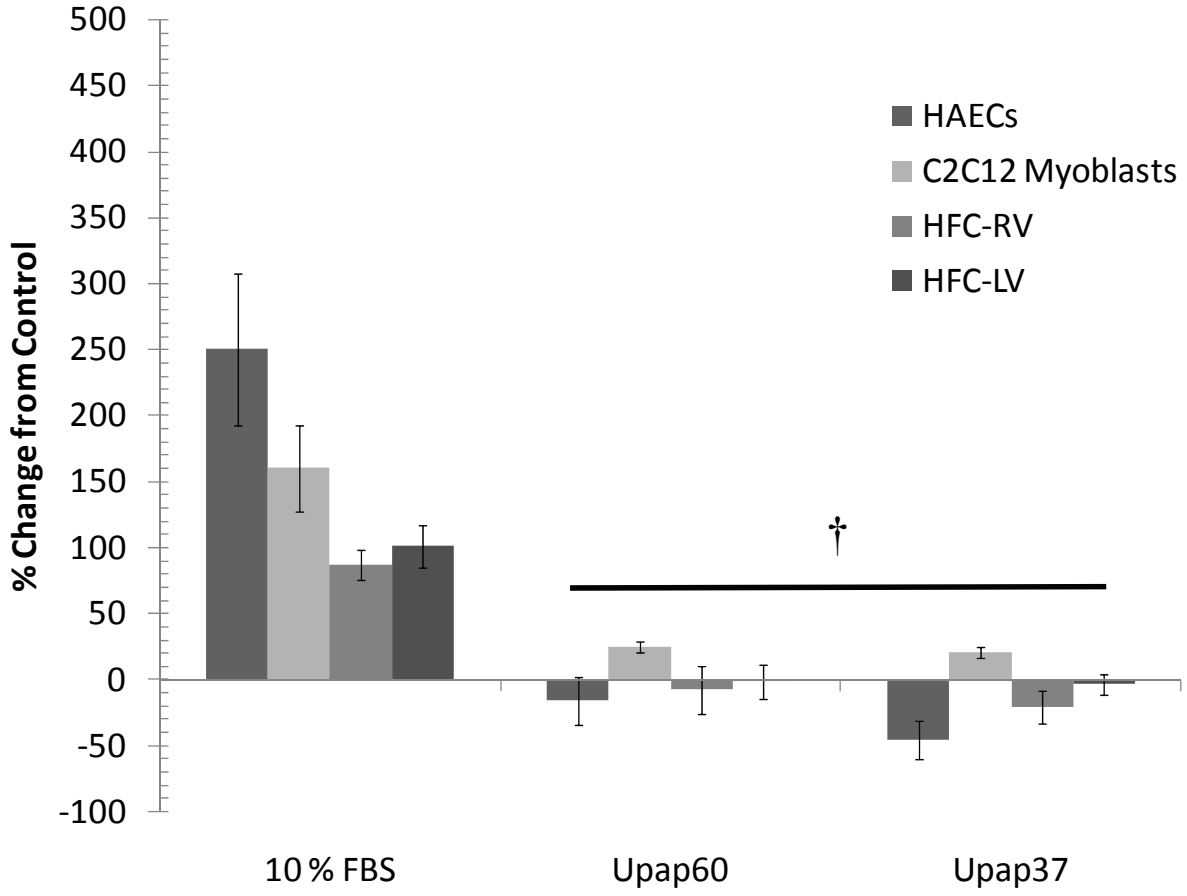

Figure 2-3: Results from the mitogenic assay for human aortic endothelial cells (HAECs), C2C12 myoblasts, and human fetal cardiomyocytes (HFCs). All cell types recovered after the addition of 10% FBS following the starvation period. Upap60 had no effect upon HAECs and HFCs but showed a slight increase in the number of C2C12. Upap37 had a slight inhibitory effect upon HAECs and HFCs and was stimulatory for C2C12 under the conditions studied. Data represents mean ± SE. † Significantly different than 10% FBS. Sample sizes: HAECs (n=6); C2C12 (n=6), HFC-RV (n=3), and HFC-LV (n=3).

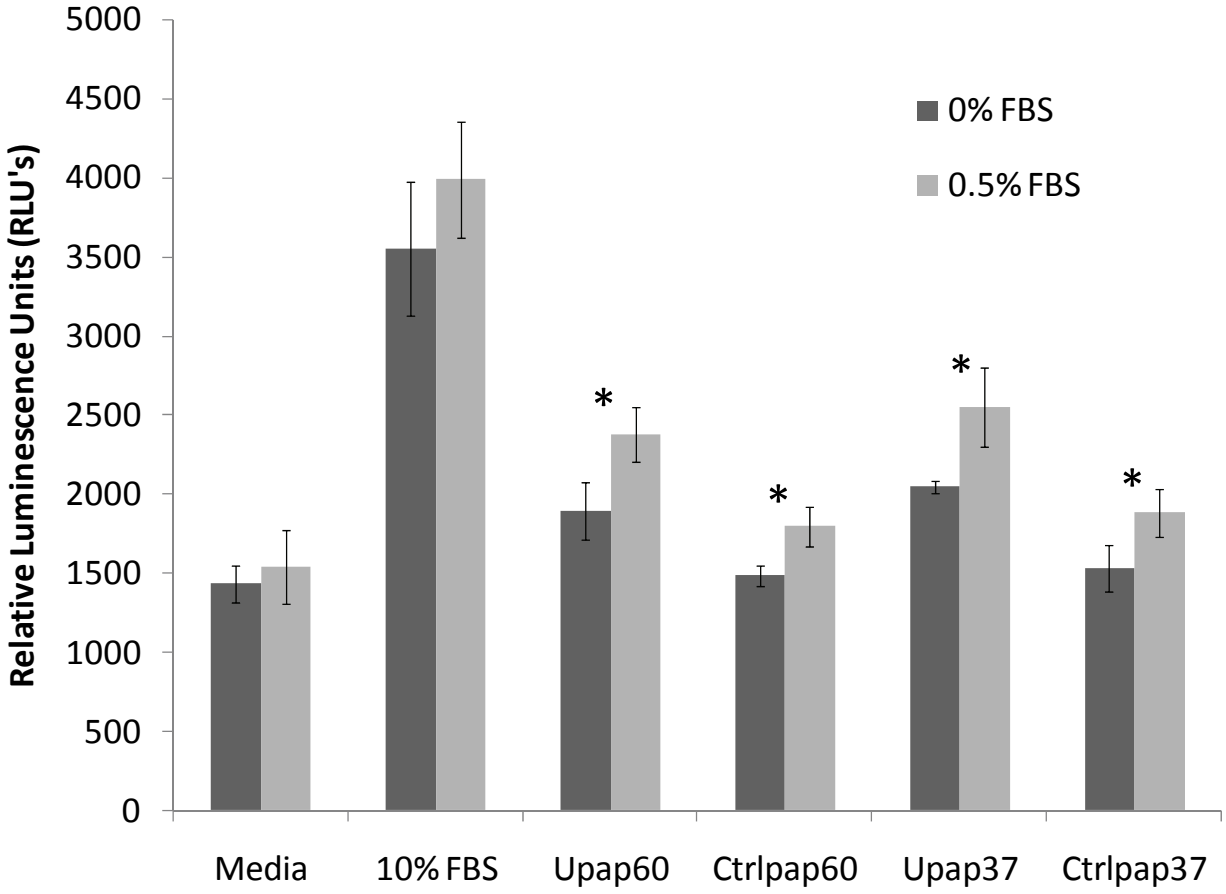

Figure 2-4: Mitogenic assay of C2C12 cells starved on DMEM or DMEM supplemented with 0.5% FBS at different concentrations. All samples showed significant differences with respect to control solutions ($p<0.05$). *Difference between starvation with 0% and 0.5% FBS ($p<0.05$).

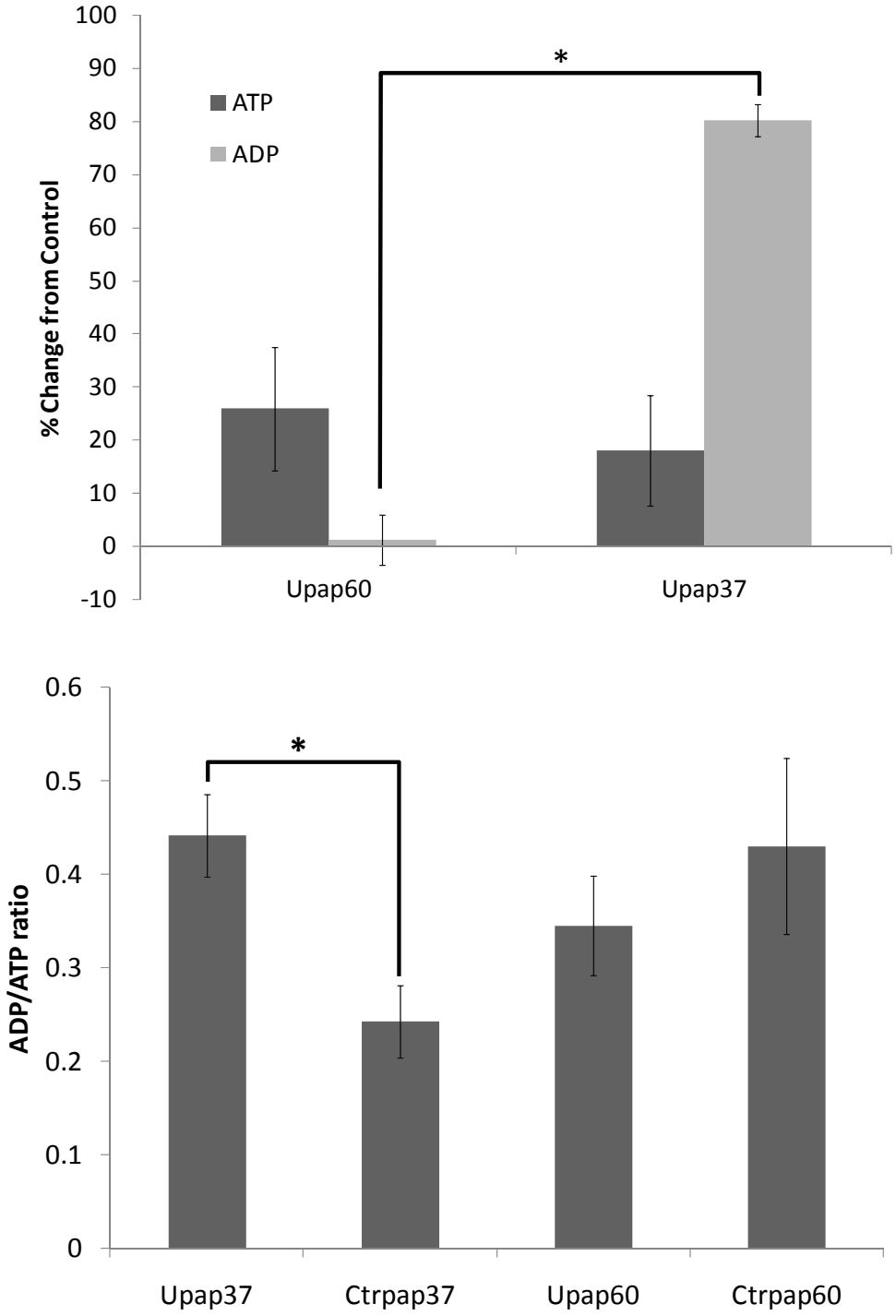

Figure 2-5: Results from the ApoGlow™ assay: Top graph shows the ADP/ATP ratio; Bottom graph shows the percent change of ATP and ADP from control (n=3). Data represents mean ± SD. *p<0.05

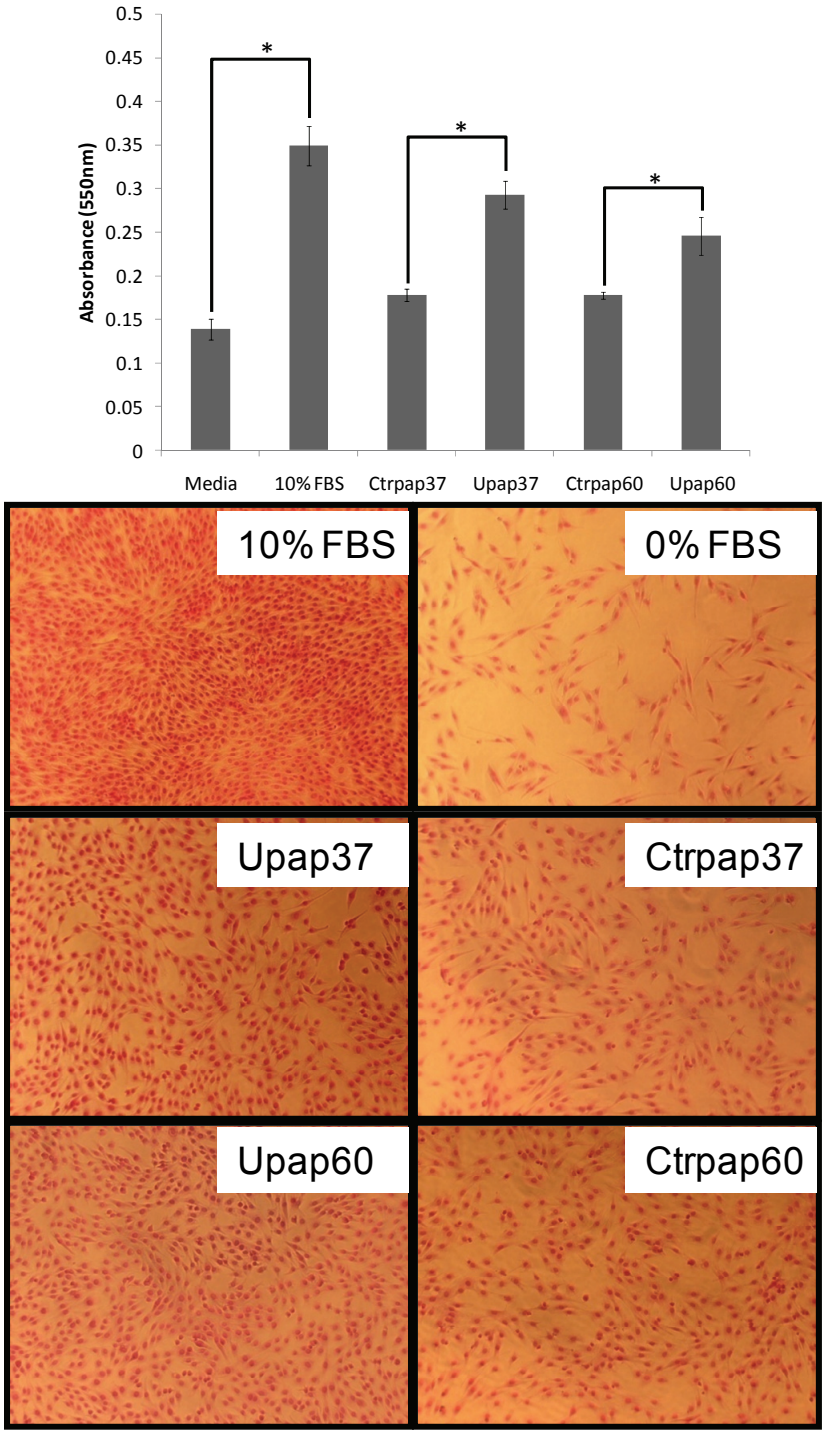

Figure 2-6: (Top) Absorbance of solubilized due; (Bottom) Pictures of C2C12 cells under different conditions. *p<0.05

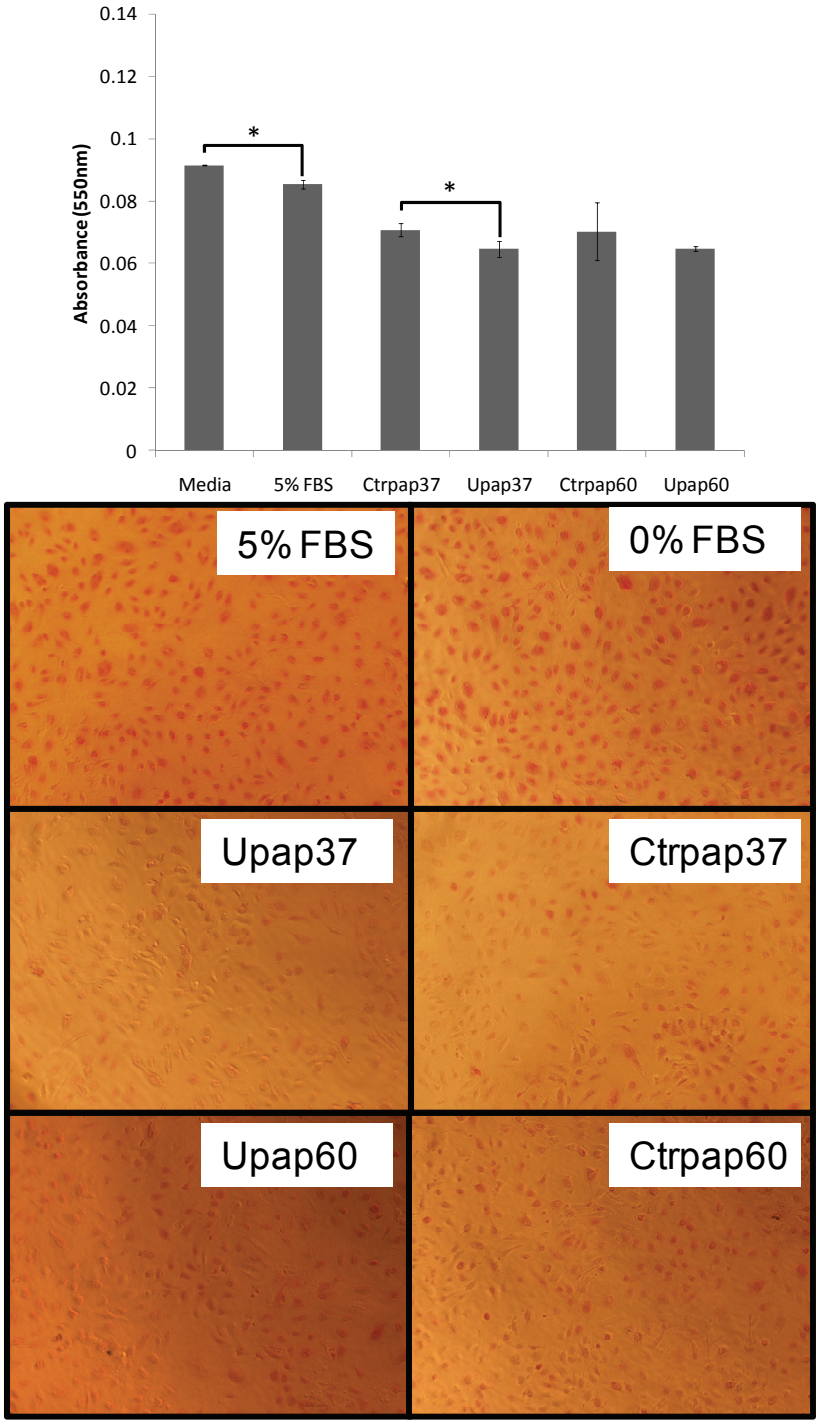

Figure 2-7: (Top) Absorbance of solubilized due; (Bottom) Pictures of HAECs cells under different conditions. *p<0.05

2.3.4 Chemotactic Assay

The results from the chemotactic assay are summarized in Figure 2-8 and Figure 2-9. HAECs migration was inhibited by all three samples of enzymatically digested UBM. There was no significant difference in the inhibition of chemotaxis between pepsin digested UBM and papain digested UBM at 37°C. There was a difference between UBM digested with papain at 37°C and 60°C. There was also a concentration dependent change in migration for pepsin digested UBM and UBM digested with papain at 37°C. ***Due to the limited availability of human fetal cardiomyocytes and MRL blastema cells, only pepsin and papain digested at 37°C were tested.*** MRL blastema cells showed an increase in migration when compared to controls but was less than the migration observed for cells exposed to 10% FBS. There was a dose dependent increase in migration of MRL blastema cells. Interestingly, human fetal cardiomyocytes (HFCs) showed no migration towards 10% FBS but did show migration towards enzymatically digested UBM. No difference was found between HFCs derived from the right and left ventricles. Figure 2-10 summarizes the results for all the cell types tested. All cell types had significantly different migration to pepsin digested UBM and UBM digested with papain at 37°C when compared to 10% FBS. MRL blastema cells and HFCs both showed migration towards enzymatically digested UBM. The results for the chemotactic assay for all cell types tested are summarized in Figure 2-10.

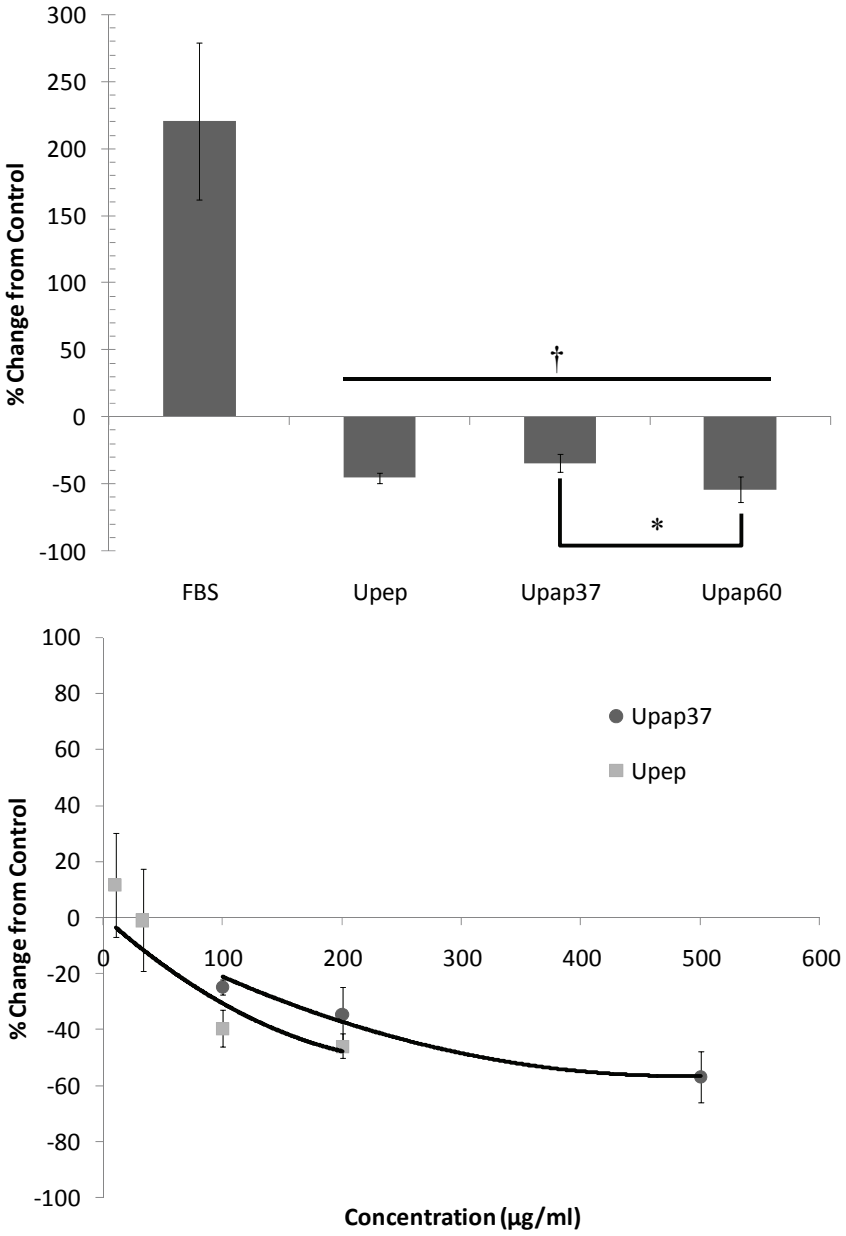

Figure 2-8: Results from the chemotactic assay for human aortic endothelial cells (HAECs): Top graph shows the percent change from control; Bottom graph shows the dose dependent response observed for papain and pepsin digested UBM. Data represents mean ± SE. † Significantly different than 10% FBS. Sample sizes for 200 µg/ml: FBS (n=5), Upep (n=3), Upap37 (n=4), and Upap60 (n=3). *p<0.05

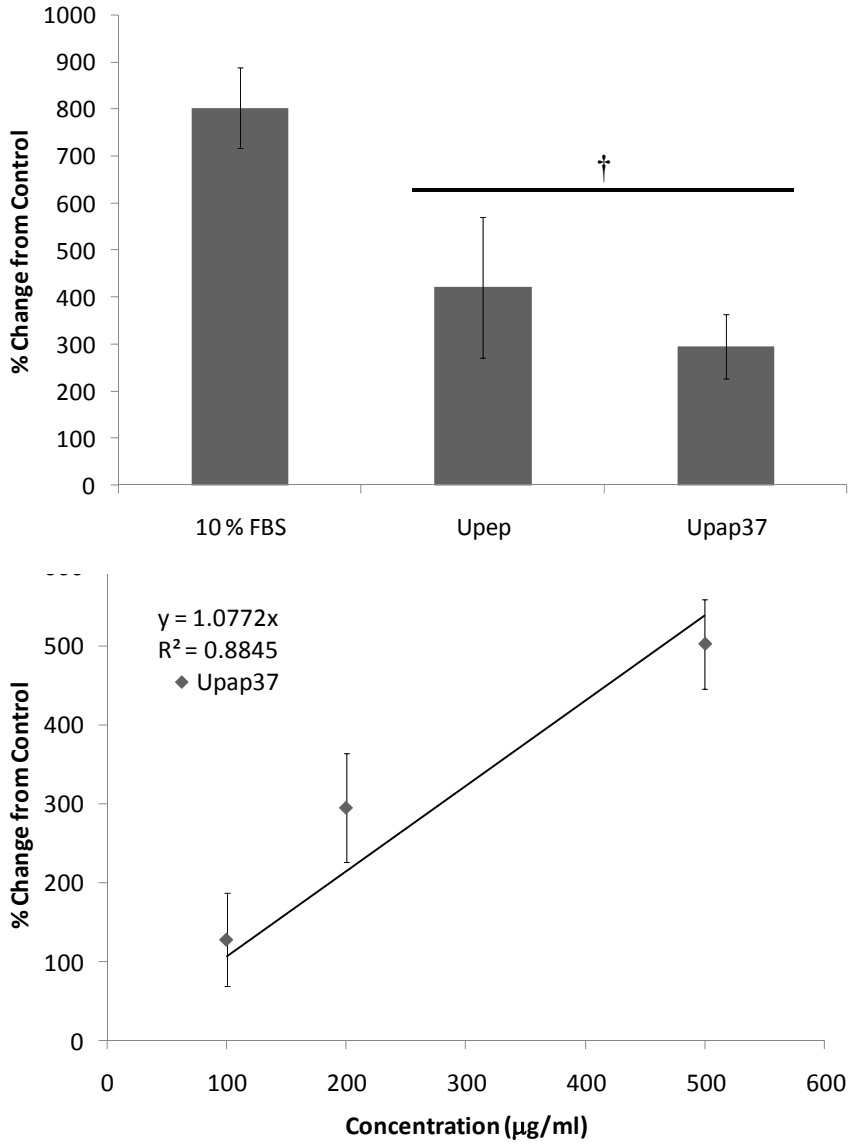

Figure 2-9: Results from the chemotactic assay for MRL blastema cells: Top graph shows the percent change from control; Bottom graph shows the dose dependent response observed for papain digested UBM. Data represents mean ± SE. Sample sizes for 200 µg/ml: FBS (n=3), Upep (n=3), and Upap37 (n=3). *p<0.05

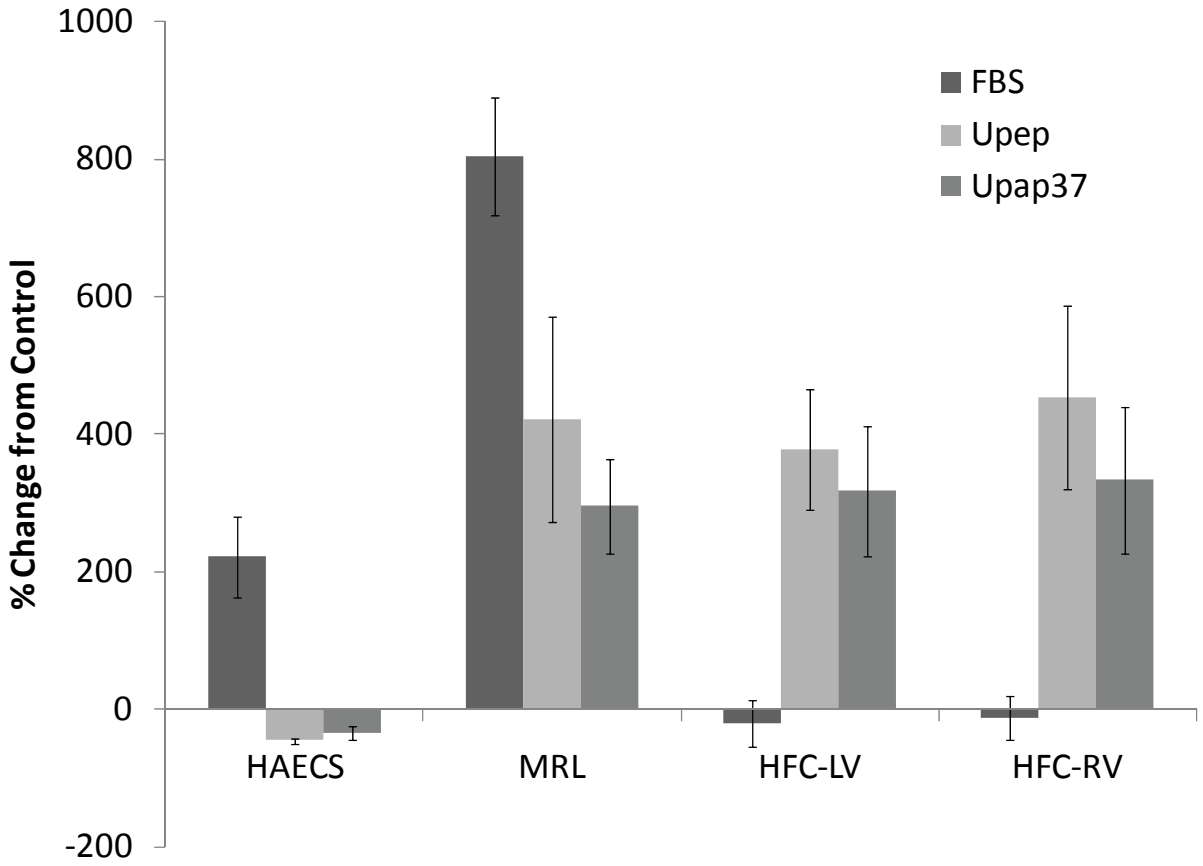

Figure 2-10: Results from the chemotactic assay for human aortic endothelial cells (HAECs), MRL blastema cells (MRL), human fetal cardiomyocytes from the right (HFC-RV) and left ventricles (HFC-LV). Data represents mean ± SE. All values were significantly different than 10% FBS. At least n=3 for all samples tested.

2.4 DISCUSSION

ECM scaffolds have been shown to be bioactive scaffolds capable of inducing constructive remodeling while avoiding scar tissue formation. The typical host tissue response after the implantation of a minimally processed ECM scaffold can be altered to one of encapsulation and fibrous tissue accumulation by chemical cross-linking prior to use suggesting that degradation of the scaffold is necessary for the constructive remodeling to occur [88]. In addition, previous studies have shown that acid digested ECM has anti-microbial and chemotactic properties [13, 15, 16]. The bioactivity observed in ECM scaffolds is most likely due to several factors such as composition, spatial distribution of bioactive molecules, and the combination of inhibitory and stimulatory molecules. However, it is reasonable to expect that solubilized ECM can retain some if not all of its bioactivity during solubilization. In addition, scaffolds can be created that extend beyond the limited two-dimensions found in the native ECM. The present study is the first step towards the solubilization of an ECM scaffold derived from the porcine urinary bladder call urinary bladder matrix (UBM).

Pepsin and papain, both commonly used endopeptidases, were selected to solubilize UBM. Both enzymes have different modes of action and act under different chemical environments. Pepsin is active under acidic pH and is involved in the hydrolysis of peptide bonds of tryptophan, phenylalanine, leucine, tyrosine, and methionine residues. The activity of pepsin is enhanced if the above mentioned amino acids are adjacent to hydrophobic amino acids [39]. Pepsin does not disrupt the helical structure of collagen but does cleave the telopeptides at both ends of the collagen molecule [38]. Pepsin is inactivated at pH values above 6. Papain is a thiol proteinase that hydrolyzes almost any residue but shows preference for arginine and lysine residues. Unlike pepsin, papain is active at a pH of 6 and requires an inhibitor [39]. Previous

studies have used both enzymes to isolate different components of the ECM in tissues [129, 139]. The conditions used in the present study were selected to minimize the use of non-physiologic chemicals and excessive purification steps that could dampen the bioactivity within the degraded ECM or that could become detrimental if incorporated into an implantable device.

A higher amount of collagen was found within pepsin solubilized UBM when compared to papain digested UBM at both 60°C and 37°C. This finding can be explained by the pH at which the digestion took place. UBM digested with pepsin was placed under acidic conditions (pH ~ 2). Collagen molecules are soluble under acidic conditions. The resulting digest was viscous and upon restoring the pH to 7.4 and the ionic strength to physiological levels, a gel formed. This further supports the presence of collagen in the pepsin solubilized ECM will be discussed in Chapter 3 and Chapter 4. Papain digests were performed at a physiological pH and under isotonic salt concentrations. These conditions might have precipitated the collagen molecules which were subsequently removed during the centrifugation step and thus resulting in lower collagen content. The pH of the solution, proteins present during the digestion process, and ionic strength of the solution may also contribute to the higher amounts of sulfated glycosaminoglycans in papain digested UBM when compared to pepsin digested UBM.

Papain digested UBM had little effect upon the proliferation of human aortic endothelial cells (HAECs). Enzymatically digested UBM was also found to have inhibitory effects upon the migration of HAECs. The inhibition of migration was dose dependent and was independent of the method used to digest the ECM. Akalu et al. have shown that a cryptic epitope (STQNASLLSLTV or STQ-peptide) present in denatured laminin, exposed after exposure to MMPs and elastase, inhibits the migration and proliferation of human umbilical vein endothelial cells (HUVECs) [140]. Laminin is a component of the basement membrane of tissues and a

component the UBM scaffold [141]. Other proteolytic degradation products from ECM molecules that inhibit angiogenesis have been reported from collagen type XVIII (Endostatin), Collagen type IV (arresten, canstatin, tumstatin, metastatin), collagen type VIII (vestatin), collagen XV (restin), fibronectin (anastellin), perlecan (endorepellin), and histidine-rich glycoprotein (HGRP) [36]. Fragments such as the ones mentioned above may be generated during the digestion of UBM and may help explain the inhibition of migration and proliferation of HAECs. Characterization of the fragments, proteins, and molecules generated from digested UBM will be the focus of future studies.

Opposite results from those seen with endothelial cells were found with progenitor like cells. Papain digested UBM showed an increase in the number of C2C12 cells when compared to controls in the mitogenic assay. There was also an increase in the activity of floppase which may suggest apoptosis or may also suggest differentiation of the C2C12 myoblasts into myotubes as a result of serum deprivation. Floppase plays a role in the externalization of phosphatidylserine (PS) which is found on non-apoptotic C2C12 cells as well [142-144]. MRL blastema cells were stimulated in the chemotaxis assays by both papain and pepsin digested UBM. HFCs were stimulated to migrate but not proliferate by pepsin and papain digested UBM. The consistency of the results between papain and pepsin digested UBM suggests that the component responsible for the stimulation and/or inhibition of migration and proliferation observed may be present in digested UBM regardless of the enzyme used. Alternatively, different inhibitory molecules or fragments may be generated by each method. Since the exact composition of UBM is unknown and the nature of the fragments and their activity is unidentified, it is difficult to speculate as to what is the mechanism responsible for the effects of digested UBM upon HAECs, C2C12, HFCs, and MRL blastema cells. No cause-effect can be

established from these experiments but the general notion that progenitor-like cells are attracted to and stimulated by degradation products of ECM scaffolds is supported by the presence of progenitor cells during *in vivo* remodeling [10]. Further *in vivo* studies will be needed to fully address this hypothesis and to correlate the results presented here with the constructive remodeling observed *in vivo*.

Since the final goal of this work is to combine the solubilized ECM with a synthetic component to create a hybrid scaffold for cardiac repair, the chemotactic property of enzymatically digested UBM upon HAECs, MRL blastema cells, and HFCs was compared. Papain and pepsin digested UBM stimulated the migration of MRL and HFCs but inhibited HAECs. This finding is consistent with previous studies that found inhibition of endothelial cells but stimulation of progenitor-like cells [138]. For cardiac tissue repair, recruitment of progenitor or stem cells either from circulation (bone marrow derived) or from adjacent tissue (cardiac or adipose stem cells) may be more beneficial during the initial stages of the remodeling process. However, chemotactic effects dependent upon the presence of ECM degradation products within the implant location is subject to the plasma proteins deposited on the scaffold and on the effects of molecules secreted by the cells deposited by circulation or migrating from adjacent tissue immediately following implantation. No clear benefit was found between papain and pepsin digestion. Pepsin digested UBM may represent a better choice as a component of a hybrid scaffold because it retains all of the constituents (digested or un-digested) present in the native UBM. The advantage of one form of digested UBM versus another will have to be addressed by *in vivo* studies.

2.5 LIMITATIONS AND FUTURE WORK

The work presented describes and characterizes the enzymatic digestion of a biologic scaffold derived from the ECM of porcine urinary bladders. Pepsin and papain were used to digest the UBM scaffold using the least amount of enzyme and avoiding excessive purification steps. The present work did not characterize the presence and activity of any growth factors or peptides generated during the digestion process. Although the focus of the work was to screen the different digests for mitogenic and chemotactic activity, future work should confirm the results presented herein by other methods such as staining for proliferation markers. *In vivo* studies will also be needed to determine if there is a clear difference between the different methods of digestion. The host tissue response is a complex mixture of events that involve the participation of circulating and surrounding cells and cannot be predicted by any *in vitro* assay alone. However, the present study represents the first steps towards creating soluble form of the UBM scaffold that can be used in mitogenic and migration assays providing clues to explain how the scaffold may exert its bio-inductive effects *in vivo*. The present work also provides a scaffold that may be used as an injectable or topical agent for tissue engineering and regenerative medicine applications.

3.0 PREPARATION AND CHARACTERIZATION OF A GEL FORM OF UBM

3.1 BACKGROUND

Biologic Scaffolds composed of extracellular matrix (ECM) have been used for the repair of a variety of tissues including the lower urinary tract [1, 2], esophagus [3, 4], myocardium [5-7], and musculotendinous [8-10] tissues, often leading to tissue-specific constructive remodeling with minimal or no scar tissue formation. These biologic scaffolds are typically prepared by decellularization of intact tissues or organs and are composed of the structural and functional molecules that characterize the native tissue ECM such as collagen, laminin, fibronectin, growth factors, glycosaminoglycans, glycoproteins, and proteoglycans [4, 12, 13]. As stated in the previous chapter, the resulting decellularized ECM is usually characterized by a two-dimensional sheet with limited ability to conform to irregular three-dimensional shapes and sizes. Therefore, the clinical utility of an ECM biologic scaffold for many clinical applications is typically restricted to topical administration or to invasive surgical procedures that can accommodate variations of the two dimensional sheet form.

UBM has been previously investigated in pre-clinical studies as a biologic scaffold for the reconstruction of damaged laryngeal tissue[66], for the reconstruction of esophageal tissue [68, 145], as a treatment for urinary incontinence [2], and as a myocardial patch [6, 7, 113] with promising results. Suspensions made from a particulate (powdered) form of lyophilized UBM

have been successfully used as an injectable scaffold for the treatment of urinary incontinence in pre-clinical studies [2] but the needle size required to accommodate the particle size was prohibitive for most clinical applications and substances such as glycerin were required to increase the viscosity of the solution.

A soluble form that can be induced to polymerize into a gel could expand the clinical utility of ECM biologic scaffolds. ECM gels with appropriate viscosities could be delivered via minimally invasive surgical techniques with the ability to conform to three-dimensional spaces after injection. Ideally this soluble form would retain the bioactivity of the ECM scaffold and its preparation would minimize or avoid purification steps that could remove growth factors and low molecular weight peptides present in the native ECM. Previous studies have described a gel form of an ECM derived from the small intestine but the preparation required an aggressive purification process that may have resulted in the loss of bioactive molecules, and the rheological properties of the gel were not determined [129]. Gels have been formed from individual components of the ECM such as collagen and from the secreted products of cell lines (Matrigel™). Matrigel™ is not used therapeutically due to its source (tumor cell line), and individual ECM components lack the bioactivity found in minimally processed ECM scaffolds in which structural and functional molecules are present in physiologically relevant amounts.

The long term objective of this work was to develop a gel form of the UBM-ECM scaffold that retains the bioactivity and ability to promote constructive tissue remodeling; properties that are characteristic of the 2-D sheet form of UBM-ECM. The present study is the first step towards this goal and describes a method to solubilize UBM-ECM without purification steps and a method to induce the self-assembly of the soluble UBM-ECM under physiological

conditions. The present study characterizes the gelation kinetics, the rheological properties, and the static *in vitro* cytocompatibility of the UBM-ECM gel.

3.2 METHODS

3.2.1 Preparation of UBM

The preparation of UBM has been previously described (Section 2.2.1) [69]. Briefly, porcine urinary bladders were harvested from 6-month-old 108-118 kg pigs immediately following euthanasia. The tunica serosa, tunica muscularis externa, the tunica submucosa, and majority of the tunica muscularis mucosa were mechanically removed. The urothelial cells of the tunica mucosa were dissociated from the luminal surface by soaking the tissue in 1.0 N saline solution. UBM sheets were placed in a solution containing 0.1% (v/v) peracetic acid (Sigma), 4% (v/v) ethanol (Sigma), and 95.9% (v/v) sterile water for two hours. Peracetic acid residue was then removed with two 15 minute phosphate-buffered saline (pH=7.4) washes, followed by two washes with sterile water for 15 minutes each. The decellularized UBM sheets were then lyophilized using a FTS Systems Bulk Freeze Dryer Model 8-54 and comminuted to a particulate form using a Wiley Mini Mill (Figure 3-1).

3.2.2 ECM Digestion

One gram of lyophilized ECM powder (Figure 3-1) and 100 mg of pepsin (Sigma, ~2,000-2,300 Units/mg) were mixed in 100 mL of 0.01 M HCl and kept at a constant stir for ~48 hours at room temperature (25ºC). The resultant viscous solution of digested UBM or pre-gel solution had a pH of approximately 3.0-4.0 (Figure 3-1). The activity of pepsin was irreversibly inactivated when the pH was raised to 7.4 (see section 3.2.4).

3.2.3 Biochemical Characterization

ECM and rat-tail collagen type I (BD, Biosciences) solutions were electrophoresed on 7.5% polyacrylamide gels under reducing conditions (5% 2-Mercaptoethanol). The proteins were visualized with Gel-Code Blue (Bio-Rad), and images recorded by a Kodak imaging station. Collagen and sulfated glycosaminoglycan (S-GAG) content of the UBM gel were determined using the hydroxyproline assay [146] and the Blyscan™ assay kit (Biocolor, Northern Ireland), respectively. The Blyscan™ assay was performed according to the manufacturer's instructions. The hydroxyproline content was determined by hydrolyzing the samples with 2 M NaOH (100 µl total volume) in an autoclave at 120ºC for 20 minutes. The samples were neutralized with 50 µl of 4 M HCl and reacted with 300 µl of 0.056 M chloramine-T (Spectrum), mixed gently, and allowed to oxidize for 25 minutes at room temperature. The samples were then mixed with 300 µl of 1 M Ehrlich's aldehyde (Spectrum) and incubated at 65ºC for 20 minutes. A standard curve was generated using rat-tail collagen type I (BD Biosciences) and used to calculate the total amount of collagen present in the digested UBM solutions. The colorimetric change was

determined by the absorbance at 550 nm using a SpectraMax spectrophotometer (Molecular Devices). Three different batches of UBM were tested (n=3).

3.2.4 Gelation Kinetics of UBM

UBM and rat-tail collagen type I gels were formed by mixing 0.1 N NaOH (1/10 of the volume of pre-gel solution) and 10X PBS pH 7.4 (1/9 of the volume of pre-gel solution) at 4°C. The solution was brought to the desired volume/concentration using cold (4°C) 1X PBS pH 7.4 and placed at 37°C for gelation to occur. Collagen and UBM gels are shown in Figure 3-1.

Turbidimetric gelation kinetics was determined spectrophotometrically as previously described [147]. Final gel solutions were kept at 4°C and transferred to a cold 96 well plate by placing 100 µl per well in triplicate. The SpectraMax spectrophotometer (Molecular Devices) was pre-heated to 37°C, the plate placed in the spectrophotometer, and the turbidity of each well was measured at 405 nm or 570 nm every 2 minutes for 1.5 hours. The absorbance values for each well were recorded and averaged. Three individual tests were performed on the same batch of collagen type I (n=3) and five (n=5) individual tests were performed on different batches of the UBM gel. Concentration dependent changes in gelation kinetic parameters and turbidity was performed at 570 nm and results represent one batch of UBM digest in triplicates. Each individual test was conducted in triplicates and averaged. The time needed to reach 50% of the maximum turbidity measurement (e.g. maximum absorbance value) was defined as $t_{1/2}$ and the lag phase (t_{lag}) was calculated by extrapolating the linear portion of the curve (see Figure 3-5). The speed (S) of the gelation based on turbidimetric measurements was determined by calculating the maximum slope of the growth portion of the curve as shown in Figure 3-5.

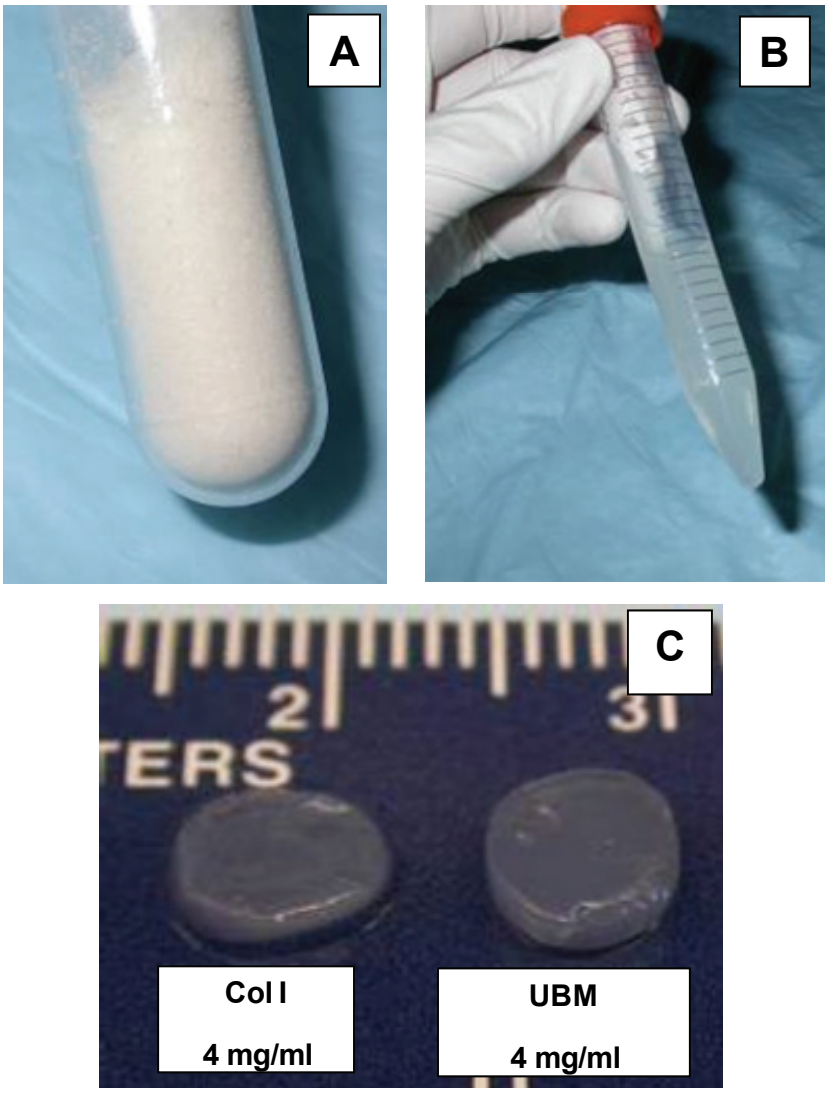

Figure 3-1: (A) Lyophilized UBM powder; (B) Pepsin digested UBM at a concentration of 10 mg/ml; (C) Collagen type I and UBM gels.

3.2.5 Rheological Characterization of UBM Gels

The sample was subjected to an oscillatory strain of:

$$\gamma(t) = \gamma_0 \cos(2\pi f t) \tag{1}$$

where γ_0 was the amplitude of the sinusoidal strain, t was the time, and f was the frequency. The sample developed a sinusoidal stress described as follow:

$$\sigma(t) = \left|G^*\right| \gamma(t) \tag{2}$$

where G* was the frequency dependent complex modulus of the sample. The real part of G*, denoted G′, was in phase with the applied strain and was called the storage modulus since it corresponded to storage of mechanical energy in the elastic deformation of the sample. The imaginary portion of G*, denoted G", was 90° out of phase with the applied strain and was called the loss modulus since it corresponded to the loss of energy by viscous dissipation within the sample. Since the sample was expected to develop solid-like characteristics as gelation proceeds, G' was expected to increase significantly.

A final property of interest was the magnitude of the complex viscosity defined as follows:

$$\left|\eta^*\right| = \frac{\left|G^*\right|}{2\pi f} = \frac{\sqrt{G'^2 + G''^2}}{2\pi f} \tag{3}$$

where $\left|\eta^*\right|$ was the frequency dependent complex viscosity, G* was the frequency dependent complex modulus, and f was the frequency. It is common to fit complex viscosity vs frequency data to a power-law of the form where k and n are both constants:

$$\left|\eta^*\right| = k \cdot f^{-n} \tag{4}$$

Rheological experiments were performed with a TA Instruments AR2000 stress-controlled rheometer using a 40 mm (diameter) parallel plate geometry and a Peltier cell to maintain the sample temperature. The samples were prepared as discussed earlier and loaded into the rheometer with the Peltier cell maintaining a temperature of 15°C. The sample edge was protected from evaporation by applying mineral oil. The temperature was then set to 37°C to induce gelation; the Peltier cell typically reached a temperature of 30°C within 10 seconds and 37°C within 50 seconds. During this increase in temperature and the subsequent gelation, the oscillatory moduli of the sample were monitored continuously at a fixed frequency of 0.159 Hz (1 rad/s) and a strain of 5%. When there was no further change in the elastic modulus (G') with time, gelation was deemed to be complete. The final linear viscoelastic properties of the gel were measured by performing a frequency sweep between 15.9 Hz (100 rad/s) and 0.08 Hz (0.5 rad/s) at 37°C and 5% strain and fitted to equation 4. The gels were then subjected to a strain sweep at 1 rad/s by increasing the strain by 50% and measuring the stress developed. A summary of the rheological testing protocol is depicted in Figure 3-2.

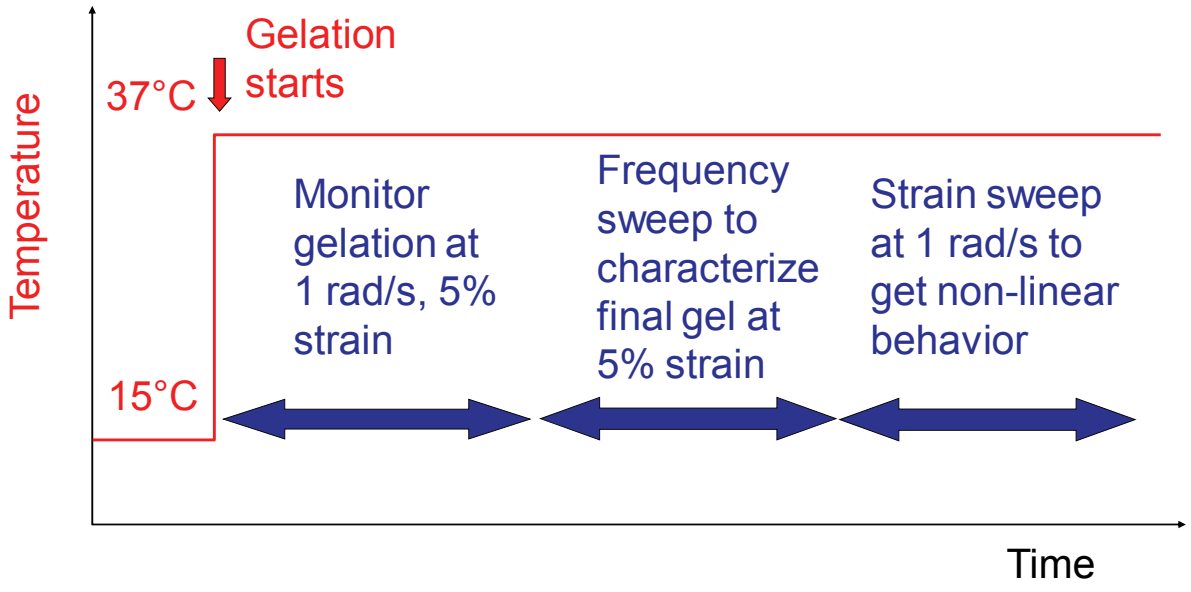

Figure 3-2: Rheological testing scheme used to characterize the UBM gels.

3.2.6 Cell Culture

Vascular smooth muscle cells (rSMCs) and chick embryonic cardiomyocytes (CECs) were harvested as previously described [148]. rSMCs were harvested from rat aortas [148] and expanded in Dulbecco's modified Eagle medium (DMEM) (Invitrogen Corporation, Grand Island, NY) with low bicarbonate and supplemented with 10% fetal bovine serum (FBS) (Hyclone, Logan, UT) and 100 U/ml Penicillin/100 µg/ml Streptomycin (Invitrogen Corporation, Grand Island, NY).

CECs were provided by Dr. Kimimasa Tobita and Dr. Bradley Keller. Briefly, CECs were harvested from fertile White Leghorn chicken eggs at the Hamburger-Hamilton (HH) stage 31 (corresponding to the developmental stage of a 6 week old embryo) and expanded in DMEM with 10% FBS, 1% chick embryo extract, and 100 U/ml Penicillin/100 µg/ml Streptomycin [149].

C2C12 mouse myoblasts were purchased from the American Tissue Culture Collection (ATCC). The C2C12 population was expanded in, low bicarbonate, supplemented with FBS 10% calf serum, and 100 U/ml Penicillin/100 μg/ml Streptomycin. HAEC were cultured in EGM-2 medium (Lonza, Walkersville, MD).

Human fetal cardiomyocytes (HFCs) were harvested as described in Section 2.2.5. Briefly, human hearts were collected from fetuses ranging 14 weeks in gestational age, within 1 hour of medically induced termination. HFCs were cultured in DMEM/F-12 supplemented with 10% FBS and 1% P/S 100 U/ml Penicillin/100 μg/ml Streptomycin. All cells were cultured under a humidified atmosphere in 95% air/5% CO_2.

3.2.7 Proliferation Assay

The 48-hour proliferation of rSMCs, C2C12, HAECs, and HFCs was measured by seeding the surface of 6 mm disks of collagen type I and UBM gels in triplicate. The collagen and UBM gels were prepared by adding 100 μl of the gel (3 mg/ml) into wells of 96 well plates. rSMCs and HAECs were seeded onto the surface of the gels at a density of 2 x 10^4 cells per well. C2C12 and HFCs were seeded onto the surface of the gels at a density of 1 x 10^4 cells per well. In the case of rSMCs, 6 mm lyophilized UBM scaffolds were seeded as well. The number of cells seeded was chosen based on pilot studies that determined the optimum cell concentration that did not reach confluency during the test period but also allowed for accurate detection of the number of cells. A well with a 6 mm lyophilized UBM disk and wells with each type of gel incubated with media without cells served as controls. After 48 hours in culture, non-adherent cells were aspirated and the activity of the attached cells was quantified using the MTT assay

(Sigma-Aldrich, St. Louis, MO) in the case of rSMCs and with the ViaLight® Plus Bioassay Kit (Lonza, Allandale, NJ) in the case of HFCs, HAECs, and C2C12 cells.

3.2.8 Histological Evaluation

Growth of rSMCs, C2C12 cells, and HFC on UBM gels was evaluated by histological methods. Disks of UBM gel were made using a stainless steel ring (1.5 cm in diameter) as a mold. The cells were seeded on the top surface of the gel at a density of 0.5 x 10^6 cells/cm^2. Media was changed every other day and the cells were allowed to grow for 7 days. The samples where then fixed with 10% buffered formalin and sections stained using Masson's Trichrome stain or hematoxylin and eosin (H & E) stain.

CECs (1-2x10^5 cells) were seeded on 1.5 cm diameter discs of collagen (3 mg/ml) and UBM (6 mg/ml) gels. Pictures were taken 24 and 36 hours after seeding using an inverted microscope using phase contrast. CECs 1.5 cm disc constructs were prepared by mixing buffered UBM pre-gel with equal parts of media containing the desired number of gels and pouring the solution into stainless steel rings. The solution was allowed to polymerize and media was added to the dish containing the gel to allow the gel to freely float in the solution. Media was changed every two days.

The preparation of the CECs constructs has been previously described [149] and the constructs were prepared by Dr. Bradley Keller's and Dr. Kimimasa Tobita's laboratory. Briefly, cells suspended on medium were mixed with neutralized UBM (approximately 200 μl) solution and poured into a 20 x 2 mm (length x width) cylindrical loading post (Tissue Train and FX-4000TT). Both ends of the constructs were fixed during polymerization in a 37°C incubator. After polymerization, the construct was allowed to float in growth medium. CECs were fixed I

4% paraformaldehyde-PBS for 15 minutes and embedded in a 13% polyacrylamide gel. Sections measuring 150 μm were cut using a standard vibrating microtome (Vibratome-100, Vibratome.com, St. Louis, MO) and the CECs were identified with α-actinin (EA-53, Sigma-Aldrich, St. Loui, MO) and nuclear stain (DAPI) and then imaged using a laser confocal microscope system (FV500, Olympus, Tokyo).

3.2.9 Scanning Electron Microscopy

The surface morphology of the UBM gels was examined using scanning electron microscopy (SEM). The specimens were fixed in cold 2.5% glutaraldehyde and rinsed in PBS, followed by a dehydration process through a graded series of ethanol (30% to 100%), and finally critically point dried in an Emscope CPD 750 critical point dryer. The samples were attached to aluminum SEM specimen mounting stubs (Electron Microscopy Sciences) and sputter coated with a gold palladium alloy using a Sputter Coater 108 Auto (Cressington Scientific Instruments). Finally, samples were examined using a scanning electron microscope (JEOL 6330F). Images were taken at a 5,000 and 10,000 X magnification.

3.2.10 Statistical Analysis

A Student t-test was used to determine significant differences between mean values of the gelation constants and the proliferation values between lyophilized UBM and UBM and collagen gels ($p<0.05$). The linear relationship between complex viscosity and frequency was determined

using a least square fit method. ANOVA was used to determine significance between mean values of the *in vitro* growth of cells on the surface of the gels (α=0.05).

3.3 RESULTS

3.3.1 Biochemical Characterization

The collagen concentration for pepsin digested UBM was 0.8 ± 0.2 mg per mg of dry lyophilized UBM powder (mean ± SD). The total S-GAG content was 7.6 ± 2.8 μg per mg of dry lyophilized UBM powder (mean ± SD). The electrophoresed solutions of UBM and purified collagen type I showed bands at similar locations confirming a large collagen type I component of UBM. UBM showed additional protein bands that were distinct from the purified collagen type I as shown in Figure 3-3. Scanning electron microscopy showed a fibrillar appearance of the UBM gels at concentrations of 3 mg/ml and 6 mg/ml (Figure 3-4).

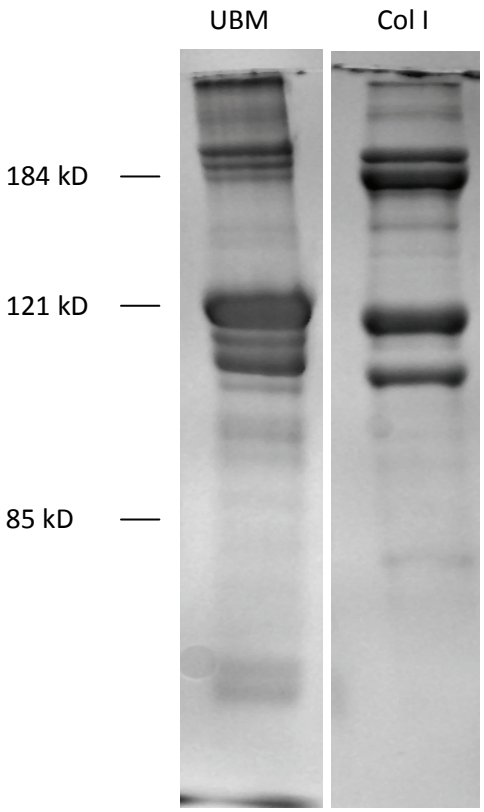

Figure 3-3: Protein gel (7.5% polyacrylamide) of collagen type I and UBM.

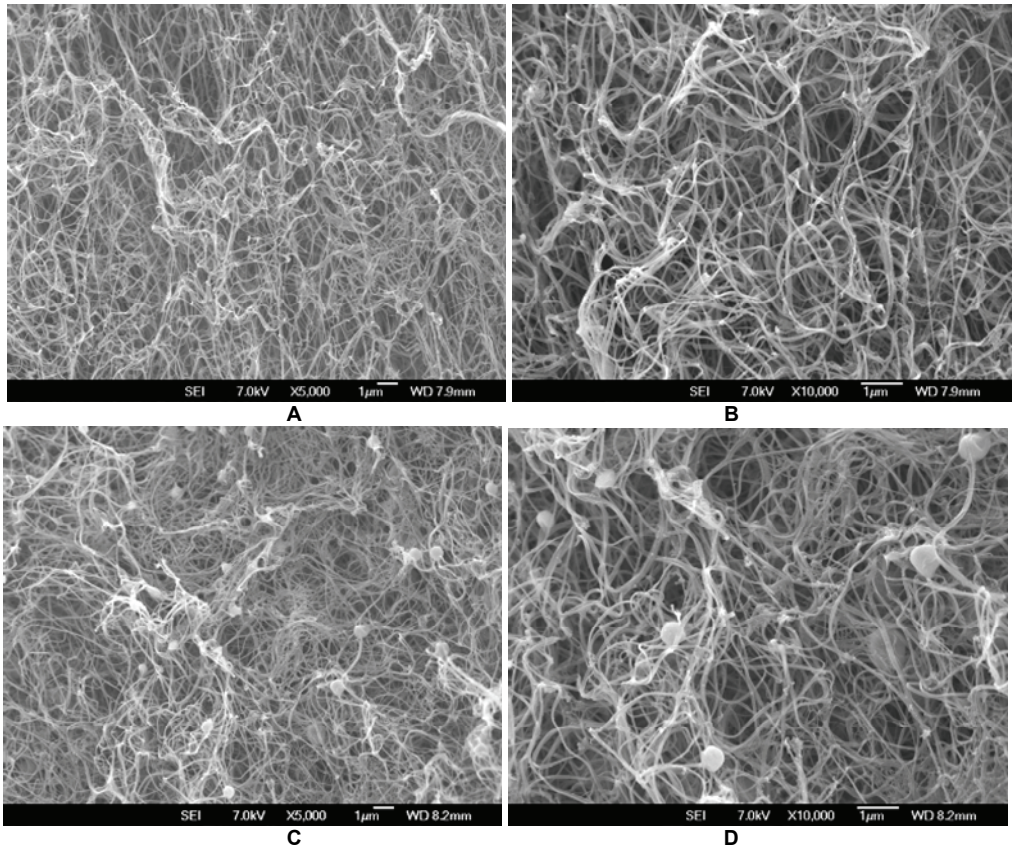

Figure 3-4: Scanning electron micrograph of UBM gels: (A) 3 mg/ml at 5,000X; (B) 3 mg/ml at 10,000x; (C) 6 mg/ml at 5,000x; (D) 6 mg/ml at 10,000x.

3.3.2 Turbidimetric Gelation Kinetics

The turbidimetric gelation kinetics and the calculated parameters are shown in Figure 3-5 and the results presented in Table 3-1. The turbidimetric gelation kinetics for UBM and collagen type I gels showed a sigmoidal shape (Figure 3-5). Collagen type I gels at a concentration of 3 mg/ml became more turbid following gelation than UBM gels at a concentration of 3 mg/ml and 6 mg/ml (Figure 3-5 and Figure 3-6). The lag phase (t_{lag}) and the time required to reach half the final turbidity ($t_{1/2}$) were greater in the UBM gels (at 3 and 6 mg/ml) than collagen type I gels (3 mg/ml). In addition, the speed of the turbidimetric gelation kinetics (S) was less for UBM when compared to collagen type I. There was no change in t_{lag}, $t_{1/2}$, and S between 3 mg/ml and 6 mg/ml UBM gels. The maximum turbidity values changed with increasing UBM concentration as shown in Figure 3-6 but were still lower than collagen type I. The values of in t_{lag}, $t_{1/2}$, and S changed at low concentrations but leveled off at concentrations above 3 mg/ml as shown in Figure 3-7. Changes in turbidity and the changes in turbidity as a function of gelation could be a result of the self-assembly molecules present within the gel, the interactions between molecules, fibril diameter, or a combination of all.

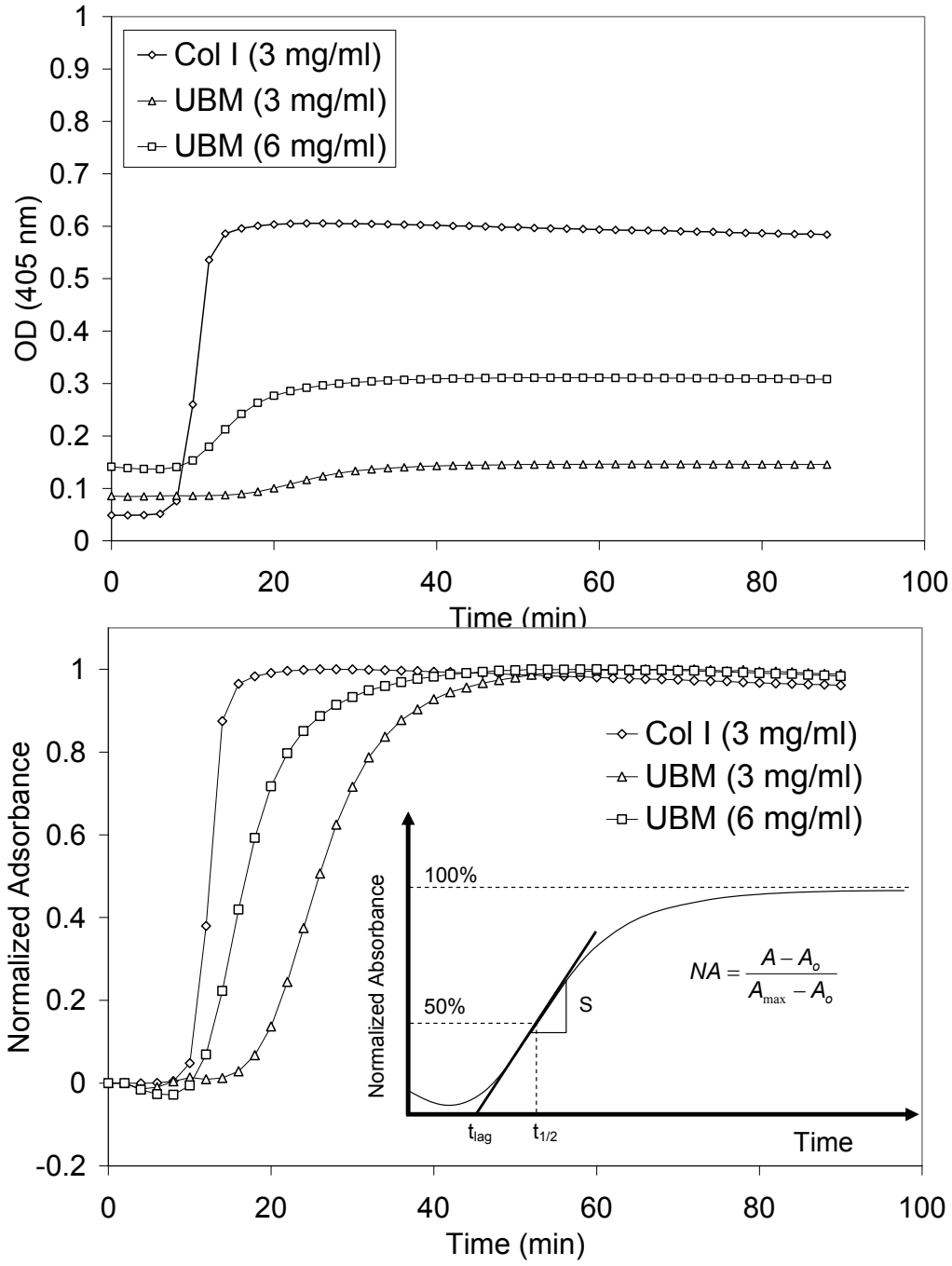

Figure 3-5: (Top) Turbidimetric gelation kinetics of collagen type I and UBM gels; (Bottom) Normalized turbidimetric gelation kinetics of collagen type I and UBM gels (inset: diagrammatic representation of the normalization and the parameters determined from the gelation kinetics).

Table 3-1: Results from the turbidimetric (405nm) analysis of the UBM gelation kinetics. Data represents mean ± SD.

Material	S	$t_{1/2}$	t_{lag}
Collagen type I 3 mg/ml	0.20 (0.01)*	12.2 (1.1)*	9.7 (0.8)*
UBM 3 mg/ml	0.07 (0.01)	24.4 (2.4)	16.8 (2.0)
UBM 6 mg/ml	0.09 (0.04)	22.4 (4.9)	15.2 (3.3)

*$p < 0.05$

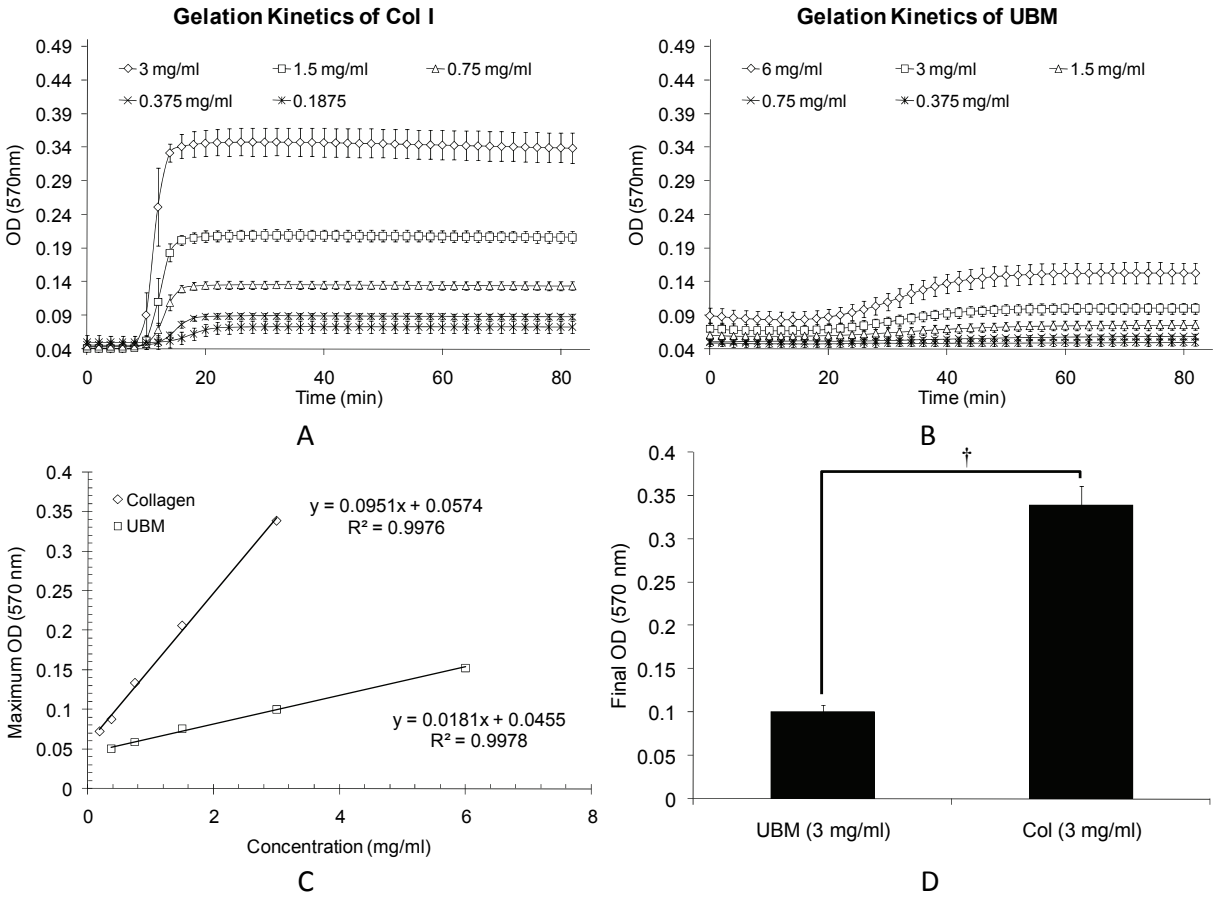

Figure 3-6: (A) Geletion kinetics of collagen type I; (B) Gelation kinetics of UBM gels; (C) Final OD versus concentration; (C) Comparison of the final OD values for collagen and UBM gels at similar concentrations. Values represent mean ± SD of quadruplicates. †p<0.05.

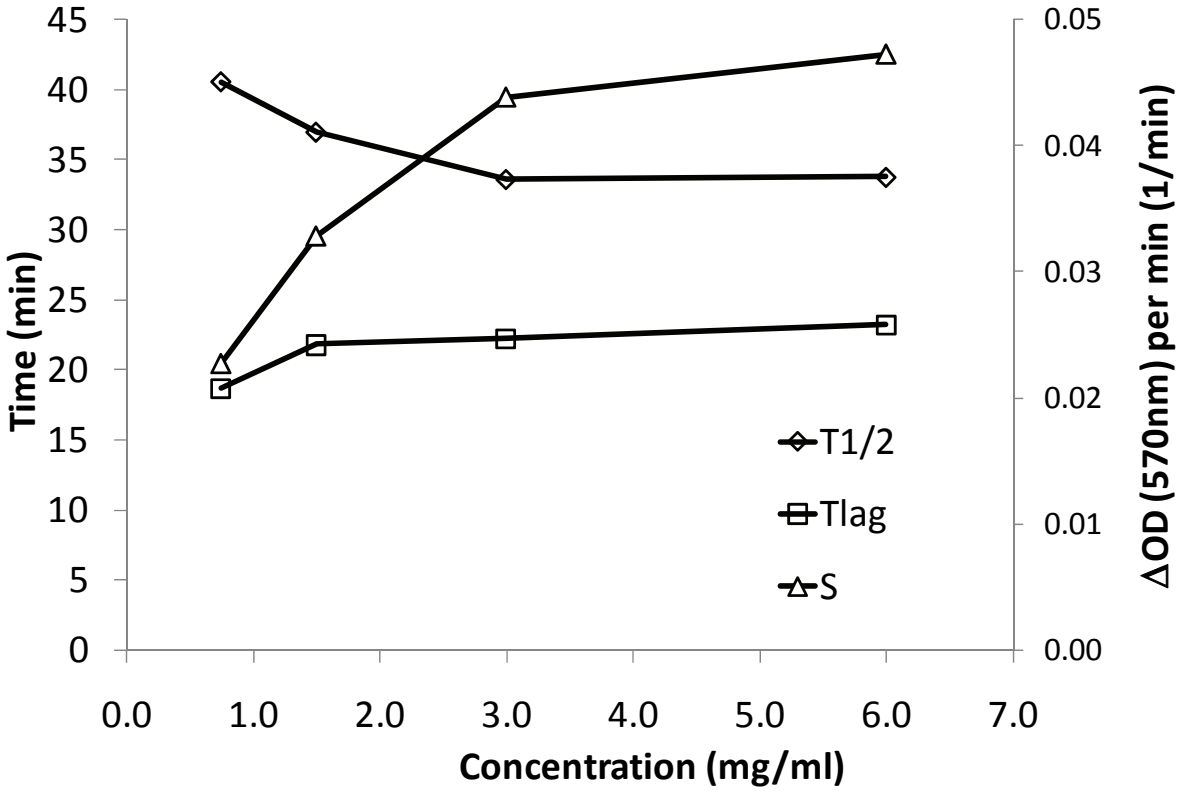

Figure 3-7: Gelation parameters as a function for UBM gels as a function of concentration. Data represent mean values from one batch of UBM digest.

3.3.3 Rheological Characterization

Both the storage modulus (G') and the loss modulus (G'') changed over time and was characterized by a sigmoidal shape after the temperature of the sample was raised from 15°C to 37°C as shown in Figure 3-8. G' and G'' reached steady state after approximately 8-12 minutes suggesting that gelation had occurred. The kinetics of G' and G'' were faster than the turbidimetric kinetics. G' and G'' slightly increased as a function of frequency as shown in Figure 3-9. There was also a concentration dependent increase in G' and G''. The dynamic viscosities of both UBM and collagen type I are shown in Figure 3-10 over a frequency range of ~0.08-15 Hz and the results are summarized in Table 3-2. The value of n~1 for both UBM and collagen type I occurs because G'>>G'' and G' is independent of frequency. Therefore, the complex viscosity of UBM and collagen were inversely proportional to frequency since $|\eta^*| \sim \frac{G'}{2\pi f}$. As shown in Figure 3-11, there was an increase in strength and stiffness as a function of strain up to a strain of 0.25 and both strength and stiffness increased with increasing concentration (from 3 mg/ml to 6 mg/ml). Strain values above 0.25 resulted in breakdown of the gel as judged by rapid decreases in stress and modulus (not shown). These findings suggest that UBM can be formed into a gel with solid like characteristics and that the mechanical properties can be tailored based on initial UBM concentrations.

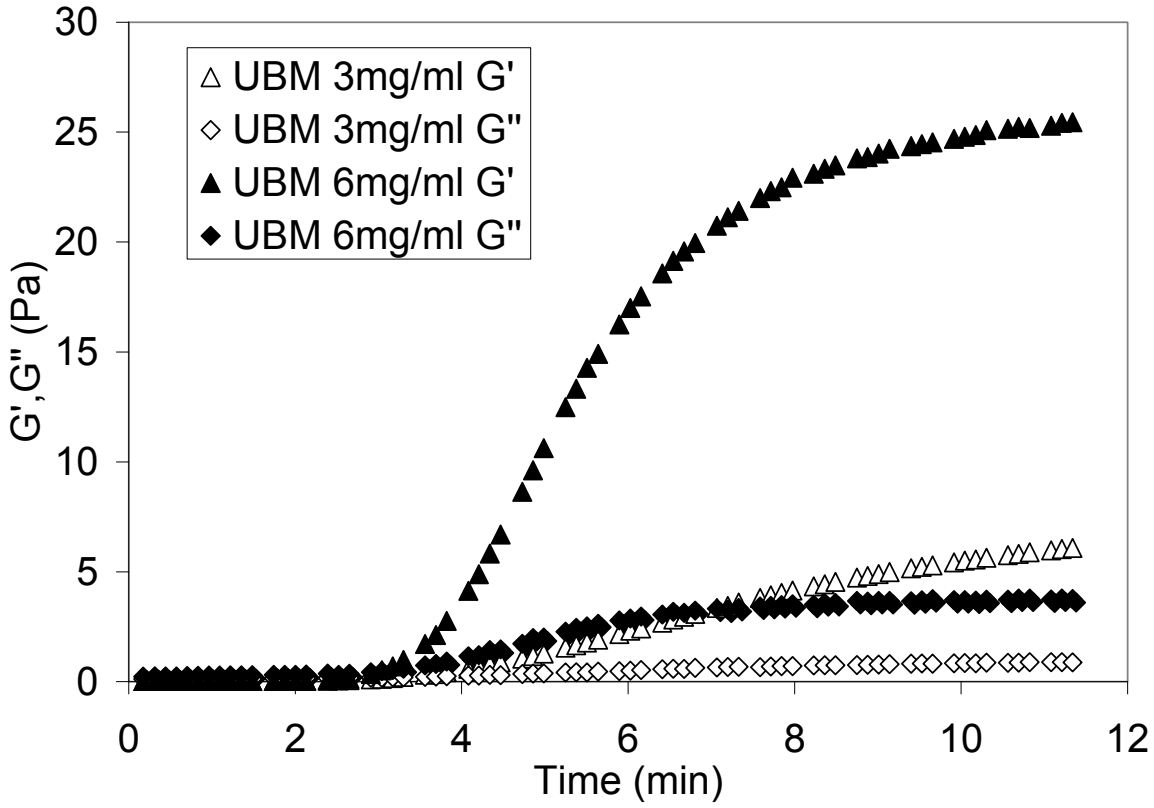

Figure 3-8: Representative curve of the gelation kinetics of UBM gels determined during the mechanical testing of the gels based on the storage modulus (G') and the loss modulus (G'').

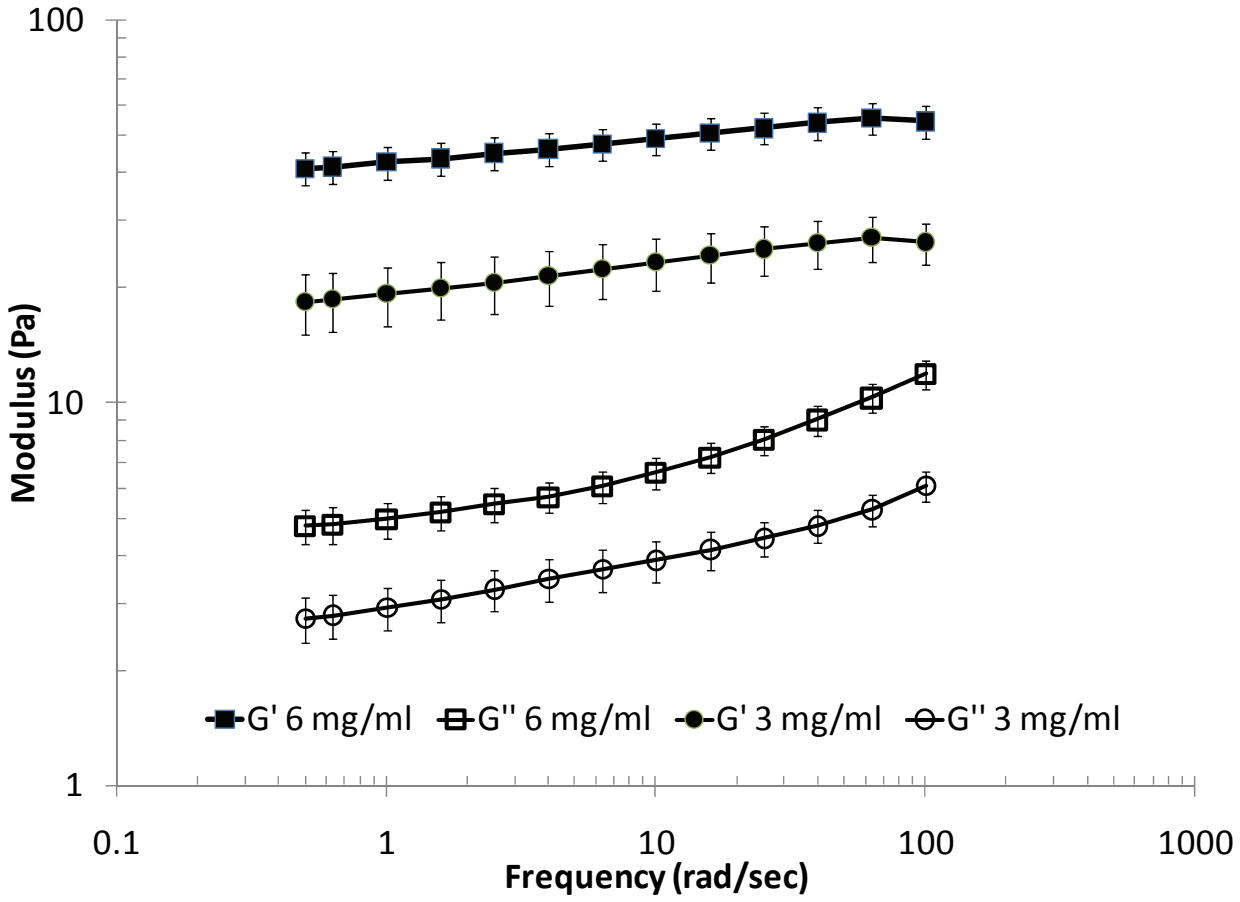

Figure 3-9: Frequency sweep for 3 and 6 mg/ml UBM gels. Data represents mean ± SE.

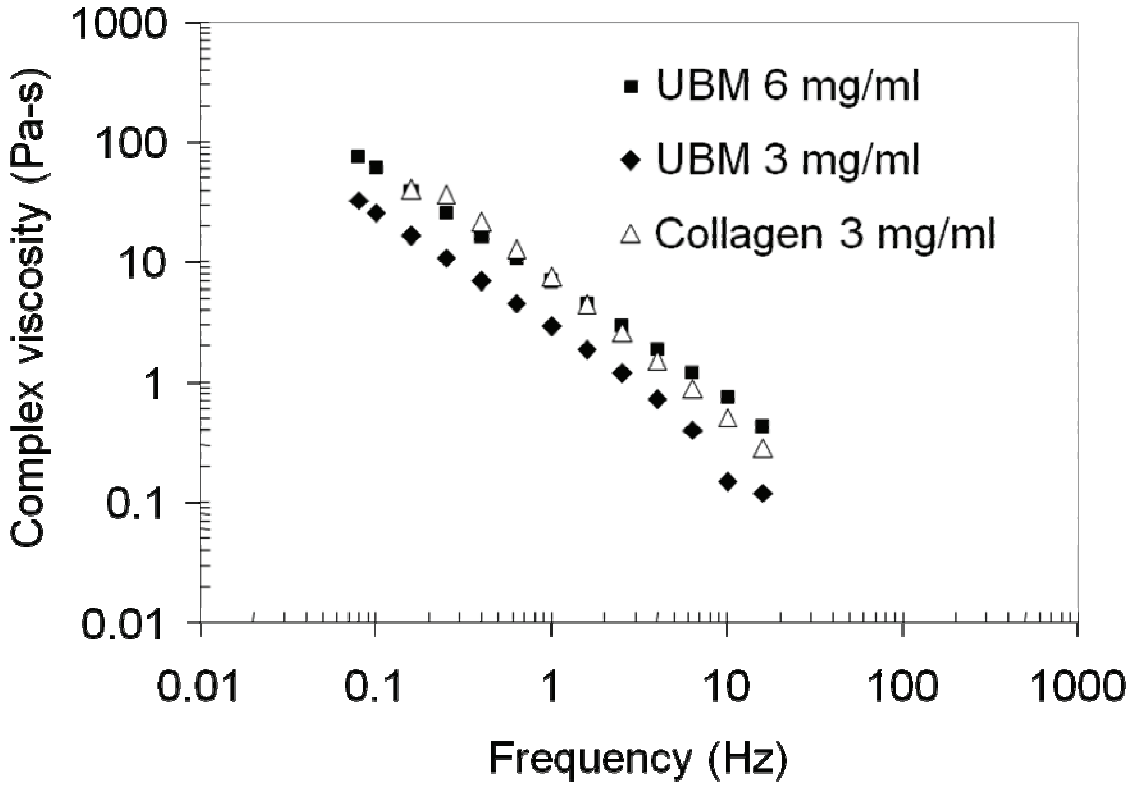

Figure 3-10: Viscosity versus frequency plots of UBM gels and collagen type I gels.

Table 3-2: Comparison of the complex viscosity of UBM gels with commercially available injectable materials.

Material	k	n	r^2	Frequency	REF
Collagen Type I 3 mg/ml	6.92	-1.117	0.995	0.01-15 Hz	--
Urinary Bladder Matrix 3 mg/ml	2.35	-1.062	0.988	0.01-15 Hz	--
Urinary Bladder Matrix 6 mg/ml	5.69	-0.955	0.999	0.01-15 Hz	--
Gelatin (Gelfoam)	149.39	-0.903	0.997	0.01-15 Hz	[150]
Zyplast™	99.851	-0.915	0.998	0.01-15 Hz	[150]
Zyderm™	66.395	-0.915	0.998	0.01-15 Hz	[150]
Zyderm™	12	-0.860	0.977	0.01-100 Hz	[151]
Cymetra®	19.9	-0.778	0.972	0.01-100 Hz	[151]
Hyaluronic Acid-DTPH	3.19	-0.744	0.974	0.01-100 Hz	[151]
Human abdominal subcutaneous fat	23.576	-0.951	0.994	0.01-15 Hz	[150]
Polytetrafluoroethylene (PTFE)	1151.9	-1.027	0.997	0.01-15 Hz	[150]

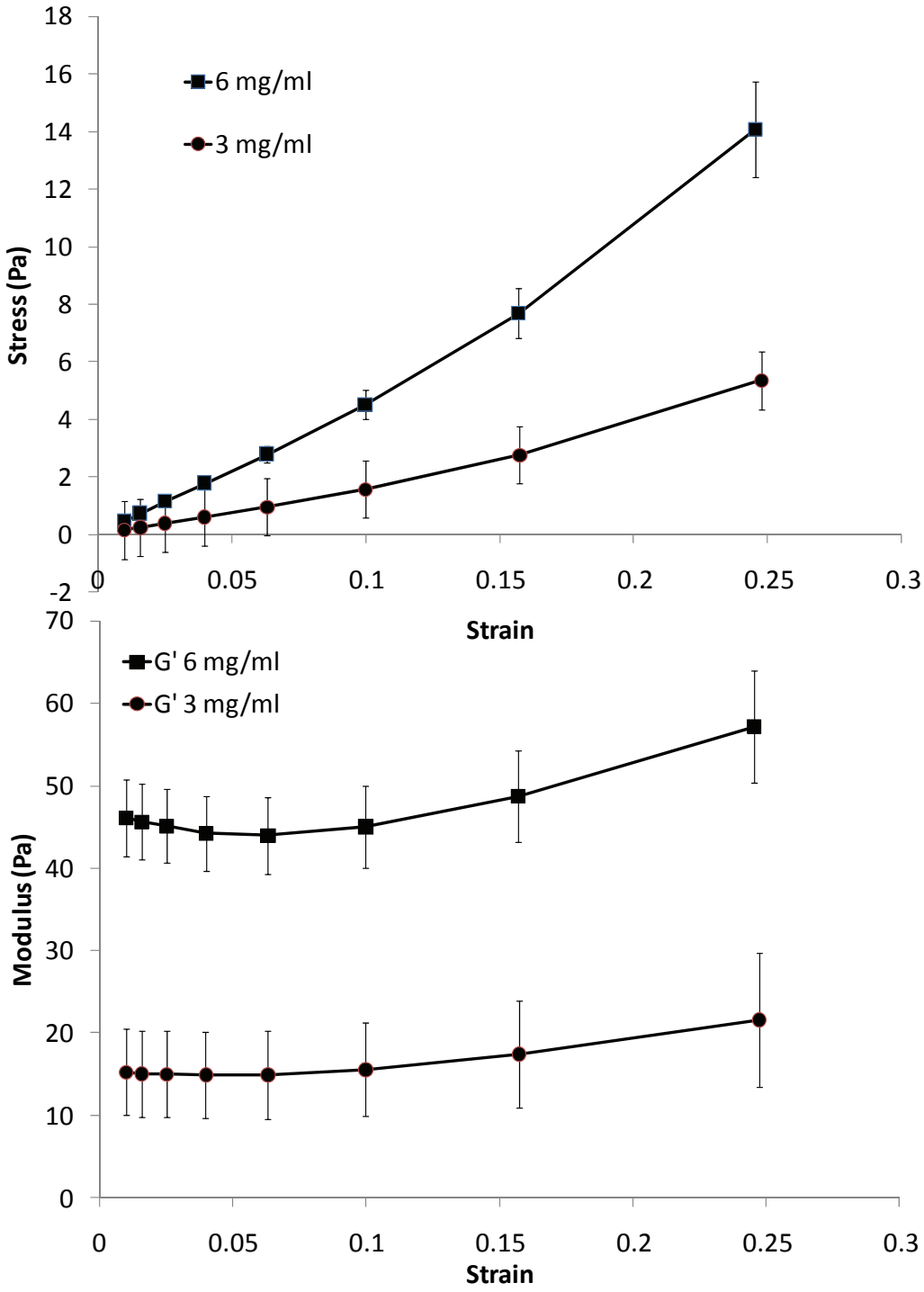

Figure 3-11: (Top) Stress versus strain plots for 3 and 6 mg/ml UBM gels; (Bottom) Modulus versus strain plots for 3 and 6 mg/ml UBM gels. Data represents mean ± SE.

3.3.4 Mitogenic Assay

Rat aortic smooth muscle cells (rSMCs), mouse C2C12 myoblasts, human aortic endothelial cells (HAECs), and human fetal cardiomyocytes (HFCs) were able to grow on UBM gels under static culture conditions. After 10 days in culture, rSMCs contracted the gels and formed a multilayer of cells as shown in Figure 3-12. The percentage of rSMCs number after 48 hrs of *in vitro* culture was greater in the UBM gels when compared to purified collagen type I as shown in Figure 3-12 when the values were normalized to the values for lyophilized UBM. The percent change in cell number between UBM gels and collagen type I gels for rSMCs, C2C12, HAECs, and HFCs is shown in Figure 3-13. It is important to note that the MTT assay and the Vialight™ assay are both influenced by cellular metabolism. Changes in the cells metabolic processes as a result of the *in vitro* growth of different substrate may also affect the results. The histological appearance of rSMCs, C2C12 cells, and HFCs are shown in Figure 3-14 and Figure 3-15. rSMCs, C2C12 cells, and HFCs contracted the gel after 7 days in culture. They formed a multilayer on the surface of the gels and some evidence of gel invasion was evident on rSMCs and C2C12 cells seeded gels.

Chick embryonic cardiomyocytes (CECs) attached and proliferated when seeded on the surface of UBM gels. They showed faster attachment and migration away from aggregates when compared to collagen type I with similar rheological properties (6 mg/ml versus 3 mg/ml) as shown in Figure 3-16. CECs were able to grow within the gels, expressed PCNA (Proliferating nuclear cell antigen), and spontaneously contracted the gels without outside stimulation (Figure 3-17). Spontaneous contraction subsided after 3 days in culture when CECs were seeded within the gels.

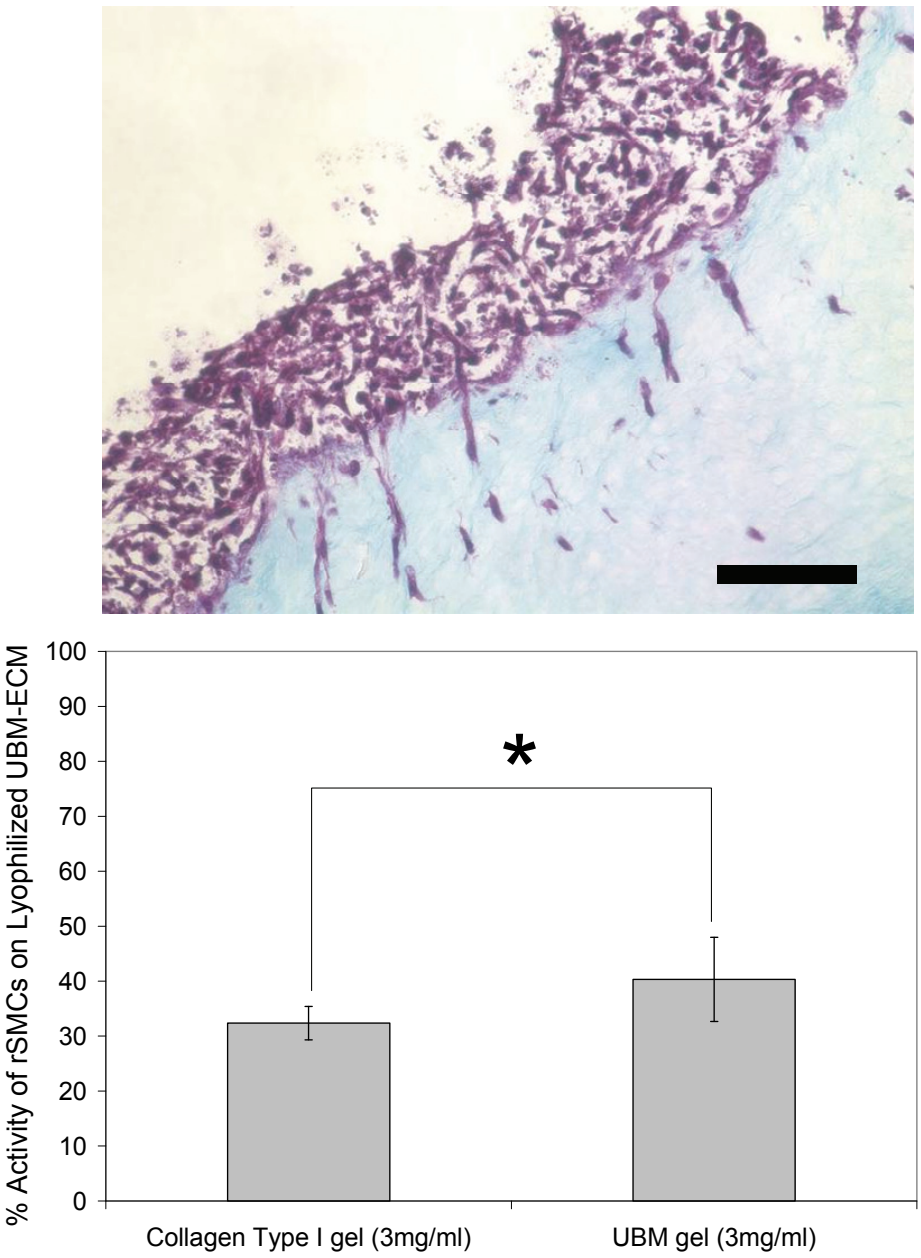

Figure 3-12: (A) Rat smooth muscle cells grown on UBM gels for 10 days (scale bar = 100 µm); (B) Comparison of the cellular activity of rSMCs on UBM and collagen type I gel when compared to lyophilized UBM-ECM scaffolds. Data represents mean ± SD. *p<0.05 (paired 1-sided t test)

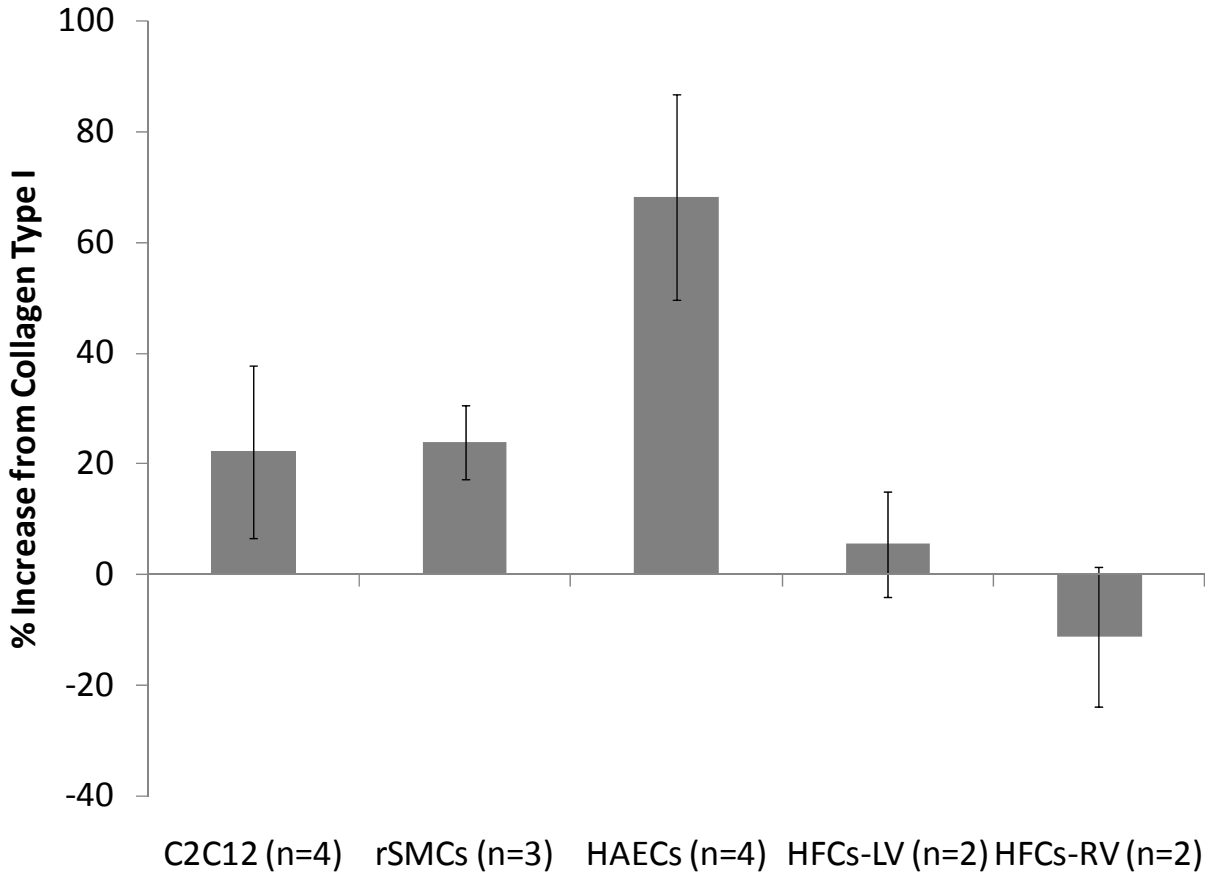

Figure 3-13: Results from the *in vitro* seeding of mouse myoblasts (C2C12), rat smooth muscle cells, human aortic endothelial cells, an human fetal cardiomyocytes derived from the left ventricle (HFC-LV) and right ventricle (HFC-RV) on UBM gels (3 mg/ml) when compared to collagen type I gels (3 mg/ml).

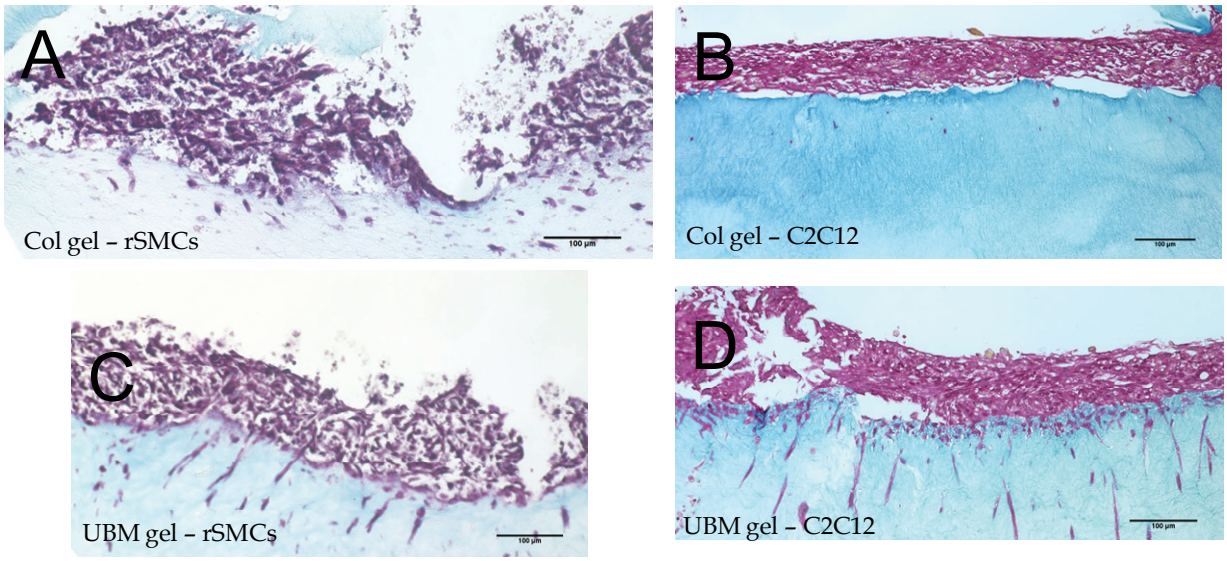

Figure 3-14: Collagen type I (3 mg/ml) gels seeded with (A) rSMCs and (B) C2C12 myoblasts; UBM (3 mg/ml) gels seeded with (C) rSMCs and (D) C2C12 myoblasts. Cells were seeded at 10^6 cells/cm^2 for seven days (Masson's Trichrome stain).

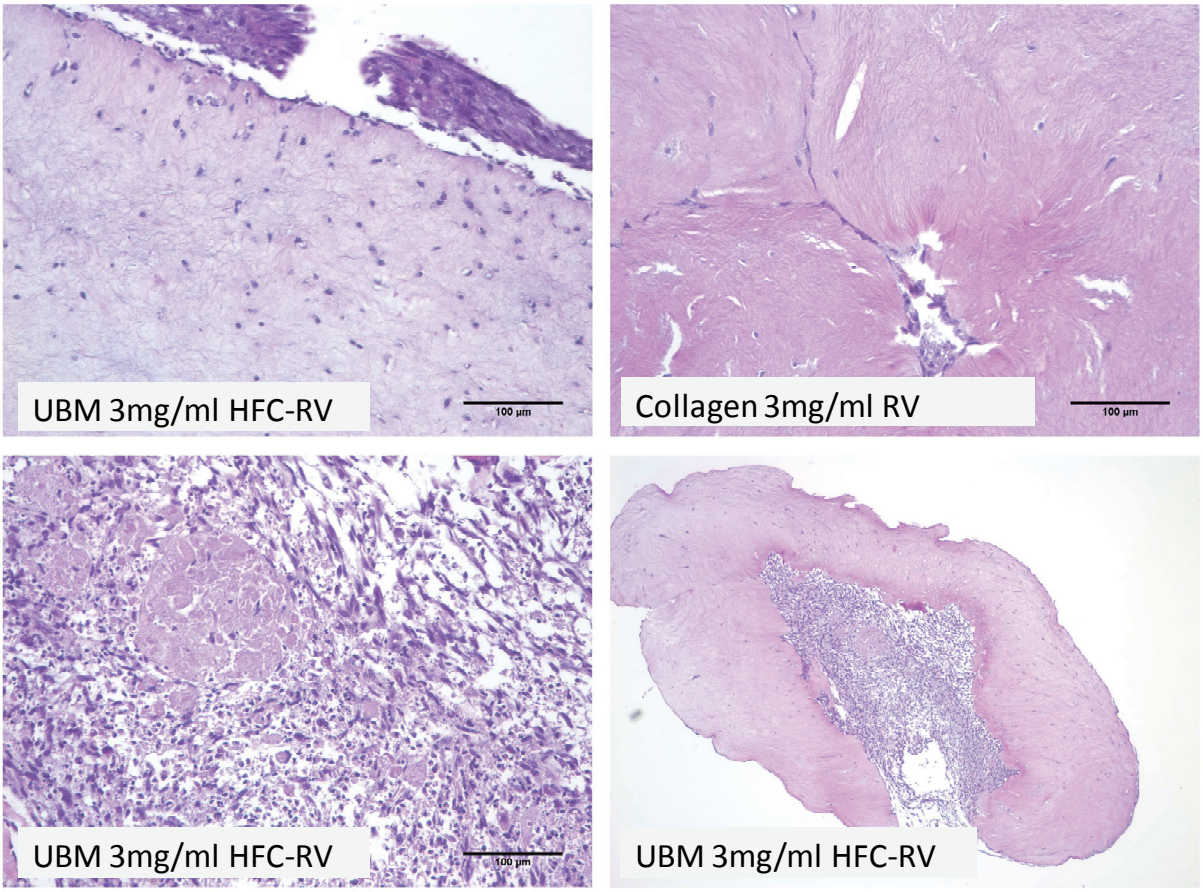

Figure 3-15: Human fetal cardiomyocytes derived from the right ventricle cultured on UBM and collagen gels (H & E). All images were taken at 200x except the image on the right-lower corner which was taken at 40x.

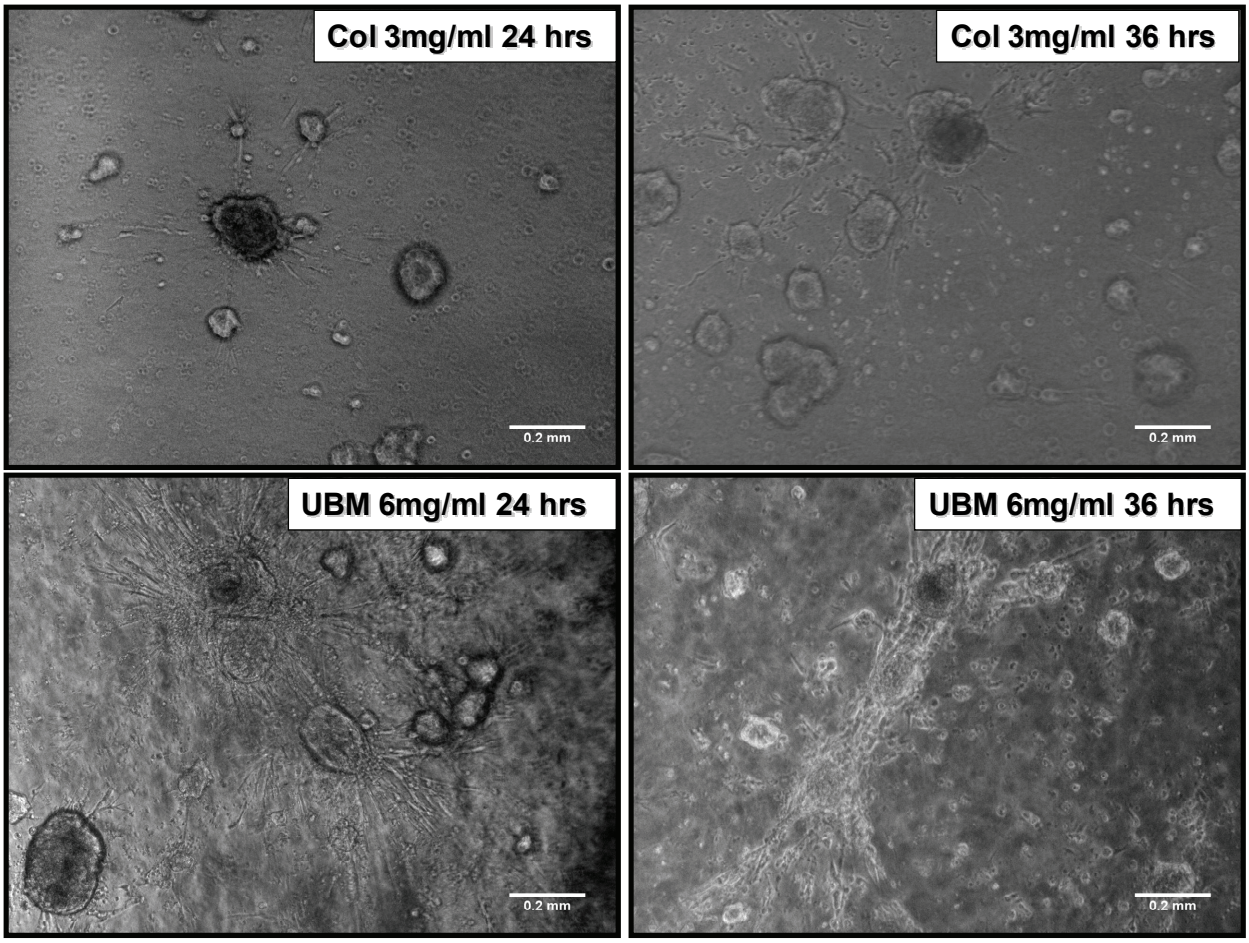

Figure 3-16: Chick embryonic cardiomyocytes cultured on the surface of UBM gels and collagen type I gels. Note the spreading of the chick embryonic cardiomyocytes (CECs) away from the aggregates in the UBM gels. The migration of CECs on collagen type I gels was less pronounced.

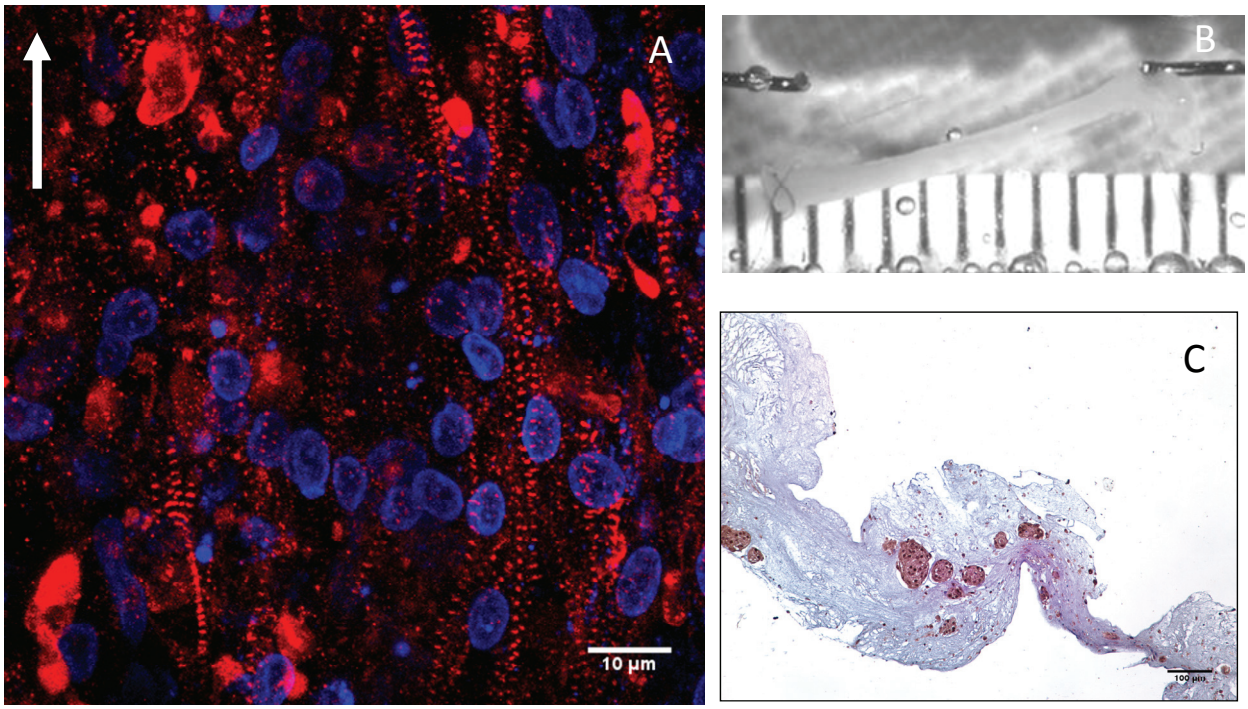

Red – *alpha sarcomeric actinin*
Blue – *nuclei*
Arrow points in the longitudinal direction

Figure 3-17: Chick embryonic cardiomyocytes cultured within the UBM scaffold. (A) Shows the confocal microscopy image of CEC (initial seeding of ~6x10^5 cells per construct) when cultured for 7 days within a 1 mg/ml gel; (B) Macroscopic image of UBM gel construct; (C) PCNA stain of CEC cultured within a UBM gel (2 mg/ml) after 4 days in culture. Construct preparation and the confocal image are courtesy of Dr. Kimimasa Tobita.

3.4 DISCUSSION

The present study characterized the gelation kinetics, rheological properties, and the cytocompatibility of a gel form of an ECM scaffold derived from the porcine urinary bladder called urinary bladder matrix. The methodology for the digestion of the UBM scaffold did not require purification steps that would adversely affect the molecular composition of the ECM. The digested UBM self-assembled into a gel when brought to physiological ionic strength, pH, and temperature. The gelation kinetics, rheological properties, and the ability of the gel to support smooth muscle cell, endothelial cells, and cardiomyocytes growth *in vitro* were also determined.

The components responsible for the gelation of UBM are unknown but most likely gelation was due to the presence of self-assembling molecules such as collagens, laminins, and proteoglycans [152, 153]. The turbidimetric gelation kinetics of UBM gels were slower than purified collagen type I at similar total protein concentrations presumably due to the presence of glycosaminoglycans in the UBM solution and/or the presence of different types of collagens or molecules such as fibronectin which are known to modulate collagen self assembly [152-156]. Glycosaminoglycans and proteoglycans cause changes in final turbidimetric absorbance and changes in gelation kinetics of collagen type I gels [155, 157, 158]. The exact reasons for the changes in turbidity and gelation kinetics remain unknown. However, the findings suggest that the process is not simply collagen chemistry but rather a result of the interplay of all of the components within the digested UBM.

Rat aortic smooth muscle cells (rSMCs) were able to adhere and proliferate upon the UBM gels. After 48 hours of incubation, greater numbers of rSMCs were found on the lyophilized sheets of UBM when compared to collagen type I and UBM gels. The greater

number of cells found on the lyophilized UBM could be due to differences in the mechanical or structural properties of the substrates (lyophilized sheet vs. gel). Interactions between cells and its substrate have been known to modulate cell behavior such as adhesion, proliferation, and migration [159]. Another plausible explanation could be the presence of bioactive proteins/peptides present at the surface of the lyophilized UBM that are no longer surface-located in the gel form. If such bioactive proteins/peptides are retained during the digestion process, it could explain the higher cellular content found on UBM gels when compared to collagen type I after the 48hrs incubation period. Future studies will determine the biochemical composition of the UBM gel as well as the retention of bioactivity after enzymatic digestion of UBM.

Mouse C2C12 myoblasts and human aortic endothelial cells (HAECs) had higher cell numbers in UBM gels when compared to collagen type I. No differences were observed on HFCs derived from either the left or right ventricle. Changes in proliferation may be due to differences in the mechanical properties of the substrate or as a result of surface bound ligands with stimulatory effects that are present in the UBM gel and not in collagen gels. The increase in HAECs in UBM gels is opposite to the findings on Chapter 2 where no change in proliferation was observed on HAECs treated with digested UBM. The mitogenic assay in Chapter two was performed with papain digested UBM and the results presented in this chapter are with pepsin digested UBM. There was no change in proliferation of HAECs under the *in vitro* conditions studied between papain digested UBM and controls. The increase in HAECs found when seeded on the surface of UBM gels could be a result of the enzyme used but most likely is a result of the type of substrate (gel versus tissue culture plate), any surface bound ligand that may interact with

HAECs, and the lack of starvation of the HAECs cells when seeded on the UBM gels. The exact reason remains unknown and will be the subject of further investigation.

CECs were able to attach and grow on the surface of UBM gels. CECs aggregates attached and spread faster on UBM gels when compared to collagen type I gels. This may be due to the presence of molecules such as laminin and fibronectin within the ECM. Zimmerman et al. and others have shown that, in some cases, Matrigel or fibronectin is needed for spontaneous contraction or stimulated contraction of cardiomyocytes [110]. The spontaneous contraction of CECs when seeded on UBM gels suggest that the mechanical properties of the gel are suitable for CECs growth and that there might be a component within the UBM gel with great affinity for CECs (i.e. fibronectin and laminin). However, the effects of the digestion process upon molecules such as fibronectin and laminin remains unknown. CECs and UBM construct began to spontaneously contract after 3 days in culture but later subsided even though the CECs had a healthy microscopic appearance. Overgrowth of fibroblasts could change the mechanical properties of the gel making it harder for the CECs to deform the matrix. As shown in the confocal images of the CECs within the UBM construct, z-bands are present when stained for α-actinin showing aligned cardiomyocytes in the longitudinal direction. However, there are nuclei within the construct that do not stain for α-actinin. The presence of nuclei negative for α-actinin supports the idea that other cell types may be populating the constructs leading to a decrease in contraction and will be the investigated in future studies.

The rheological properties of the UBM gel were determined and showed that both the storage modulus (G') and the loss modulus (G'') increased as function of time after the temperature of the buffered solution was increased to 37°C. The gelation of UBM observed by turbidimetric and rheologic methods showed a sigmoidal shape. After approximately ~20-30

minutes, the turbidity and the shear moduli of UBM reached a constant value at which point gelation was deemed complete. After the gelation period, G' was greater than G'' suggesting that the gel behaved as a solid-like structure. This transition to a solid structure occurred for both 3 mg/ml and 6 mg/ml UBM gels. As seen by the changes in G', G'', and the dynamic complex viscosity (η^*) as a function concentration, the rheological properties under dynamic loading change as a function of the final concentration. In addition, strength and stiffness can also be increased with increasing concentration. These findings suggest that changes in concentration can be used to tailor the rheological properties of the gel for specific applications.

The UBM gels developed in the present study have lower viscosity values than some of the injectable materials currently in clinical use [150, 151, 160]. Also, high UBM concentrations (6 mg/ml) were required to obtain gels with similar rheological properties to collagen type I gels (3 mg/ml). The increase in protein concentration needed to obtain the desired rheological properties (similar to collagen or hyaluronic acid) may affect the diffusion of oxygen, nutrients, and waste across the gel. Changes in diffusion may affect the behavior of cells if the gel is intended as a cell delivery material or if cells are embedded within the gel [161, 162]. The *in vitro* response of cells when seeded within the gel as well as the host tissue response to the gel will be the subject of future studies.

3.5 CONCLUSIONS

The present study showed that UBM can be successfully solubilized and formed into a gel form. The rheological properties of the gel can be tailored to specific applications by changing the concentration of the gels. The present study also shows that UBM gels support the adherence and growth of rat aortic smooth muscle cells, mouse C2C12 cells, human aortic endothelial cells, and human fetal cardiomyocytes.

3.6 LIMITATIONS AND FUTURE WORK

The work presented examines a soluble form of UBM that can be polymerized into a gel. Currently, the gelation kinetics of UBM might be too slow for some applications. If faster polymerization is needed, hybrids can be created. For example, UBM can be mixed with fibrin and use fibrin as the trigger for polymerization rather than the UBM itself. Of course, the mixture of UBM with another component raises other questions such as what are the optimum concentrations, what are the changes in mechanical properties, and is there any shadowing of the bioactivity of UBM.

Future studies should address the cell-matrix interactions and most importantly the effects of the gel form *in vivo*. The bioactivity and the benefits of using the UBM gel will be better understood if we could show favorable changes *in vivo* when compared to standard therapies. Another potential application could be use of the gel as a cell deliver vehicle after an MI. The benefit of the use of UBM gels for cell engraftment and cell survival *in vivo* should be investigated and warrants further study.

4.0 PREPARATION AND CHARACTERIZATION OF AN ELECTROSPUN HYBRID SCAFFOLD

4.1 BACKGROUND

Biologic scaffolds derived from the extracellular matrix (ECM) are characterized by their ability to support the adhesion, proliferation, and differentiation of a variety of cell types both *in vitro* and *in vivo* and by their ability to promote constructive tissue remodeling [30, 163-167]. However, ECM derived scaffolds can be limited to the inherent geometrical and mechanical properties of the tissue from which they are derived and the manufacturing process do not allow for the same degree of control over the material properties (i.e. porosity, strength, elasticity, etc) found in synthetic materials. In addition, the mechanical and material properties of ECM derived scaffolds are subject to biologic variations dependent upon the age of the host, the tissue of origin, and the specific methods of processing.

As discussed in Chapter 1, biodegradable synthetic scaffolds represent an alternative to biologic scaffolds derived from ECM. Elastomeric properties are attractive for the repair of soft tissues because elasticity is inherent to most soft tissues. Currently there is a need for biomaterials that are biodegradable, bio-inductive, and that have mechanical properties that match the mechanical properties of the tissue which they are intended to replace. One attractive elastomer is the biodegradable and cytocompatible poly(ester-urethane)urea (PEUU). PEUU has

reproducible elastomeric properties, is biodegradable, and the degradation products are cytocompatible. However, apart from some bioactivity inherent in one of its degradation products (putrescine), PEUU scaffolds lack the inherent bioactivity present in biologic scaffolds such as UBM.

Methods such as electrospinning allow for the fabrication of PEUU scaffolds with microscopical morphologies and mechanical properties that closely resemble the native extracellular matrix (ECM) [168, 169]. Furthermore, the fiber size and orientation can be controlled to produce mechanical anisotropy that approximates certain native tissues. However, they do not possess the bioactivity inherent in biologic scaffolds derived from the ECM. Attempts to impart bioactivity during the manufacture of PEUU scaffolds have been described by the addition of collagen, growth factors, peptide sequences, and cells [20, 22-24, 27, 28, 90]. Although promising results have been obtained, there are still limitations. Even if growth factors and peptide sequences promote cell adhesion, migration, and proliferation *in vitro*, it is uncertain if one molecule alone can modulate the host tissue response enough to push the outcome toward constructive remodeling *in vivo*. Cell seeding of the PEUU may improve the cellular content within the scaffold after implantation, but issues such as cell viability from the "bench" to the patient and cell source remain a problem.

The objective of the present study was to combine the digested UBM described in Chapter 2 to create an elastomer composed of a biodegradable polyurethane (PEUU) and solubilized UBM. Electrospinning was chosen as the method of fabrication due to early success with electrospinning blends of PEUU/UBM scaffolds and to closely mimic the ultrastructural morphology of the native ECM [29]. The following chapter describes the preparation and characterization of hybrid scaffolds composed of enzymatically digested UBM and PEUU.

4.2 METHODS

4.2.1 Preparation of UBM/PEUU Hybrid Scaffolds

The preparation of UBM and PEUU has been previously described [29]. The following section describes the process used by our collaborating laboratory to synthesize and create the electrospun hybrid scaffolds. The preparation of UBM will be briefly described.

4.2.1.1 Poly(ester urethane)urea Synthesis

All monomers and reagents were acquired from Sigma unless otherwise noted. 1,4-diisocyantobutane (BDI) and 1,4-butanediamine were purified by vacuum distillation. Poly(ε-caprolactone) diol (PCL, M_n = 2000) was dried under vacuum at 50°C for 48 h. Solvents dimethyl sulfoxide (DMSO) and N,N-dimethylformamide (DMF) were dried on 4-Å molecular sieves. Stannous octoate and 1,1,1,3,3,3-hexafluoro-2-propanol (HFIP, Oakwood) were used as received.

Biodegradable poly(ester urethane)urea (PEUU) was synthesized from PCL and BDI with chain extension by putrescine as previously reported [170]. The reaction occurred as a two-step solution polymerization in DMSO with a monomer feed molar ratio of 2:1:1 BDI: PCL:1,4-butanediamine. After PEUU precipitation and drying, PEUU transparent films were cast from a 3 wt% solution in DMF and dried under vacuum for 48 h.

4.2.1.2 Preparation of UBM

The preparation of the porcine urinary bladder matrix has been previously described in previous chapters [165]. Briefly, porcine urinary bladders were harvested from pigs immediately following euthanasia. Connective tissue and adipose tissue were removed from the serosal surface and any residual urine was removed by multiple water rinses. The tunica serosa, tunica muscularis externa, the tunica submucosa, and most of the muscularis mucosa were mechanically removed and the luminal urothelial cells were dissociated by soaking in 1.0 N saline solution. The remaining basement membrane plus the subjacent tunica propria was referred to as urinary bladder matrix (UBM). UBM sheets were disinfected for two hours on a shaker in a solution containing 0.1% (v/v) peracetic acid, 4% (v/v) ethanol, and 95.9% (v/v) sterile water. Peracetic acid residue was removed by washing twice with sterile PBS (pH = 7.4) and twice with sterile water for 15 min each time. UBM sheets were subsequently lyophilized and comminuted to form a powder [171].

4.2.1.3 Preparation of Pepsin Digested UBM

UBM was digested with pepsin by mixing 1 g of lyophilized and powdered UBM with 100 mg of pepsin (~2,000-2,300 Units/mg, Sigma-Aldrich, St. Louis, MO) in sterile 100 mL 0.01 N HCl. This solution was stirred constantly at room temperature (25°) for 48 hours. The resultant viscous solution of digested UBM had a pH of approximately 3.0-4.0. A control solution was made in parallel by keeping a portion of the pepsin-HCl solution used to digest the UBM under similar conditions but without the addition of the UBM powder.

4.2.1.4 Preparation of Papain Digested UBM

One gram of lyophilized, powdered UBM was mixed with 100 mL of phosphate buffered saline (PBS) containing 1 U/mL of papain (Sigma-Aldrich, St. Louis, MO). The flask was covered to minimize evaporation, placed inside an incubator at 37°C or on hot plate at 60°C, and kept under constant stir for a total of 24 hours. After the 24 hour digestion period, the solution was brought to room temperature, spun at 1000 RPM for 6 minutes, and the supernatant collected. For each milliliter of solution, one milliliter of 1 mM E-64 protease inhibitor (Sigma-Aldrich, St. Louis, MO) was added to inactivate the papain.

The digested pepsin and papain digested UBM scaffolds were poured onto polystyrene dishes and frozen at -80°C. The digest were then lyophilized and stored under dry conditions before use.

4.2.1.5 Electrospinning

Hybrid scaffolds were made via electrospinning. UBM and PEUU were dissolved and blended in HFIP at a total concentration of 6 wt% at a 50:50 ratio and then electrospun. ***The 50:50 ratio was selected for all in vitro studies based on previous studies suggesting that 50:50 PEUU/Upep scaffolds had sufficient mechanical strength for left ventricular reconstruction. For subcutaneous implantation of hybrid scaffolds (described in section 4.2.4) 75:25 and 25:75 ratios were selected to study the host tissue response to a high and low concentration of UBM with respect to the PEUU.*** A similar technique to that described previously was utilized for electrospinning [169]. The electrospinning process consisted of feeding the polymer or the polymer/ECM solution at 1.0 mL/h through Teflon tubing to a stainless steel capillary (type 316, 1.2-mm I.D.) located 15 cm from an aluminum disc target. Samples were electrospun by charging the polymer solution at 15 kV and the aluminum target at -10 kV. The target was also

attached to x-y linear stages repeatedly translating in a square pattern with 5-cm sides to produce scaffolds of uniform thickness. Scaffolds were subsequently dried under vacuum at room temperature for 24 h. Electrospun scaffolds were placed on sterilization pouches and gamma irradiated at a dose of 2.0 Mrads.

4.2.2 Characterization of PEUU/UBM Hybrid Scaffolds

4.2.3 Scanning Electron Microscopy

Scaffolds were imaged via scanning electron microscopy (SEM) to characterize scaffold fiber morphology. The samples were attached to aluminum SEM specimen mounting stubs (Electron Microscopy Sciences, Hatfield, PA) and sputter coated (Sputter Coater 108 Auto (Cressington Scientific Instruments, Valencia, PA) with a gold palladium alloy. Finally, samples were examined using a scanning electron microscope (JEOL 6330F).

4.2.4 Differential Scanning Calorimetry

Differential scanning calorimetry (DSC) was performed on a differential scanning calorimeter (Shimadzu, DSC 60) under helium and nitrogen purge. Approximately 3 mg of hybrid scaffold material was loaded onto DSC stubs and placed on the DSC machine. Temperature scanning rates of 20°C/min were employed over a range of -100°C to 200°C.

4.2.5 Mechanical Testing

Tensile testing was performed on a horizontal MTS Tytron™ 250 machine. Specimens were cut into a dog-bone shape specimen with a mid-substance width of 2.5 mm and length of 7 mm and mounted on the mechanical testing machine maintaining a gage length from clamp to clamp of 8 mm. Samples were subjected to five 0.7 mm elongation-relaxation cycles at a rate of 10 mm/min and then immediately pulled to failure at the same rate. Data acquisition was performed 10 data points per second with a personal computer connected to the MTS machine. From the raw data, maximum force and elongation (grip-to-grip), and maximum tangential stiffness (K) were computed as shown [127]. The tangential stiffness was calculated as follow:

$$K^i = \frac{F^{i+10} - F^{i-10}}{e^{i+10} - e^{i-10}} \tag{5}$$

where i is a data index indicator, F is the force recorded, and e is the recorded elongation. The maximum tangential stiffness was taken as the maximum value of K^i. A diagrammatic representation of these parameters is shown in Figure 4-1.

The stress, σ, and strain, ε, were determined as follows:

$$\sigma = \frac{F}{A_o} \tag{6}$$

$$\varepsilon = \frac{L - L_0}{L_0} \tag{7}$$

where F is the force recorded, A_o is the un-deformed cross-sectional area, L is the deformed length, and L_o is the initial length of the specimen. Maximum tangential stiffness (MTM) was computed as shown in equation (1) by converting Force (F) to Stress (σ) and elongation to strain (ε).

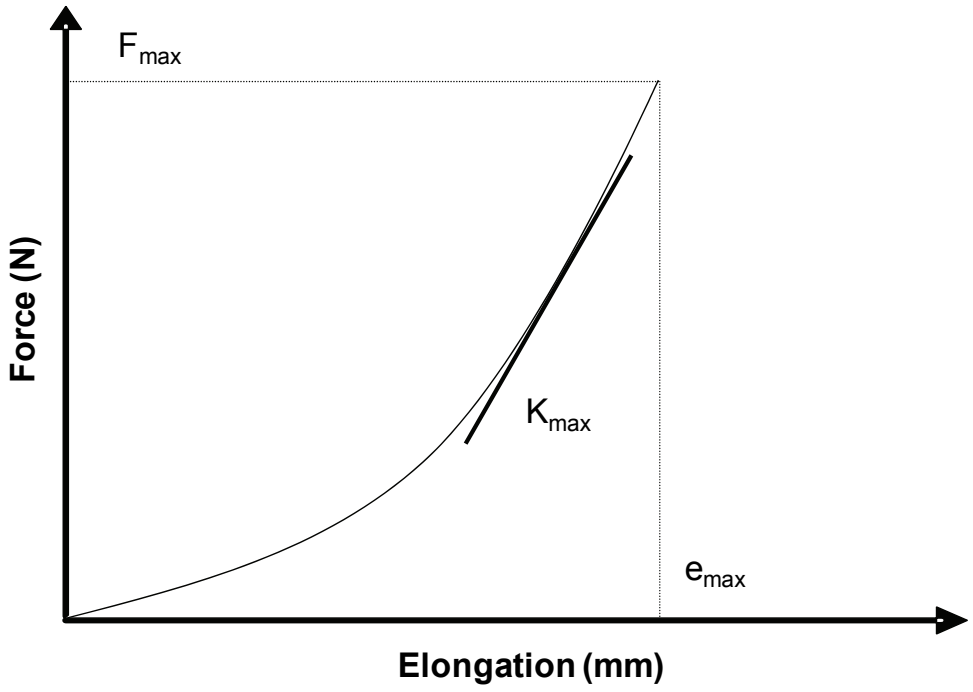

Figure 4-1: Diagrammatic representation of the force versus elongation curve obtained from the mechanical testing.

4.2.6 In Vitro Degradation

*In vitro s*caffold mass loss was measured in 15 ml of PBS at 37°C for 1 and 7 days. Dry scaffolds were weighed and immersed in 15 mL of PBS (pH = 7.4) and incubated at 37°C. Samples were removed at one and seven days and placed in a lyophilizer for 2 hours prior to weighing (sufficient time for complete dehydration). Mass loss was calculated as:

$$\text{mass loss (\%)} = \left(1 - \frac{m_2}{m_1}\right) \cdot 100 \qquad (8)$$

where m_1 and m_2 are the masses of films before and after degradation, respectively.

4.2.7 In vitro Growth of Human Aortic Endothelial Cells

Human aortic endothelial cells were purchased from Cambrex and expanded in EGM-2 media as described in section 2.2.5.1. HAECs were sub-cultured and statically seeded at 200 μL of 15 x 10^4 cells / mL on 7-mm scaffold discs firmly placed into the bottoms of 96-well TCPS plates. Empty TCPS wells were used as controls. Scaffolds were gamma irradiated at a dose of 2.0 Mrads prior to seeding. Media was replaced in the wells every 2 days. Cell viability was evaluated 1 and 4 days after seeding using the ViaLight™ assay (n = 3 per sample).

4.2.8 In vivo Host Tissue Response to PEUU/UBM Scaffolds

The host tissue response to implanted hybrid scaffolds was determined using a rat subcutaneous implant model. All animal procedures were performed in accordance with the National Institutes of Health guidelines for care and use of laboratory animals and with the approval of the Institutional Animal Care and Use Committee.

Sprague-Dawley rats (Charles River Laboratories) weighing less than 500 g were anesthetized via induction of isofluorane (2% in oxygen), shaved, and prepped for surgery. Bi-lateral subcutaneous pockets were created in the subcutaneous tissue by making incisions of approximately 5-mm in length caudal to the scapula. Scaffold discs (10-mm diameter) were placed in the subcutaneous pocket and secured at two locations with 2-0 prolene sutures. A bovine collagen type I hybrid scaffold was prepared as described in section 4.2.1.3 and included in the *in vivo* studies. Test samples consisted of PEUU, PEUU/UBM (25/75), and PEUU/UBM (75/25) scaffolds sterilized via exposure to UV light for 2 h or gamma irradiated at a dose of 2.0

Mrads and randomly assigned to either the left or right subcutaneous pocket. Incisions were closed using a non-absorbable suture and the animals were recovered from anesthesia and allowed normal ambulation and normal diet for the remainder of the study period. Bupronex (0.02 mg) was administered subcutaneously the day of surgery and one day post-surgery. Gentamicin (2mg) was administered subcutaneously the day of the surgical procedure and for two days post-surgery. The animals were survived for 28 days. Following euthanasia, the operative site was identified and the excised tissues were placed in 10% neutral buffered formalin fixative. The harvested specimens were then trimmed, embedded in paraffin, sectioned, and stained with Masson's Trichrome stain.

4.2.9 Statistics

Results for the mechanical and *in vitro* testing are displayed as the mean ± standard deviation. One-factor analysis of variance (ANOVA) was utilized to evaluate cell viability and cell growth of human aortic endothelial cells using the Neuman-Keuls test for *post hoc* assessments of the differences between samples.

4.3 RESULTS

4.3.1 Characterization of UBM/PEUU Scaffolds

Papain and pepsin digested UBM were blended and electrospun with PEUU at a 50:50 ratio. Papain digested UBM at 60°C and 37°C did not blend as readily as pepsin digested UBM leading to precipitation of the UBM in the ejecting needle. The ultrastructure of hybrid scaffolds was imaged using scanning electron microscopy and representative images are shown in Figure 4-2. Pepsin digested UBM readily dissolved in HFIP with the PEUU. Pepsin hybrid scaffolds (PEUU/Upep) showed a fibrillar ultrastructure with UBM fibers that are indistinguishable from the PEUU fibers by scanning electron microscopy. Papain hybrid scaffolds (PEUU/Upep60 and PEUU/Upep37) had a fibrous ultrastructure and UBM agglomerates distributed throughout the scaffold. The hybrid scaffolds lost about 30-40% of its mass after 1 day of static immersion in PBS (results shown in Figure 4-3). There is a slight but not statistically significant increase in the mass loss after 1 week. Differential scanning calorimetry analysis of the hybrid scaffolds shows different curves with a shift in the melting point temperature (T_m) of the PEUU. There is also a broadening of the melting point peak on scaffolds blended with UBM (results shown on Figure 4-4).

Table 4-1 and Table 4-2 summarize the results of the structural and material properties for the hybrid scaffolds. There was a decrease in ultimate strength and maximum strain and an increase in the maximum tangential modulus for all hybrid scaffolds when compared to the pure polymer scaffold. Representative strain versus strain curves are shown in Figure 4-5. Average stress versus strain curves for PEUU, hybrid scaffolds, and UBM up to a strain of 30% is shown in Figure 4-6.

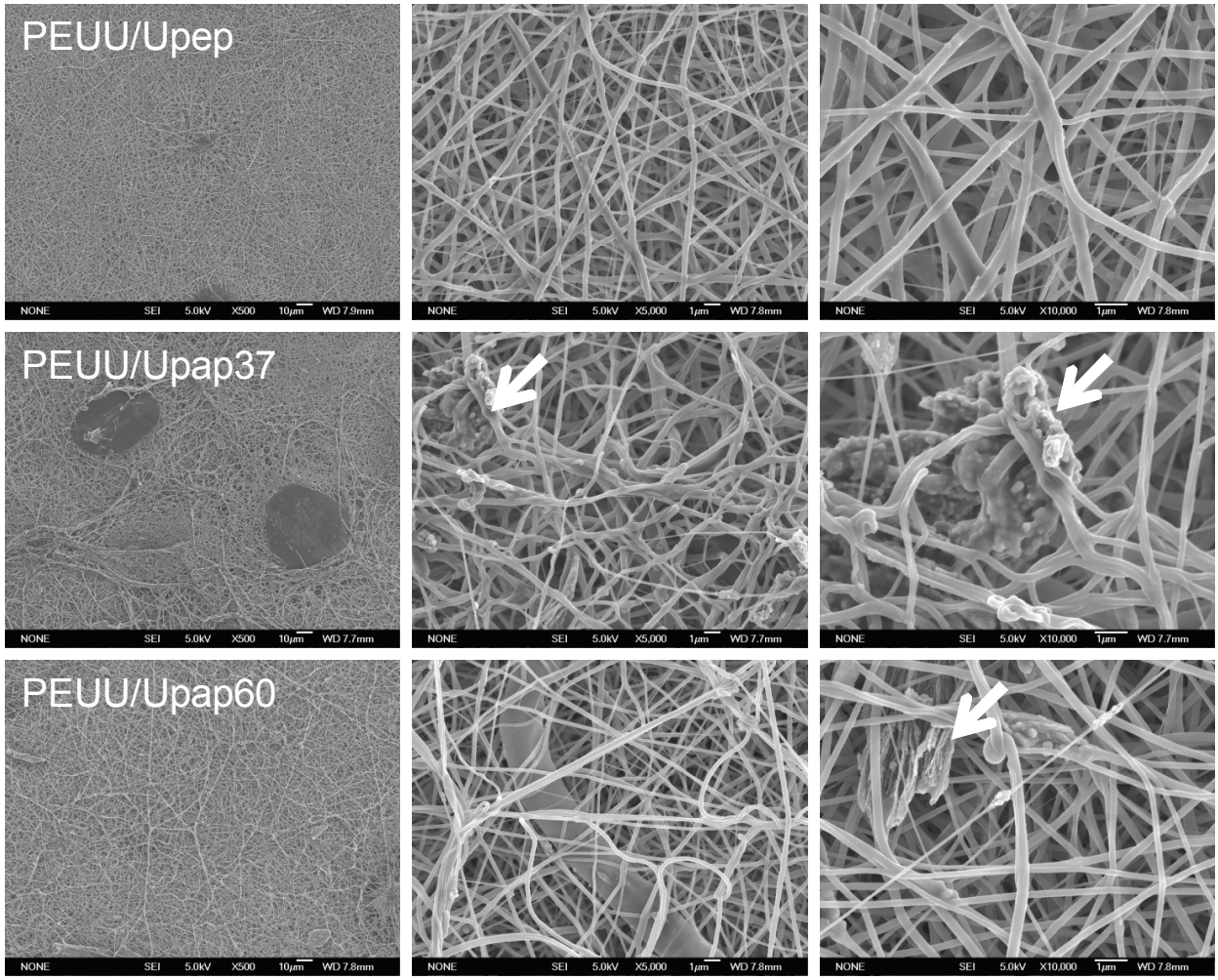

Figure 4-2: Scanning electron microscopy images of hybrid scaffolds at 500x, 5,000x, and 10,000x. Arrows point to UBM particles present on the hybrid scaffolds.

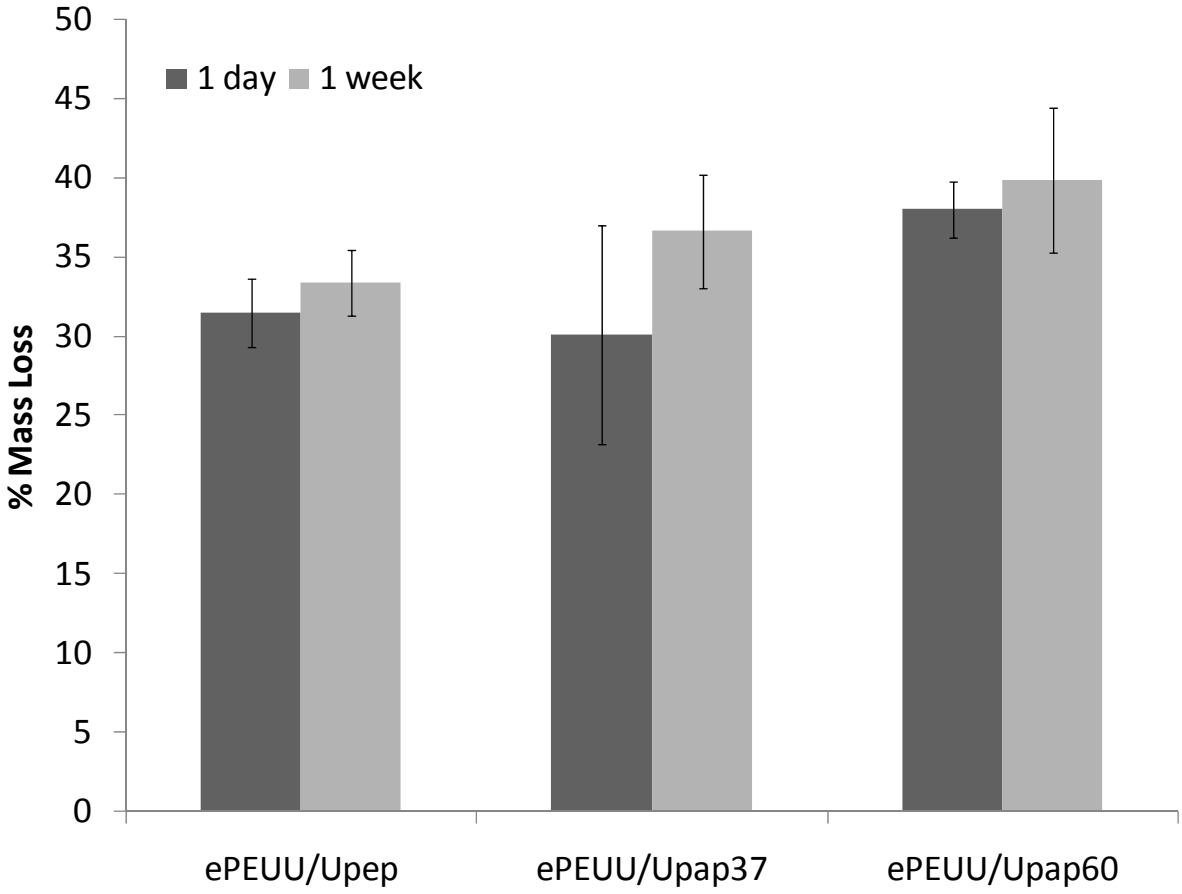

Figure 4-3: Mass loss of hybrid scaffolds after 1 day and 1 week of static *in vitro* incubation (n=3 per sample).

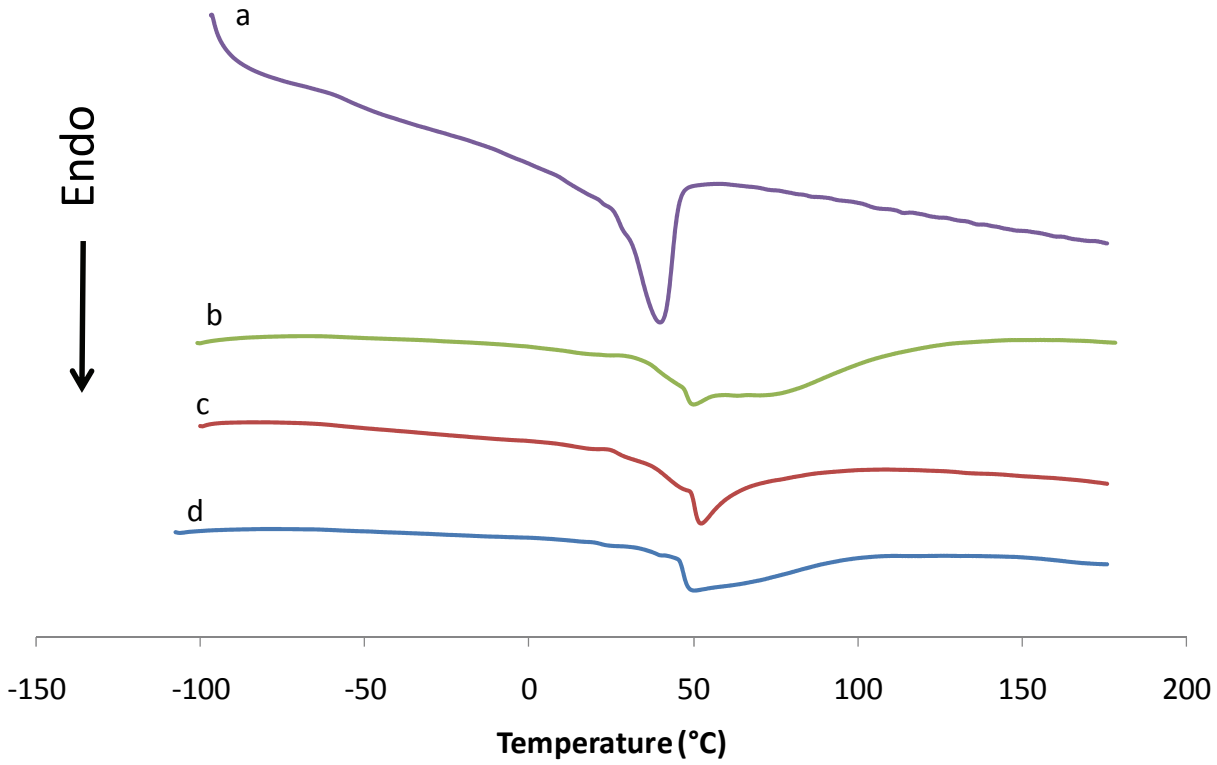

Figure 4-4: Differential scanning calorimetry results for (a) ePEUU, (b) ePEUU/Upap60 (50:50), (c) ePEUU/Upap37 (50:50), and (d) ePEUU/Upep (50/50).

Table 4-1: Structural properties of hybrid scaffolds pre-implant. Mean ± SD

	Structural Properties							
	F_{max} **(N)**		e_{max} **(mm)**		S_{max} **(N/mm)**		$S_{max\ cycle\text{-}1}$ **(N/mm)**	
ePEUU	8.50	(4.24)	28.63	(6.16)	0.65	(0.26)	0.34	(0.14)
ePEUU\Upep	1.87	(1.36)	11.64	(1.43)	0.26	(0.13)	0.12	(0.08)
ePEUU\Upap37	1.91	(1.44)	9.09	(0.66)	0.39	(0.12)	0.15	(0.06)
ePEUU\Upap60	2.17	(1.10)	12.51	(0.75)	0.51	(0.25)	0.14	(0.05)

Table 4-2: Material properties of hybrid scaffolds pre-implant. Mean ± SD

	Material Properties							
	$Stress_{max}$ **(MPa)**		$Strain_{max}$ **(%)**		***MTM*** **(MPa)**		$MTM_{cycle\ 1}$ **(MPa)**	
ePEUU	10.68	(2.84)	408.99	(87.98)	6.45	(2.78)	3.08	(0.65)
ePEUU\Upep	5.73	(1.21)	166.35	(20.43)	6.21	(0.79)	3.33	(2.42)
ePEUU\Upap37	5.85	(0.96)	129.92	(9.48)	10.15	(3.44)	3.71	(1.42)
ePEUU\Upap60	8.29	(1.75)	178.77	(10.66)	14.19	(4.79)	4.20	(1.91)

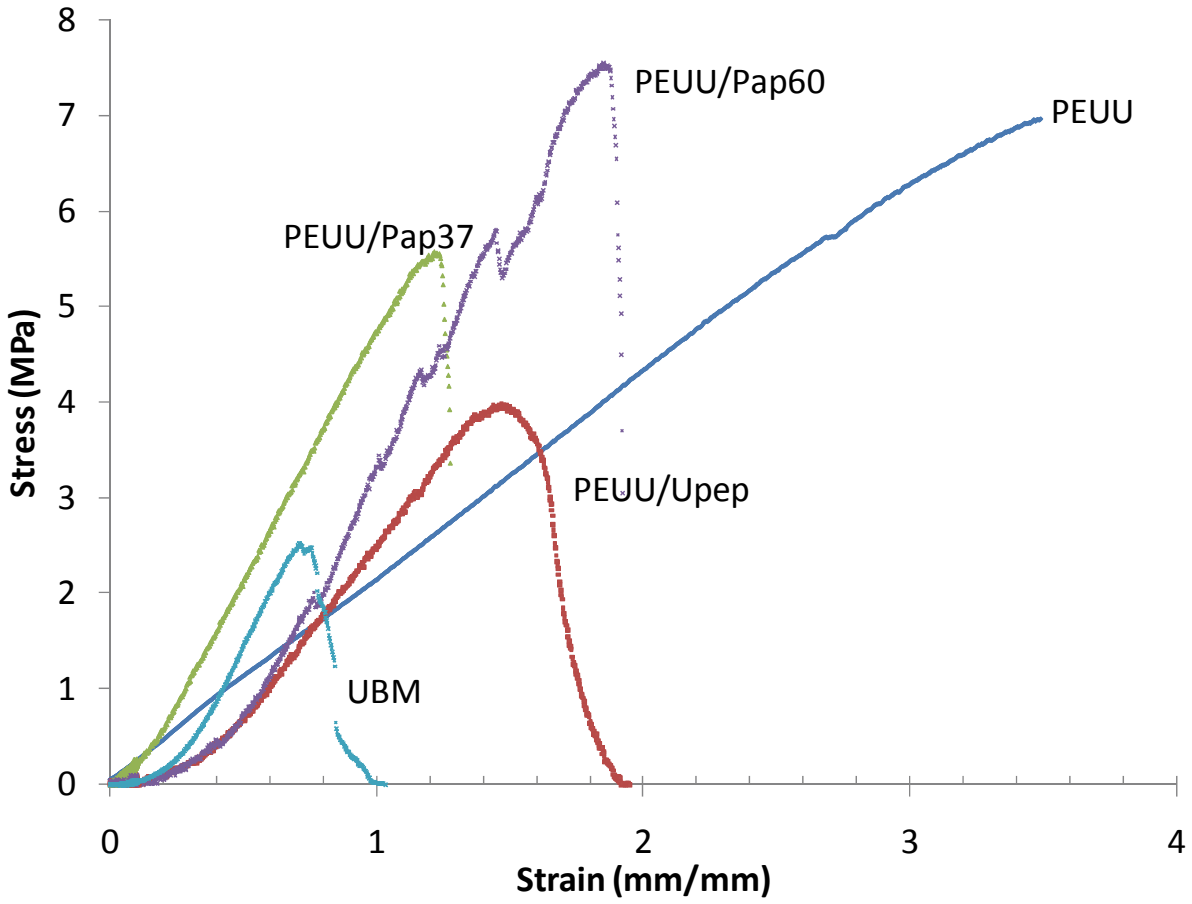

Figure 4-5: Representative stress versus strain curves for PEUU, PEUU/Upep, PEUU/Upap37, PEUU/Upap37, and UBM (pre-implant).

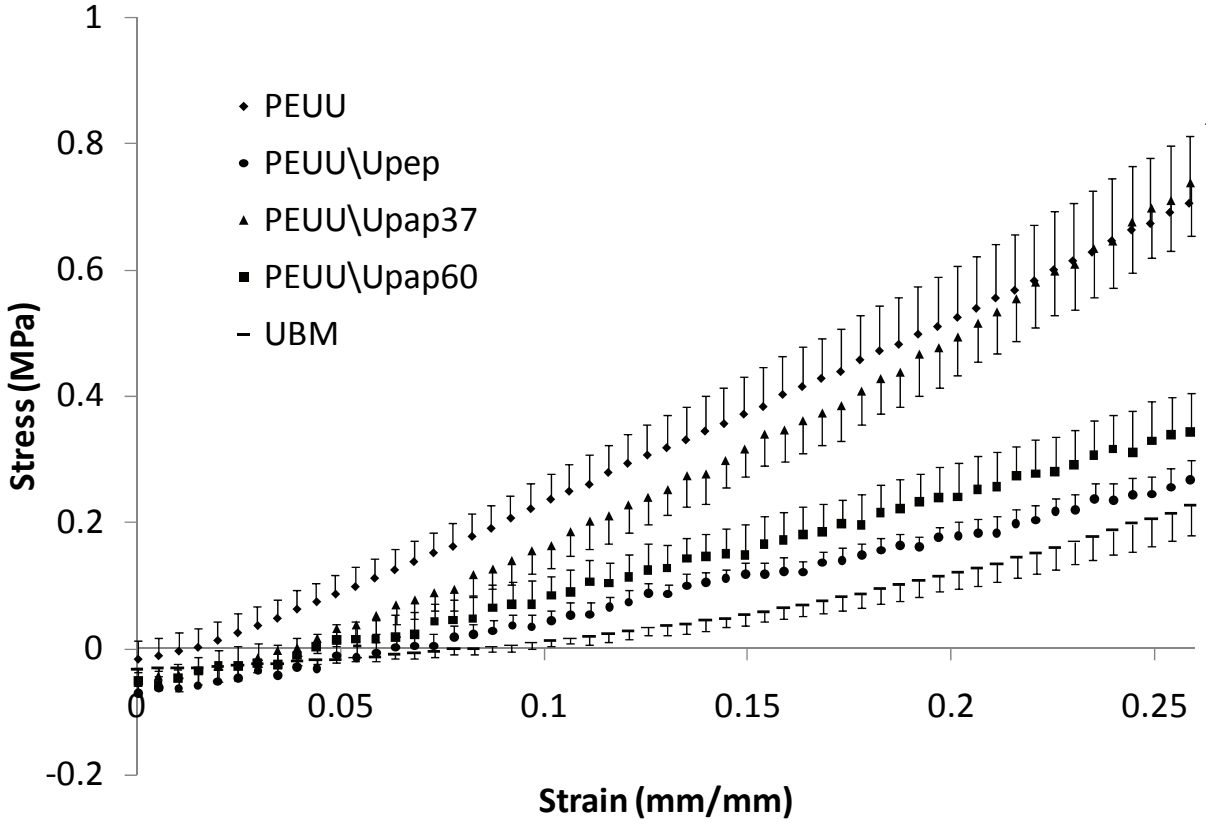

Figure 4-6: Stress versus strain curves for PEUU, PEUU\Upep, PEUU\Upap37, PEUU\Upap60, and UBM. Mean ± SE.

4.3.2 In vitro Growth of Human Aortic Endothelial Cells

Human aortic endothelial cells (HAECs) were grown on tissue culture plate (TCP), PEUU, and hybrid scaffolds for 1 and 4 days. Results from the *in vitro* culture of HAECs on PEUU and hybrid scaffolds are summarized in Figure 4-7. All scaffold materials supported the growth human aortic endothelial cells. PEUU and hybrid scaffolds had fewer cells than tissue culture plate. There was no difference in the number of HAECs grown on PEUU versus the hybrid scaffolds after one and four days of culture. There was a decrease in cell number between 1 and 4 days for PEUU/Upep and PEUU/Upap60 ($p<0.05$). There was a slight difference in cell numbers between 1 and 4 days of culture for PEUU and PEUU/Upap37 ($p<0.1$).

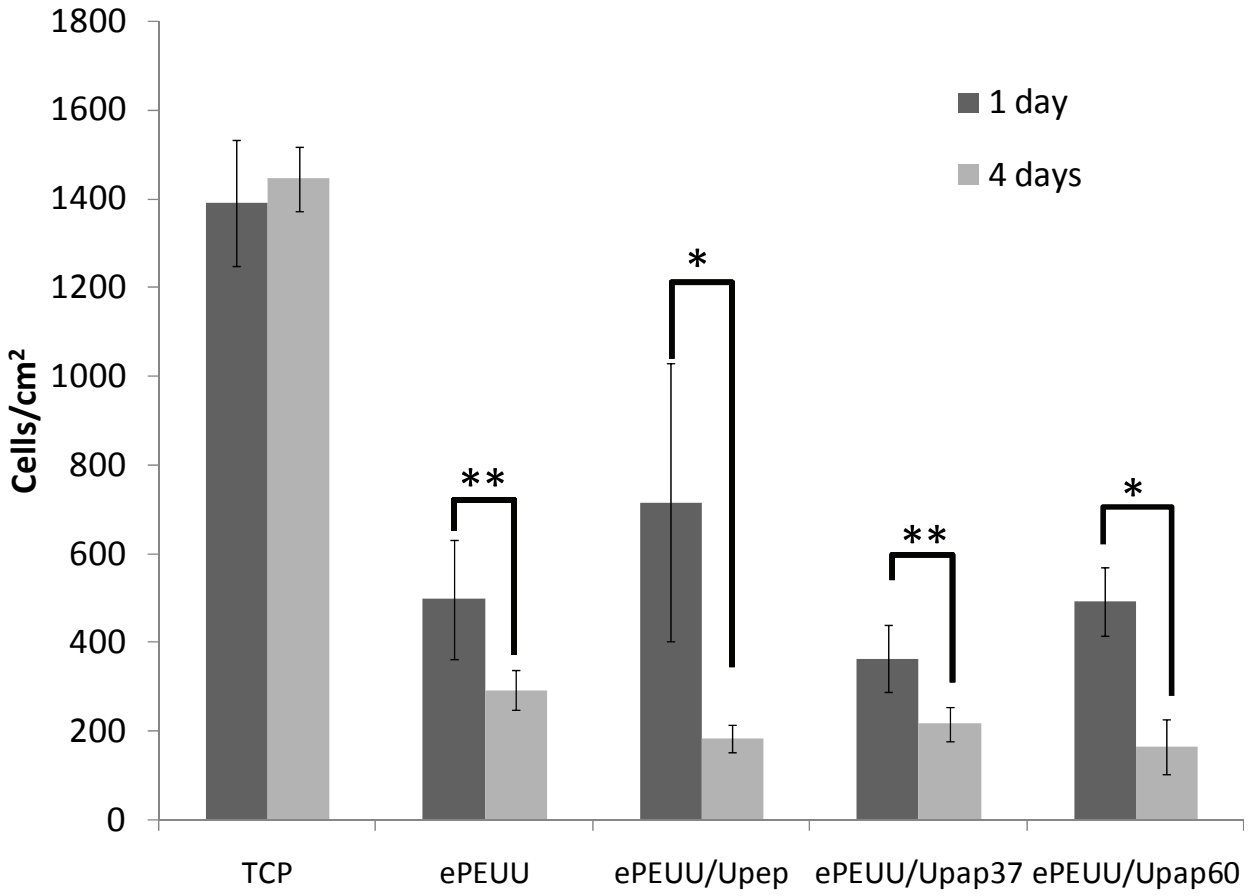

Figure 4-7: Results from 1 a 4 day culture of human aortic endothelial cells on tissue culture plate (TCP), PEUU, PEUU/Upep, PEUU/Upap37, and PEUU/Upap60. *p<0.05; **p<0.1

4.3.3 In vivo Host Tissue Response to UBM/PEUU Scaffolds

The host tissue response and *in vivo* degradation of electrospun PEUU and UBM/PEUU hybrid scaffolds were evaluated using a rat subcutaneous tissue implant model. There was no gross evidence of infection at the time of harvest for both the PEUU and the PEUU/UBM scaffolds. The host tissue response to the PEUU scaffold was characterized by the encirclement of the scaffold by mononuclear cells with little or no scaffold invasion or scaffold degradation as shown in Figure 4-8. PEUU/Upep (75/25) scaffolds were characterized by a thick cellular layer

surrounding the scaffold with small amounts of cellular infiltration when compared to the PEUU scaffold alone and a small amount of delamination as shown in Figure 4-8. Degradation of the lamellae was more pronounced in the PEUU/Upep (25/75) scaffolds when compared to PEUU alone or PEUU/Upep (75/25) (Figure 4-8).

The increase in *in vivo* scaffold degradation and cellular infiltration found with greater UBM concentration *in vivo* is consistent with the degradation rates and cellular adhesion and proliferation observed *in vitro*. PEUU/Upep (25/75) scaffolds were partially degraded and were infiltrated with cells throughout the cross-section of the material. New ECM present within the scaffold material and it is most likely that this neo-ECM was deposited by the cellular infiltrate (Figure 4-8). The histologic appearance of the scaffolds after 28 days in a subcutaneous location showed that the addition of the UBM to the electrospun scaffolds resulted in changes in the host tissue response. Figure 4-9 shows that the method of sterilization did not affect the histological appearance of the host tissue response to the hybrid scaffolds. Future studies will be necessary to characterize the phenotype of the cells that are recruited as a result of the UBM component of the hybrid materials. It is also important to note that although the initial mechanical properties can be controlled during the manufacturing of the scaffold, long-term outcome and clinical efficacy of the scaffold will ultimately depend upon the host tissue response and tissue remodeling.

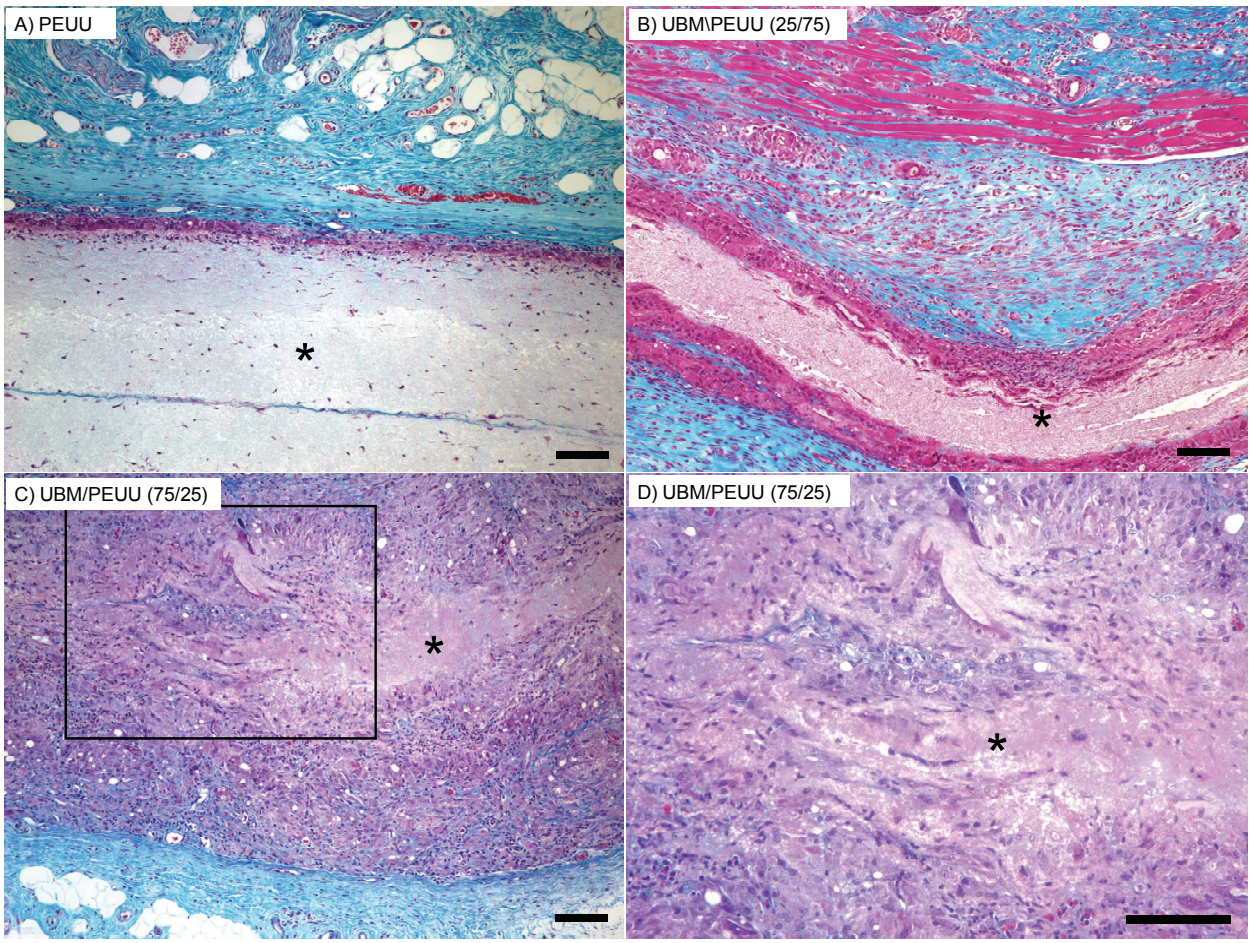

Figure 4-8: Masson's Trichrome stain of cross-sectional views of scaffolds implanted in a subcutaneous pocket of rats for 28 days: (A) PEUU scaffold 10x ; (B) UBM/PEUU (25/75) scaffold 10x; (C) UBM/PEUU (75/25) 10x; (D) UBM/PEUU (75/25) 20x magnification of box shown in (C) [29]. Star (*) denotes the scaffold material. (scale bars = 100 μm)

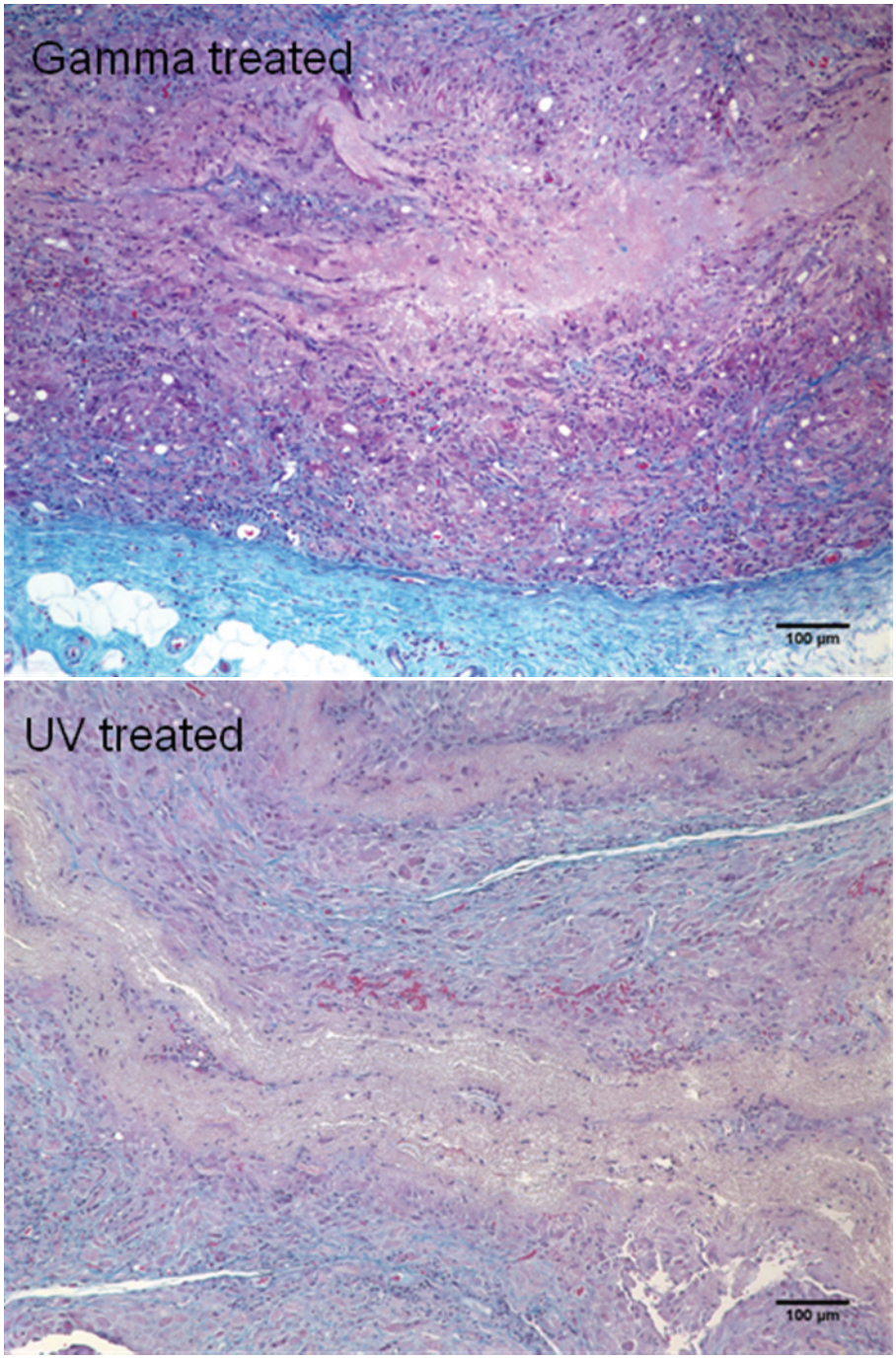

Figure 4-9: Host tissue response to PEUU/Upep (25/75) after 28 days in a subcutaneous tissue pocket in a rat model. Top picture shows the host tissue response to a hybrid scaffold sterilized by gamma irradiation 2.0 Mrads; Bottom image shows the host tissue response to a hybrid scaffold sterilized via exposure to UV for 2 hours. Both images are 100x. Both images show delamination of the scaffold with a dense mononuclear cellular infiltrate.

4.4 DISCUSSION

Electrospinning has been used to create different types of scaffolds for tissue engineering and regenerative medicine applications by re-creating fiber morphology and ultrastructure that is similar to the ECM of tissues. Electrospinning can be used to create scaffolds with anisotropy that mimic tissues or can be used to micro-integrate cells to create a scaffold-cell construct [27, 28]. Poly(ester-urethane)ureas (PEUU) are among the new line of biodegradable elastomers that can be electrospun to create elastic scaffolds suitable for cardiac tissue engineering applications [25, 100]. PEUU can also be combined with other biologic components such as collagen, growth factors, and bioactive peptides to impart bioactivity to the scaffold and guide the host tissue response when used as an implantable material [20, 22, 23, 27, 28, 90]. As stated in Chapter 1, extracellular matrix (ECM) scaffolds have been shown to have bio-inductive properties leading to the constructive remodeling of tissues [4, 12, 30, 172]. The constructive remodeling response is most likely a result of a complex interplay of inhibitory and stimulatory molecules that affect cell migration, activation, and proliferation. One of the objectives of the present work was to combine the constructive remodeling characteristics found in ECM scaffolds with PEUU, a biodegradable elastomer, to create a bioactive hybrid scaffold. The rational was to use the PEUU component to control the ultrastructural morphology (such as fiber morphology) and mechanical properties of the scaffold while using the ECM to impart bioactivity in order to induce a constructive remodeling. The present study characterized hybrid scaffolds processed via electrospinning of a mixture of PEUU and enzymatically digested UBM. The ultrastructural

morphology, mechanical properties, *in vitro* growth of human aortic endothelial cells, and the *in vivo* host tissue response were studied. This chapter describes the first steps towards the manufacture of hybrid scaffolds composed of an elastomer and a biologic scaffold material.

Papain digested UBM was not readily soluble in hexafluoroisopropanol (HFIP) while papain digested UBM was soluble in HFIP at 6 wt%. The concentration used in the present study was selected based on previous studies showing 6 wt% as the optimum concentration for electrospinning UBM [29]. Electrospun pepsin digested UBM formed a fibrous structure that was indistinguishable from the fibrous structure from the electrospun PEUU. Electrospun papain digested UBM (at 37°C and 60°C) showed agglomerates found throughout the hybrid scaffolds. The differences in ultrastructural appearance of the hybrid scaffolds could be attributed to the differences in the constituents within each type of UBM digest. As described in Chapter 2, there are some differences in the solubility, collagen content, and sulfated glycosaminoglycans content between papain and pepsin digested UBM. The chemical environment used to enzymatically digest UBM using pepsin allows for the solubilization of collagen molecules which can be electrospun using the techniques described here without the need of a synthetic component. However, electrospun collagen molecules lack the mechanical properties and stability needed to create scaffolds for load bearing applications and often require chemical cross-linking as a final step during its preparation. Papain digested UBM did not exhibit the same degree of solubility in HFIP and may be elctrospun as UBM particles as shown in the scanning electron microscopy images. It is unclear if papain digested UBM can be electrospun into fibers alone as the case for pepsin digested UBM.

Stankus et al. previously looked at the incorporation of collagen into electrospun PEUU scaffolds [23]. Our group, in collaboration with Dr. William Wagner's laboratory, has also

investigated the incorporation of pepsin digested UBM into electrospun PEUU scaffold with encouraging results [29]. The present study focused on a 50/50 blend of pepsin and papain digested UBM for *in vitro* experiments to maximize the mechanical integrity of the scaffold and the amount of UBM present within the scaffold material. There was a rapid decrease in weight after 1 day of static *in vitro* degradation for all the hybrid scaffolds. There was a 30-40% mass loss in all scaffolds and the trend was sustained after 7 days. The mass loss is less than the loss reported after 2 weeks of static *in vitro* degradation of an unsterilized 50/50 UBM/PEUU hybrid scaffold [29]. The thermal properties of electrospun scaffolds were also compared using DSC. PEUU has been shown to have a glass transition temperature (T_g) of -56°C and a soft segment melting temperature of ~41°C [23, 29]. UBM by itself has been shown to have a very broad transition between 30°C and 108°C (data not shown) which could represent dehydration of the UBM. A similar transition has been observed by Guan et al. in collagen and PEUU/collagen combinations manufactured using thermally induced phase separation (TIPS) [18]. The hybrid scaffolds showed a slight increase in the melting temperature and a broadening of the peak found between 50°C and 100°C. The broadening of the peak represents the change in melting temperature caused by the addition of the UBM component. The shift in the melting temperature of the scaffold could be due to the addition of the UBM as well. The glass transition temperature was not apparent in the UBM hybrid scaffolds although a previous study showed that a PEUU/Upep (25/75) hybrid scaffold did not affect the glass transition temperature of the PEUU; a finding that suggests that the UBM and PEUU were immiscible.

The addition of UBM to the PEUU altered the shape of the stress-strain curves as shown in Figure 4-5. Figure 4-6 shows the average stress-strain curves of hybrid scaffolds, PEUU, and UBM. The extent of the contribution of UBM to the mechanical properties of the hybrid

scaffolds is not clear. Based on observation and the rapid burst release of the UBM, it is more likely that the PEUU component carries the mechanical load of the hybrid scaffolds. The Hybrid scaffolds and UBM have similar stress-strain relationships under low strain values (<0.1). Cardiac patches should undergo ~30-40% strain based on native *in vivo* strain measurements [173]. At these values, differences in the mechanical behavior between the hybrids and UBM begin to become more evident. The high tensile strength and breaking strains of the hybrid scaffolds make them suitable for cardiac tissue engineering where strength is needed to withstand the pressure of the ventricle soon after implantation and during the entire remodeling process. Ideally, the mechanical stability imparted by the PEUU will allow for cellular in growth and cardiac tissue reconstruction to occur. The *in vivo* assessment of the hybrid scaffold as a cardiac patch will be discussed in Chapter 5.

Hybrid scaffolds are more hydrophilic than the PEUU and hydrate much faster (based on observation). The increase in hydrophilicity of PEUU after the addition of collagen was also documented by Stankus [23]. Hydration of the scaffold could be responsible for the changes in shape between PEUU and hybrid scaffolds. Differences could also be attributed to the mass loss that occurs when a sample is hydrated prior to mechanical testing. Hybrid scaffolds shrink in size after hydration and such change could affect the mechanical behavior of the scaffolds. As shown in Table 4-3, the mechanical properties of the electrospun PEUU match the values obtained in previous studies with the exception of a higher maximum strain value on the PEUU tested in this study [23, 29]. Since one objective of the present work was to eventually use the PEUU as a cardiac patch, thicker scaffolds were constructed (~600μm in thickness). The higher breaking strain found on the PEUU samples when compared to previous studies could be due to the thickness of the scaffold prepared and used in the present study. Similar tensile strengths

were observed between collagen hybrids and UBM hybrids (comparisons are summarized in Table 4-3). UBM hybrids had a lower breaking strain than collagen hybrids. The differences could arise from the sterilization step or differences during the processing of the scaffold material (i.e. different polymer batch, differences in collagens present in the UBM, etc). Gamma irradiation can also affect the mechanical properties of a scaffold by creating cross-links and/or backbone scissions of the polymer fibers [17]. However, no differences were observed between gamma treated and UV sterilized PEUU/Upep hybrid scaffolds suggesting that sterilization by exposure of the scaffolds to 2.0 Mrads of ionizing radiation does not affect mechanical properties of hybrid scaffolds. Exposure of UBM scaffolds to ionizing radiation has been shown to decrease the maximum strength and elongation values [70]. The PEUU component might not be as susceptible to backbone scission when compared to lyophilized UBM scaffolds.

Table 4-3: Comparison of the mechanical properties of the present study with previous studies using electrospun PEUU.

	Stress$_{max}$ **(MPa)**		***Strain$_{max}$*** **(%)**		***MTM*** **(MPa)**		***REF***
ePEUU	10.68	(2.84)	408.99	(87.98)	6.45	(2.78)	Present Study
ePEUU\Upep	5.73	(1.21)	166.35	(20.43)	6.21	(0.79)	Present Study
ePEUU\Upap37	5.85	(0.96)	129.92	(9.48)	10.15	(3.44)	Present Study
ePEUU\Upap60	8.29	(1.75)	178.77	(10.66)	14.19	(4.79)	Present Study
ePEUU*	13	(4)	220	(80)	8	(2)	[23]
PEUU (Film)	27	(4)	820	(70)	60	(10)	[23]
ePEUU\Col*	6	(1)	240	(3)	3	(1)	[23]
ePEUU*	12.9	1.7	220	(77)	--	--	[29]
ePEUU\Upep*	4.8	(1.6)	143	(10)	--	--	[29]

*Non-sterilized scaffolds

Stankus et al. showed an increase in the growth of rat smooth muscle cells on electrospun PEUU/Upep scaffolds when compared to PEUU scaffolds and tissue culture plate [29]. There was no difference between PEUU and hybrid scaffolds in the present study using human aortic endothelial cells and there was a decrease in cell numbers when compared to tissue culture plate. The apparent disagreement between both studies could be a result of the type of cells used. Rat smooth muscle cells are a rapidly proliferating cell type when compared to human aortic endothelial cells. The scaffolds in the present study were moved to different wells during the *in vitro* seeding to allow cells that attached to the scaffolds to proliferate without the involvement of cells that attached to the bottom of the well. If the cell attachment strength was low, the transfer between wells could potentially disrupt the attachment a significant number of cells

appearing as a decrease in cell numbers. Such decrease was observed in the present study between 1 and 4 days in culture. HAECs could also be responding to the UBM component in the hybrid scaffolds. As stated in Chapter 2, enzymatically digested UBM showed no mitogenic properties for HAECs cells while showing a slight stimulatory effects upon a myogenic cell line (C2C12 myoblasts). If this activity was present and sufficient in the hybrid scaffolds, the involvement of UBM could also explain the differences observed between the present study using HAECs and the study by Stankus et al. Future studies will address this discrepancy and will examine the growth of C2C12 on hybrid scaffolds. If the growth of myoblasts on hybrid scaffolds mimic those reported in Chapter 2, the lower numbers of HAECs and the higher numbers of myogenic cells could be explained by the presence of UBM in the hybrid scaffolds.

The present study also examined at the *in vivo* host tissue response of the PEUU/Upep hybrid scaffold in a subcutaneous model. PEUU/Upep at 25/75 and 75/25 ratios were used in the *in vivo* study of hybrid scaffolds to ensure that changes in the host tissue response could be detected by histological evaluation after the 14 and 28 days of implantation period. The increase in scaffold degradation and cellular infiltration with increasing UBM concentration *in vivo* is consistent with the degradation rates and cellular adhesion and proliferation reported in previous *in vitro* studies. PEUU/Upep (25/75) hybrid scaffolds were degraded *in vivo* and showed cells present throughout the cross-section of the material. Newly deposited ECM was also a product of the cellular infiltrate. The degree of cellular infiltration appears to be directly related to the extent of degradation of the scaffold materials or likely there was positive feedback between these processes. The morphological appearance of the scaffolds after 28 days in a subcutaneous location showed that the addition of the UBM to the electrospun scaffolds resulted in changes in the host tissue response. In addition, the sterilization of the scaffold using UV or

gamma irradiation did not affect the histological appearance of the host tissue response. Future studies will be necessary to characterize the types of cells that are recruited as a result of the UBM component of the hybrid materials. Preliminary results show (see Figure 4-10) that the cells found around and within the scaffolds after 28 days are CD68 positive cells. CD68 is a positive phenotypic marker for macrophages. Macrophages can be found in two distinct subpopulations with a unique phenotypic profile depending on the type of host tissue response elicited [174-176]. This macrophage response is analogous to the Th-1 and Th-2 response described in the transplant immunology literature. Future studies will look at the host tissue response and determine if the hybrid scaffolds elicit a type I or a type II macrophage response. It is also important to note that although the initial mechanical properties can be controlled during the manufacturing of the scaffold, long-term outcome of the scaffold will ultimately depend upon the host tissue response and tissue remodeling.

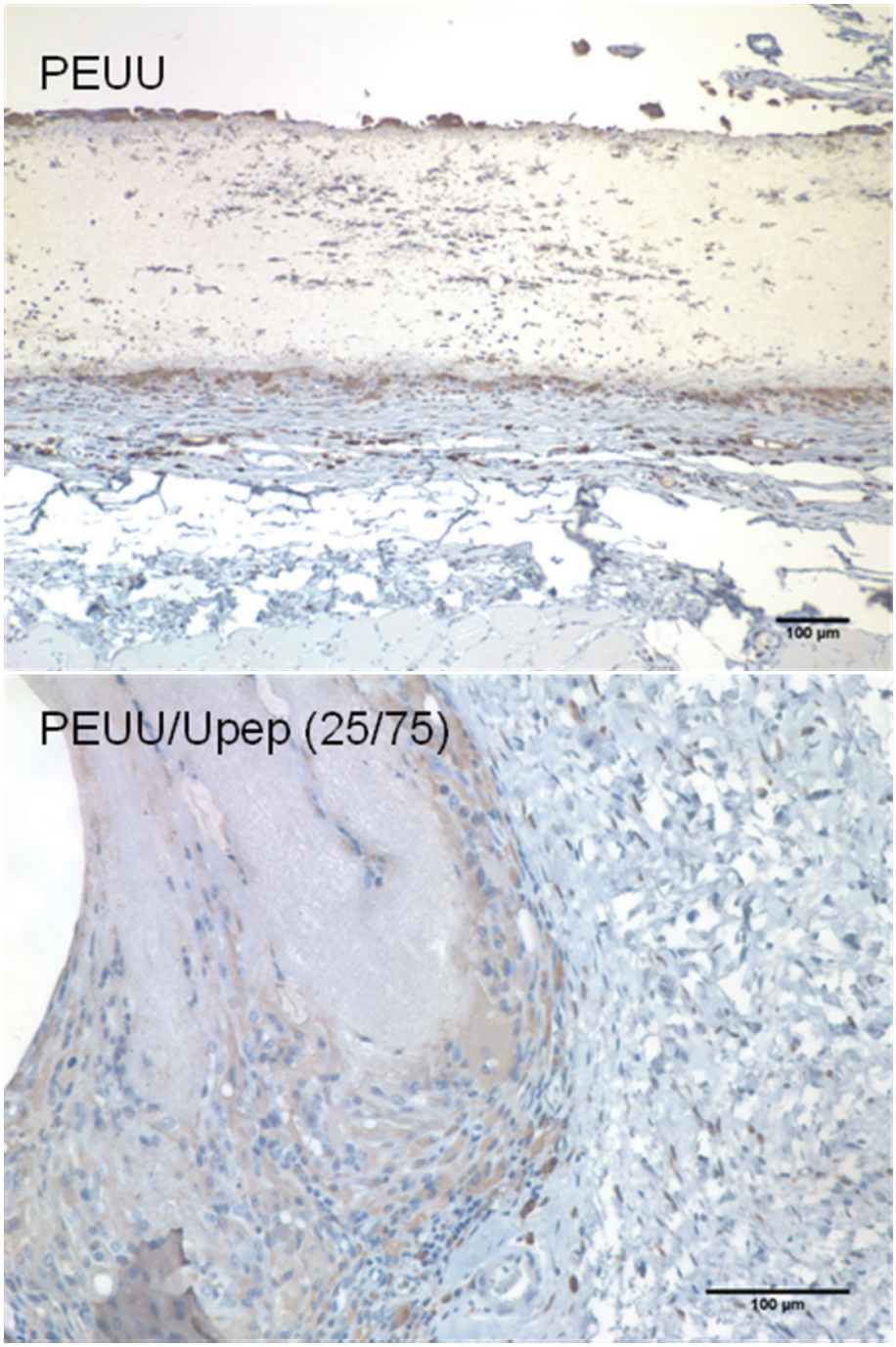

Figure 4-10: Histological section of samples implanted in a subcutaneous pocket for 28 days in a rat model stained for CD68: (Top) PEUU and (Bottom) PEUU/Upep 25/75. Stain courtesy of Bryan Brown.

4.5 LIMITATIONS AND FUTURE WORK

The work presented provided the first attempt at creating a hybrid scaffold created from the electrospinning of enzymatically digested UBM and PEUU. Papain and pepsin digested UBM can be used in combination with PEUU to create hybrid scaffold for soft tissue reconstruction and more specifically for cardiac tissue engineering.

For practical purposes, only 50/50 blends were studied. A 1:1 ratio allowed for equal amounts of synthetic and natural components while retaining suitable mechanical properties to withstand the pressures in the left ventricle. However, other blends could be attempted. Since the optimum concentration of UBM needed to tilt the balance towards a more constructive remodeling and away from fibrous encapsulation is unknown, the exploration of different blends remains hard to assess. Based on these studies and a study recently published, regardless of the type of UBM used and the selected ration, there is always a large amount of mass lost during the first day of *in vitro* degradation. Although not directly tested, this burst release most likely occurs during the first few hours of hydrolytic degradation. This suggests that regardless of the amount of UBM used (75, 50, or 25) only ~10-20% of it will remain after hydration. This limits the amount of UBM that can be delivered to the site of implantation. Other methods should be employed to retain the UBM component in the hybrid scaffolds in order to have a controlled release of bioactive molecules. Future work should focus on the retention of the UBM.

Another limitation of the present study is that only material properties and *in vitro* growth of HAECs were used to assess the differences between the different types of hybrid scaffolds. No differences were found *in vitro* and there for *in vivo* work is the next logical step and the most accurate way to determine any advantage. This should also be the focus of future studies.

5.0 HYBRID SCAFFOLDS AS A LEFT VENTRICULAR PATCH

5.1 BACKGROUND

Heart failure (HF) is the inability of the heart to pump blood in sufficient amounts to maintain adequate tissue perfusion [93]. HF can be the end manifestation of nearly all cardiac diseases including coronary atherosclerosis, myocardial infarction, valvular diseases, hypertension, congenital heart diseases, and cardiomyopathies. One of the most common causes of HF is acute myocardial infarction (MI) where one or more blood vessels supplying the heart are occluded inhibiting the transfer of oxygen and nutrients to regions of the myocardium [93, 94]. This ischemic insult leads to irreversible cell death within the myocardium, changes in the geometry of the ventricle, and results in impaired ventricular contractility and increased myocardial stiffness. Decrease in left ventricular contractility will reduce the stroke volume (the volume pumped by the heart) and the heart will attempt to compensate by increasing the force of contraction via dilation of the ventricle. The increase in contraction as a result of dilation occurs due to the stretch of the myofibers and thus increasing the affinity of Troponin to calcium (two components important for cardiac muscle contraction) resulting in an increase in the force of contraction [93, 94]. However, this compensatory mechanism only works for small deformations and for a short period of time. As dilation increases, the stresses and energy consumption on the ventricular wall increases. The end result is a decrease of the cardiac output

to levels of inadequate perfusions and to progressive heart failure [93, 94]. Figure 5-1 shows the progression of ventricular dilation as a result of myocardial infarction.

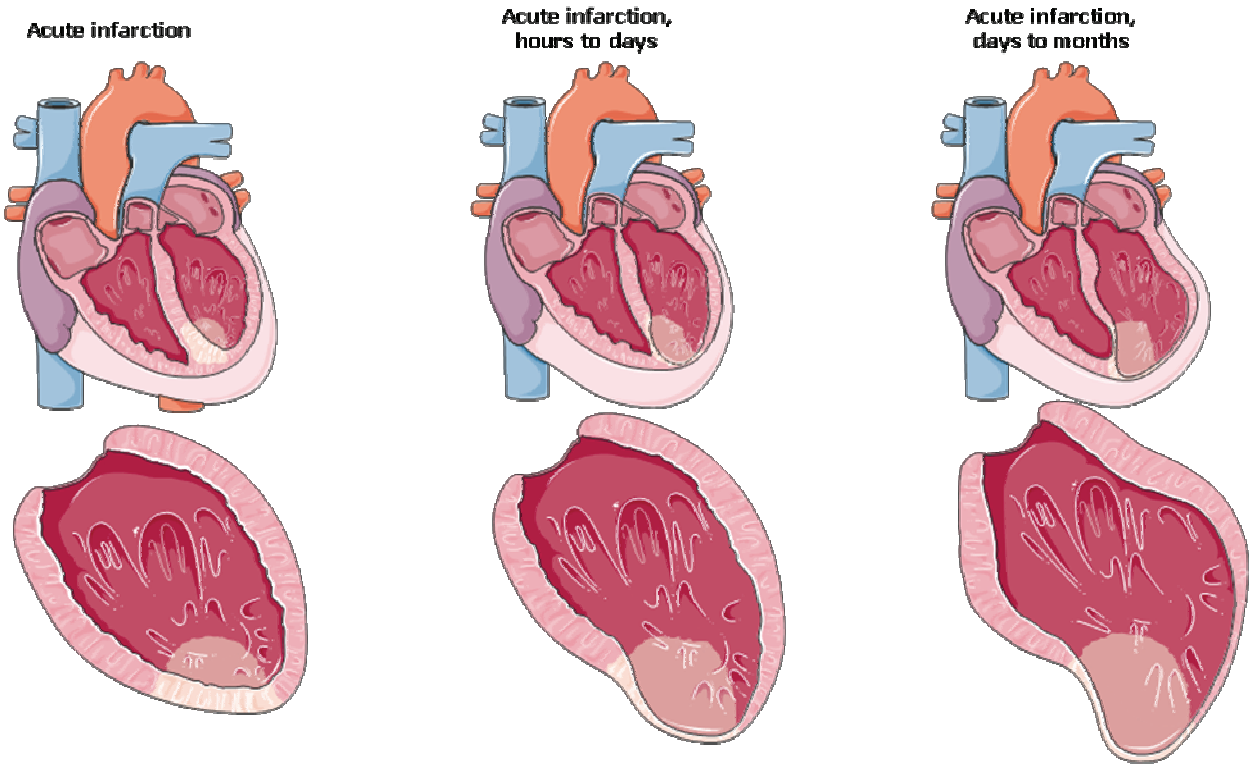

Figure 5-1: Progression of heart failure after myocardial infarction (From Servier Medical Art at www.servier.com).

The current "gold standard' of treatment for heart failure is heart transplantation. However, there is a large gap between available donors and the number of patients in need of a heart transplant. Current surgical treatments attempt to restore the geometry of the ventricle by removing the dilated ventricular tissue. The most common surgical techniques used are endoventricular circular patch plasty (EVCPP), partial left ventriculectomy (Batista operation), or the use of cardiac support devices (such as the Apicorn CorpCap mesh). In the EVCPP procedure, the non-viable tissue is removed and replaced by a synthetic patch resulting in

improved systolic and diastolic functions due to the reshaping of the ventricle. However, the use of a synthetic patch leads to fibrous encapsulation of the surgical mesh without the integration of the surrounding tissue or the infiltration of cardiomyocytes to the scaffold [92]. An ideal scaffold could be used to reshape the ventricle and would promote reconstruction of normal myocardium. One such mechanism may involve degradation of the scaffold at an appropriate rate while attracting resident and circulating stem cells and progenitor cells to the remodeling site culminating in the formation of functioning myocardium. Stated differently, the ideal scaffold would degrade while instructing the host tissue to create functioning myocardium.

ECM scaffolds have found encouraging success for the repair of cardiac tissue by avoiding scar tissue formation and by inducing constructive remodeling. UBM was used by Kochupura et al. to repair a full thickness defect in the right ventricle in a canine model with a single sheet of UBM [113]. After 8 weeks, the UBM patch improved regional mechanical function and cardiomyocytes were found within the remodeling tissue. Another study used a single sheet of UBM to repair a 2 cm^2 full thickness defect in a canine model showing improvements in regional systolic contraction when compared to defects repaired with Dacron after 8 weeks [6]. The scaffold was degraded and cardiomyocytes were found randomly distributed within the remodeling site. However, UBM was not completely replaced by functioning myocardium, remains constrained to the mechanical properties of the urinary bladder, and may not possess the appropriate mechanical properties needed for the reconstruction of cardiac tissue.

PEUU scaffold manufactured using thermally induced phase separation (TIPS) have been investigated as a myocardial patch in LV infarcted myocardium or in a surgical defect in the right ventricular outflow tract. Six millimeter defects created in the right ventricular outflow

tract of rats repaired with PEUU showed cellular integration with endothelialization. The same patch placed on the surface of infarcted myocardium showed the in-growth of contractile smooth muscle tissue formation and improvement in long-term contractile function [25, 100]. However, the constructive remodeling observed with the ECM scaffolds was not observed in the PEUU scaffolds under the conditions studied.

The present study uses the hybrid scaffold created by electrospinning of PEUU and UBM to repair a full thickness defect in the left ventricle in a canine model. A 50/50 blend was selected based on mechanical properties and to maximize the amount of UBM delivered per scaffold material.

5.2 EXPERIMENTAL DESIGN AND DISCUSSION

5.2.1 Animal Model

The present study examined the differences between the synthetic control material (PEUU) and a hybrid scaffold composed of both PEUU and enzymatically digested UBM. All animal procedures were performed in accordance with the National Institutes of Health guidelines for care and use of laboratory animals and with the approval of the Institutional Animal Care and Use Committee. The parameters of interest were degree of remodeling and tissue contractility. Four dogs (n=4 each) were subjected to a partial sternotomy and were placed on cardiovascular bypass (CBP). A 2 cm^2 left ventricular defect was created and the defect was surgically repaired by direct placement of a PEUU/Upep (50/50) scaffold or a PEUU scaffold.

Clinically healthy dogs were anesthetized (Acepromazine (0.1-0.5 mg/Kg IV)). Animals were maintained at a surgical plane of anesthesia with Isoflurane (1-3% in oxygen). Blood pressure was monitored via a pressure transducer in the femoral artery and ECG was monitored throughout the surgical procedure. The animals were infused with 2 ml/kg/h of lactated Ringer's solution or equivalent solution throughout the procedure.

Prior to undergoing the sternotomy, the wound edges were infiltrated with local anesthetic (marcaine or bupivicaine, ~10-15 ml) to decrease pain in the early post-op period thereby improving comfort. A sternotomy was performed and followed by a pericardiotomy and placement of suspension sutures to cradle the heart. Visualization of the heart, the pulmonary valve outflow tract, aorta, and right atrium was accomplished. Heparin was administered intravenously (110-500 IU/kg) and the animal was placed on cardiopulmonary bypass (CPB) by cannulation of the right atrium and aorta or the right atrium and the carotid artery. Canine blood was purchased from Cleveland Scientific (Cleveland, OH) and Marshal Bioresources (North Rose, NY). The first trial used heparinized blood (Cleveland Scientific) while the rest of the surgeries used ACD treated blood (Marshal Bioresources). After draining the left ventricle, a left ventricular defect was created and repaired using the PEUU or hybrid scaffold (see Figure 5-3). The scaffolds were sewn into its place with 7-0 non-absorbable suture material (e.g. Prolene). At the conclusion of surgery, the chest was closed and the animal was weaned off cardiopulmonary bypass. A chest tube was placed prior to closing the chest and maintained up to 72 hours to ensure negative pressure compliance in the chest and to remove any excess drainage present after a procedure of this type. The chest was closed using routine thoracic closure technique (1-0 Prolene for closure of the ribs, 2-0 PDS for SQ and 2-0 Prolene or staples for skin closure).

Following the surgical procedure and cessation of inhalation anesthesia, the animals were continually monitored for 24 hours and the following parameters were recorded every hour: *pulse rate, strength of pulse, capillary refill time, and amount of fluid removed from chest via the chest drain, respiratory rate and the ability to maintain an open airway, urinary output, and defecation*. Body temperature was measured and recorded every 2 hours. Each animal was kept warm and dry to prevent hypothermia and was rotated once per half-hour until it can maintain a sternal position.

Extubation of each dig was performed when the animals exhibited a swallowing reflex and the protective cough reflexes were functional. The pulse, respiration, body temperature, jaw tone, capillary refill time, and mucous membrane color were evaluated prior to the removal of the endotracheal tube. An animal's overall health status was required to be stable prior to extubation, and after extubation the animal was required to maintain an open airway, stable heart rate, respiration rate, body temperature, jaw tone, capillary refill time (3-4 sec), and good (pink) mucous membrane color. Following extubation, the animal began to respond to touch and sound.

Buprenorphine hydrochloride (0.01-0.02 mg/kg, SQ, q12h), was administered at regular intervals for pain. Acute pain in animals is expressed by guarding, vocalization, mutilation, restlessness, recumbency for an unusual length of time, depression (reluctance to move or difficulty in rising), or abnormal appearance (head down, tucked abdomen, hunched, facial distortion). A Lee-White clot time was performed before and after surgery to assess coagulation status. Heparin was titrated with Protamine sulfate (1 mg/100 IU of Heparin) based on the dose of Heparin administered during surgery for the first surgery. Protamine sulfate was not administered to rest of the animals. Blood loss was monitored with a packed cell volume (PCV -

dog, 37-55%, hematocrit -dog, 29.8-57.5) performed at the time of surgery, immediately post-operatively, and after surgery every 2-4 hours for the first 24 hours.

Figure 5-2 and 5-3 shows the macroscopic appearance of the cardiac patches prior to implantation and after implantation and prior to closing the chest wall. Figure 5-4 shows the macroscopical cross-sectional view the first PEUU implant and the histological view of a cross-section. All samples could be handled surgically and were sutured to the adjacent myocardium. PEUU and PEUU/Upep patches were able to withstand left ventricular pressures after implantation and removal of cardiopulmonary bypass. Four animals were implanted with a cardiac patch, three received a PEUU patch and one received a PEUU/Upep 50/50 patch. Table 5-1 compares the mechanical properties of the hydrated PEUU and PEUU hybrid scaffold prior to implantation with synthetic polymers and with the native myocardium. Although not as strong or as stiff as PGA and PLA scaffolds, PEUU and hybrid scaffolds have sufficient mechanical properties for use as a myocardial patch.

Table 5-1: Comparison of the material properties of PEUU with other synthetic polymers and with the native myocardium. For values obtained in the present study data represents mean ± SD.

	$Stress_{max}$ (MPa)		*MTM* (MPa)		*REF*
ePEUU	10.68	(2.84)	6.45	(2.78)	Present Study
ePEUU\Upep	5.73	(1.21)	6.21	(0.79)	Present Study
ePEUU\Upap37	5.85	(0.96)	10.15	(3.44)	Present Study
ePEUU\Upap60	8.29	(1.75)	14.19	(4.79)	Present Study
ePEUU	13	(4)	8	(2)	[23]
PEUU (Film)	27	(4)	60	(10)	[23]
ePEUU\Col	6	(1)	3	(1)	[23]
ePEUU	12.9	1.7	--	--	[29]
ePEUU\Upep	4.8	(1.6)	--	--	[29]
PGA	70		>7000		[177]
PLLA or PDLA	30-80		>1000		[178]
PHB	36		2000		[179]
TMC	12		6		[102]
TMC-PDLL (50:50)	10		16		[102]
PGS	~0.2-0.5		0.04-1.2		[180]
Rat Myocardium	0.03-0.07		0.001-0.14		[180]
Human Myocardium	0.003-0.015		0.02-0.5		[180]

Unfortunately, none of the animals survived beyond 12 hours after surgery. The first animal suffered a stroke after surgery and the rest of the animals were unable to completely come off anesthesia and the animals were euthanized. The reasons for the failure of the dogs to survive are unknown but the cardiopulmonary bypass remains the suspect and the use of whole blood to prime the bypass circuit. All animals were able to breathe on their own after surgery but were not responsive. The first dog expired within 6 hours of surgery with bleeding into the chest cavity. The bleeding was not due to failure of the patch material. Cardiac tamponade and a stroke were suspected in this case. The second dog expired within 8 hours of surgery and was not responsive. The third dog experienced a cardiac arrest during the operation but cardiac function was restored. Blood pressure and heart rate remained excessively high and the animal was euthanized. The fourth animal showed normal clinical signs after surgery (stable BP and HR) but the blood pressure suddenly increased and respiration rate decreased with no obvious explanation. The animal was euthanized.

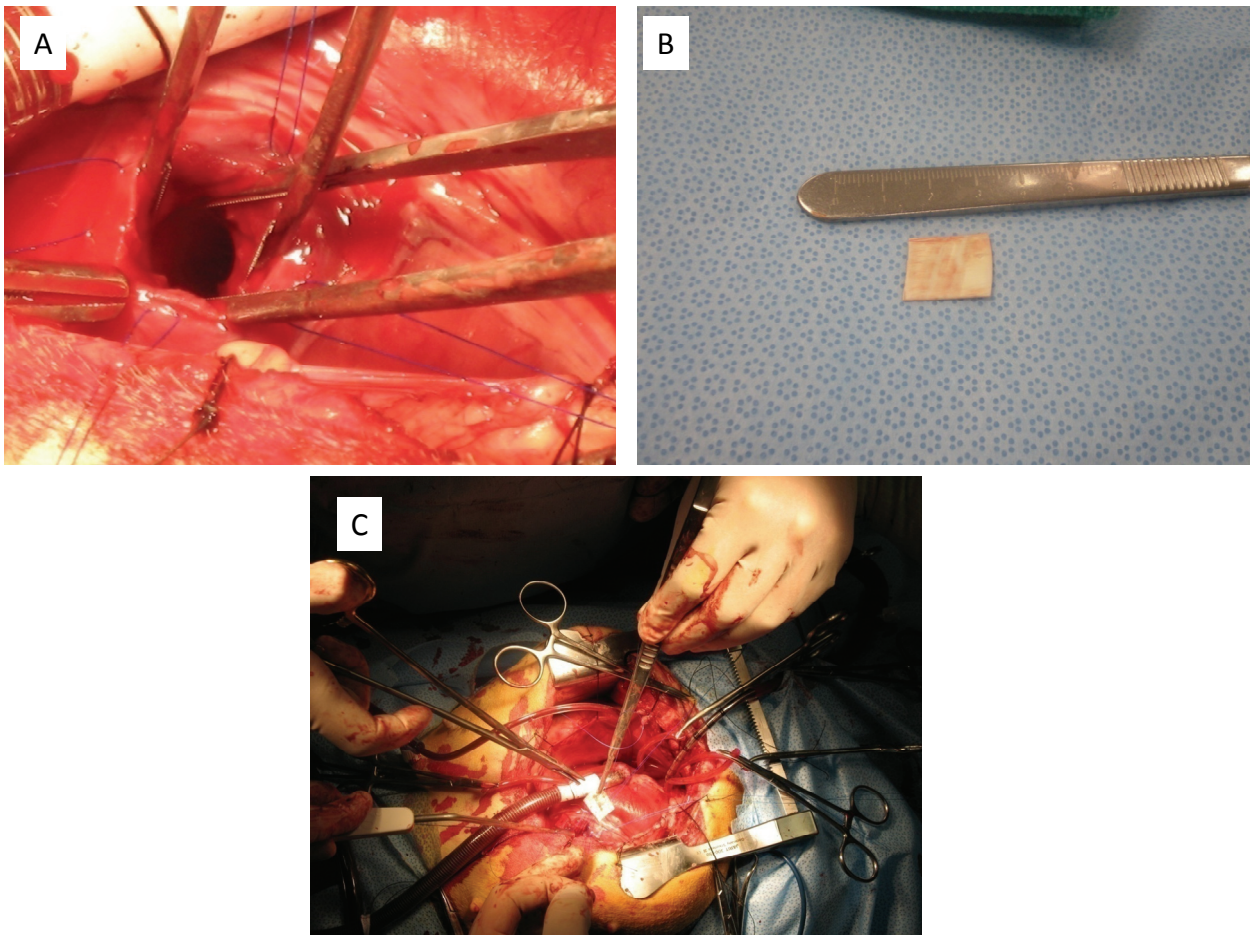

Figure 5-2: (A) Full thickness defect created in the left ventricle; (B) PEUU patch cut before surgery; (C) Placement of the PEUU patch as a left ventricular patch.

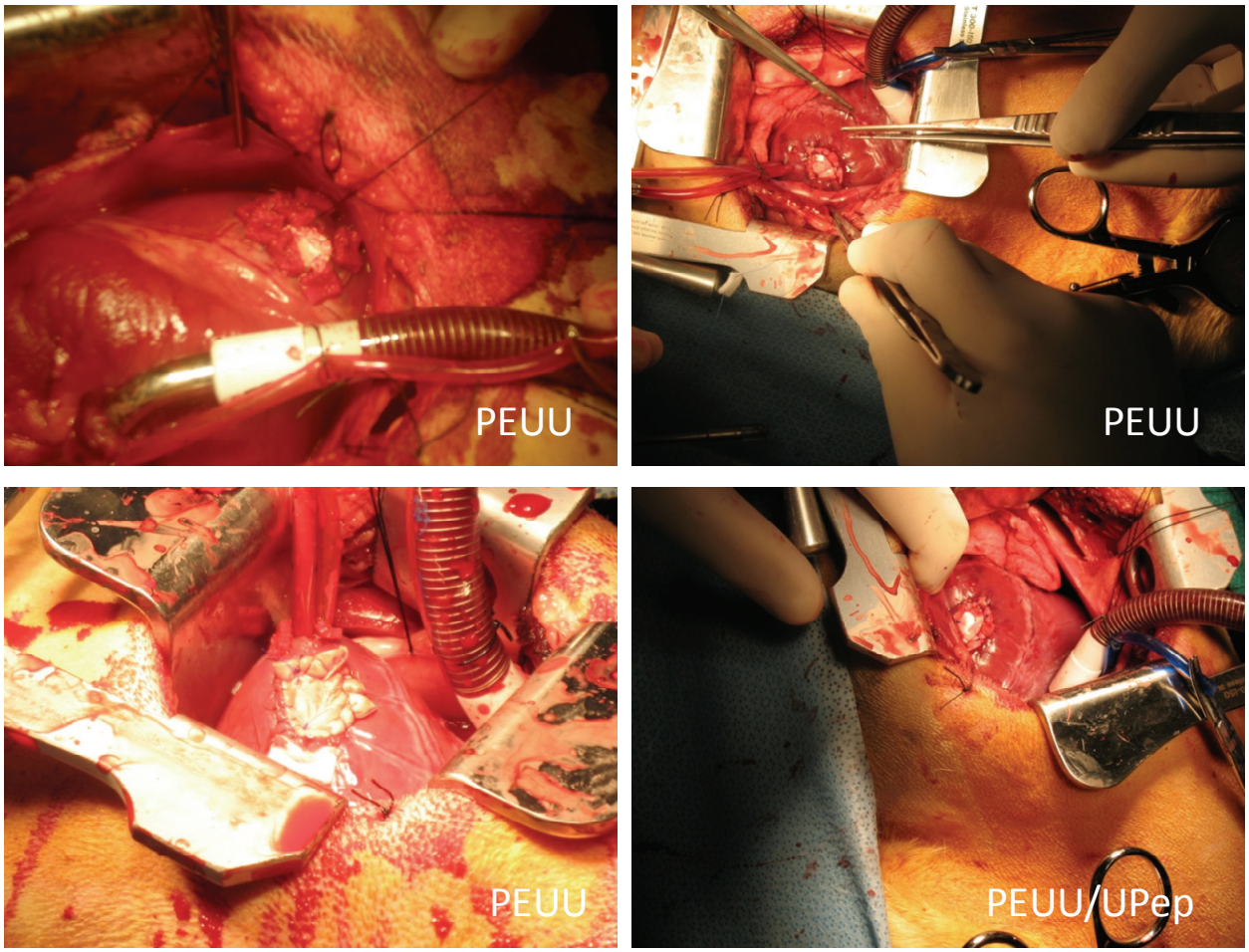

Figure 5-3: Scaffold implanted in a left ventricular defect. Each patch showed excellent surgical manageability. After placing the patch and re-filling the left ventricle, there was no leaking and the patch could withstand the ventricular pressures.

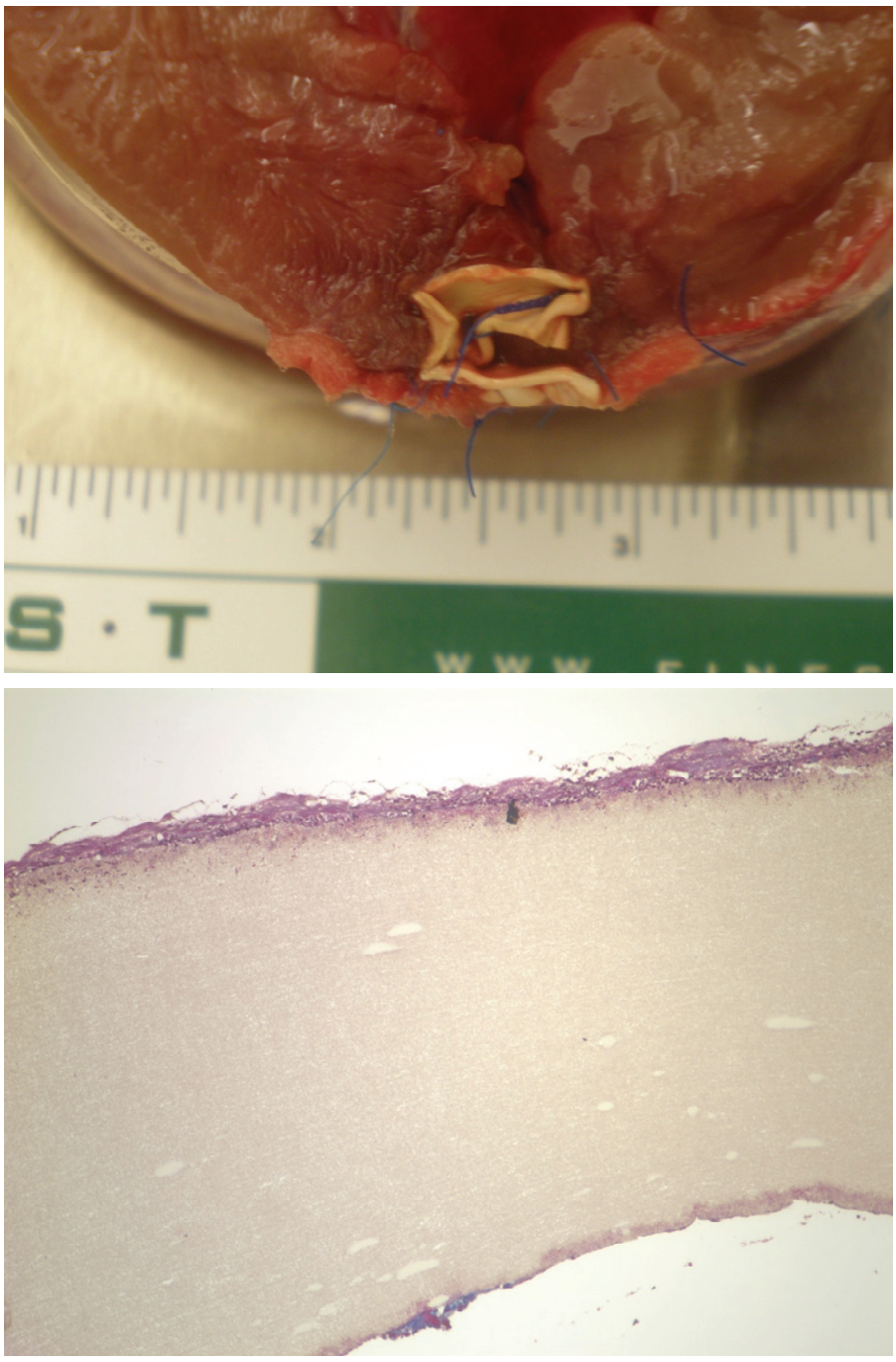

Figure 5-4: (Top) Placement of PEUU graft on a full thickness defect. In this particular case there were to patches placed on the ventricular defect: one patch on the endocardial surface and one patch on the epicardial surface. (Bottom) Histology of the graft after 6 hours.

5.3 LIMITATIONS AND FUTURE WORK

The present work had several challenges. The first challenge was placing dogs under cardiopulmonary bypass. Whole blood was chosen as a perfusion solution due to its relative availability and low cost. However, problems arise from storage and transporting the blood. The typical volume of blood needed was around 200mL to prime the CP circuit. Donor dogs could have been used but only 1% of the total weigh the animal could have been collected and the animal could not be used for a total of 3 weeks due to the university's Division of Laboratory Animal Resources (DLAR) regulations. The recovery period required for the donor animal significantly affected the timely completion of this study. Plasma or other fluids may be a better choice since hemolysis and micro-emboli can cause problems.

Future work will look at either moving to the right ventricle or using another animal model. Dogs did not recover well after cardiopulmonary bypass and perhaps better outcome will be achieved if bypass can be avoided completely. Removing a section of the right ventricle does not require bypass and can be performed without arresting the heart. The heart was not arrested in the present study to minimize the effects of the surgery on the animal. Another possibility would be to change animal models. Using a sheep model may help in the post-operative care and blood products are more readily available. All these possibilities are being considered. These first steps can also help lead the way to more pathological relevant animal model such as subjecting the animals to an acute MI prior to implantation of the scaffold material.

6.0 DISSERTATION SYNOPSIS

6.1 MAJOR FINDINGS

The present work described the enzymatic digestion of an ECM scaffold derived from the urinary bladder called urinary bladder matrix or UBM. UBM was enzymatically digested using pepsin and papain. The biochemical composition of the UBM was determined and the chemotactic and mitogenic properties towards different cell types were tested. Pepsin digested UBM was self-assembled into a gel form. The *in vitro* growth of multiple cell types on the surface of the gels was measured and the rheological properties of the gel determined. Finally, enzymatically digested UBM was combined with a synthetic elastomer to create hybrid scaffold materials. The material properties of the hybrid scaffolds were measured and the scaffolds were used as a left ventricular patch in a canine model. A description of the scaffold materials used in the present study is summarized in Table 6-1.

Table 6-1: Description and limitations of the bioscaffolds used in the present study as potential materials for cardiac tissue engineering.

Scaffold	*Description*	*Limitations*
Lyophilized UBM	Minimally processed ECM Inherent bioactivity present Biodegradable	Limited elastic properties Invasive surgical delivery
UBM Gel	Viscous solution Some bioactivity Biodegradable Minimally invasive delivery	Limited strength
PEUU	Elastomeric scaffold Adequate strength Biodegradable	No inherent bioactivity Invasive surgical delivery Slow degradation *in vivo*
Hybrid	Elastomeric scaffold Adequate strength Biodegradable Some bioactivity	Invasive surgical delivery Rapid loss of bioactive component

Following are the major finding of the present work:

Specific Aim 1

1. Papain and pepsin digested UBM have different collagen and sulfated glycosaminoglycan content.
2. Papain and pepsin digested UBM inhibited the migration of human aortic endothelial cells (HAECs).
3. Papain and pepsin digested UBM stimulated the migration of MRL blastema cells and human fetal cardiomyocytes.

4. Papain digested UBM had no effect upon the mitogenicity of HAECs and human fetal cardiomyocytes.
5. Papain digested UBM showed a mitogenic effect upon C2C12 myoblasts.

Specific Aim 2

1. Pepsin digested UBM can be self-assembled into a gel form.
2. The rheological properties of the UBM gel were measured and the strength and stiffness of the gels was found to change as a function of the final concentration of the gel.
3. UBM gels were able to support the *in vitro* growth under static culture conditions of HEACs, human fetal cardiomyocytes, chick embryonic cardiomyocytes, and C2C12 myoblasts.

Specific Aim 3

1. Enzymatically digested UBM can be electrospun with poly(ester-urethane)urea scaffolds to create hybrid scaffold materials.
2. The mechanical properties of the hybrid scaffold materials were characterized. Hybrid scaffolds retain sufficient mechanical integrity for use as scaffold material in tissue engineering and regenerative medicine applications.
3. There was no change in the static *in vitro* growth of human aortic endothelial cells cultured on hybrid scaffold materials.
4. When placed in a subcutaneous pocket, hybrid scaffolds effectively change the host tissue response when compared to the polymer alone.

Specific Aim 4

1. PEUU and hybrid scaffolds composed of pepsin digested UBM showed appropriate mechanical integrity as a replacement of a full thickness myocardial defect in the left ventricle.

6.2 CONCLUSIONS

Several conclusions can be drawn from this work. Enzymatically digested UBM solutions were shown to have stimulatory and inhibitory effects upon the migration and proliferation of different cell types. Pepsin digested UBM can be self-assembled into a gel form providing a new form of the UBM scaffold with potential uses in tissue engineering and regenerative medicine application. In addition, enzymatically digested UBM can be combined with an elastomer to create hybrid scaffold that elicit a different host tissue response when compared to the polymer alone and with sufficient mechanical strength for use to repair full thickness defects in the left ventricle of canine hearts.

6.3 OVERVIEW OF FUTURE WORK

Future work has been expanded at the end of each chapter. Overall, the work presented in this dissertation are the first steps towards the creation of an optimum hybrid scaffold that takes advantage of the attractive properties of synthetic scaffolds and the bioactivity found in ECM scaffolds.

The bioactive component of enzymatically digested UBM should be identified and isolated. The current work used the entire solution obtained after the enzymatic digestion of UBM but no clear answer was found on what molecule or molecules were responsible for the stimulatory or inhibitory effects observed. This type of work will require an extensive, comprehensive, and systematic approach and should be the focus of future studies. Understanding what types of molecules are generated may help us understand constructive remodeling as well as allow us to engineer better tissue scaffolds.

The gel form of UBM should be expanded and used for other types of ECM. Our laboratory has successfully formed ECM gels from liver, heart, small intestine, pancreas, and skin. Each should have unique digestion protocol with different constituents and rheological properties. The use of the ECM gel *in vivo* will also be needed to determine if the constructive remodeling characteristic typical of the native form is retained in the gel form. Future studies should also focus on the gelation kinetics after injection *in vivo* and at alternative chemistries to control gelation kinetics and the final rheological properties of the scaffold material.

The present study shows that hybrid scaffolds can be manufactured via the electro pinning of an ECM/Polymer solution. Our laboratory has found that some cells grow better and express tissue specific markers when cultured on tissue specific ECM scaffolds [181]. To further expand the clinical utility of the hybrid scaffolds, other ECM digests derived from the heart, liver, and skin digests should be used and tested for specific applications. Skin ECM digests could be used for scaffolds intended as a skin substitute or scaffolds that will be in close contact with skin. Also, hybrid scaffolds manufactured with heart ECM digests could be used as an alternative to UBM for cardiac tissue engineering applications. Other processing methods could also be explored such as thermally induced phase separation (TIPS). Scaffolds prepared using

TIPS have had relative success as cardiac patches in rat models and could be the base for a new generation of hybrid scaffold materials using ECM as a bioactive component.

In the present dissertation, it was shown that there was a burst release of ECM from the hybrid scaffolds after one day of static *in vitro* incubation. The electrospinning technique could be modified to form a layer of pure PEUU first followed by a layer of the PEUU/UBM mixture and then finished with another layer of PEUU. The proposed manufacturing process should trap the UBM within the scaffold and slow down the release of the UBM.

The animal studies will continue. Our laboratory is assessing the best course of action to address the question: Does a hybrid scaffold restore contractility in a full thickness defect when compared to the synthetic component alone. Future studies should increase the number of animals and increase the time points to fully understand the effects of the hybrid scaffolds upon myocardial reconstruction and the host tissue response. In addition, future studies should also explore the use of the scaffolds under pathological conditions such as after an MI.

APPENDIX A

LEFT VENTRICULAR CONTRACTILITY

In order to measure contractility without the need of keeping the animal under anesthesia, an isolated heart preparation was assembled to perfuse the heart *ex vivo* and to measure left ventricular contractility. This section describes the isolated heart system assembled and tested on donor hearts.

A constant pressure isolated heart system (also known as a Langendorff's preparation) was used to perfuse canine hearts due to its relative simplicity when compared to a working heart preparation. The system uses a hydrostatic pressure to maintain a constant pressure in the heart's vasculature after cannulation of the aorta. The aortic valve is forced closed due to the hydrostatic pressure and the perfusion solution is pushed throughout the heart via the coronaries in a retro-grade fashion collecting in the coronary sinus and the right atrium. The hearts were paced using a Grass Stimulator at a rate of one beat per minute and a voltage of 2-5 V and kept at 37°C using a thermostatically controlled water jacket. The isolated heart system was purchased from Radnoti Glass Technology Inc (Monrovia, Ca). A schematic of the isolated heart system is shown in Figure A1.

To procure the heart animals are subjected to a surgical plane anesthesia with Isoflurane (1-3% in oxygen). A bolus injection of heparin was administered when possible and the heart

extracted. Immediately following extraction, the aorta was cannulated and, using a 50-ml syringe plunger, cold perfusate was pushed through the heart via retro-grade perfusion. The hearts were then placed in ice cold perfusate solution and transported to the isolated heart system (performed as soon as possible with an optimum transit time of 5-10 minutes). The left ventricular contractility would then be measured using the Sonometric System (London, Ontario, Canada). Sonometric system is a self sufficient system with all the components needed for data acquisition (combination of personal computer, data boards, and crystals).

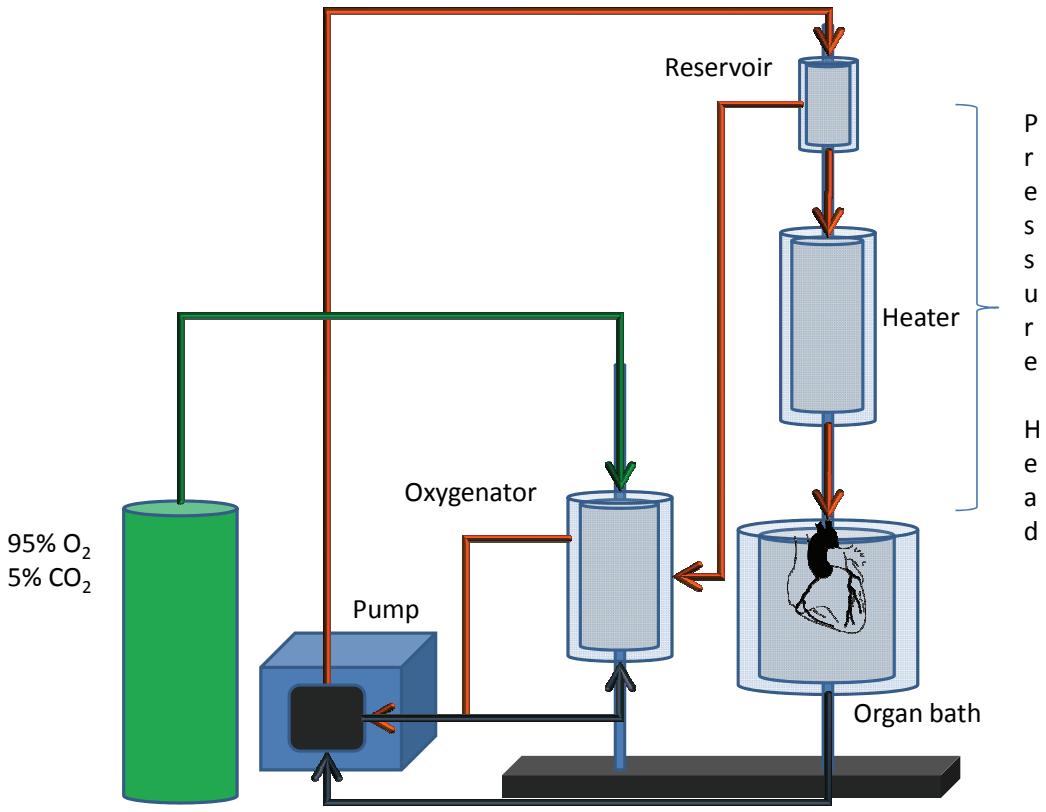

Figure A-1: Diagrammatic representation of the constant pressure isolated heart system used.

The perfusate solution consisted of a combination of salts and glucose based on the solution described by Krebs and Henseleit. The fluid should mimic the ionic content of plasma and have physiological pH values. Table A1 shows the concentrations of the reagents used to make the perfusate solution. This solution was chosen since canine blood products were difficult to obtained in the quantities needed for a large animal isolated heart system (>10 L) and since the oxygenator of the isolated heart system was not designed to oxygenate blood (oxygenates by bubbling oxygen into the solution). Also, the isolated heart system is made of glass which could lead to hemolysis and unwanted by products from the blood. The reagents were mixed at room temperature under constant stir and the pH measured to ensure a pH value of 7.4. There was no need to adjust the pH of the perfusate solution used. The perfusate solution is then sterile filtered before use.

Table A-1: Recipe for the perfusate used for the isolated heart system.

Reagents	***mM***
NaCl	118.5
NaHCO3	25
KCl	4.7
MgSO4	1.2
KH2PO4	1.2
Glucose	11
CaCl2	1.5

Prior to use, the isolated heart system was primed and the water jackets filled with warm water. Perfusate was then pumped into the oxygenator and thought the rest of the isolated heart system. The temperature of the perfusate was monitored and the flow of the pumps and the temperature of the water bath adjusted to reach a constant temperature of 37°C. A mixture of 95% O_2 and 5% CO_2 was used to oxygenate the perfusate by constant bubbling in the oxygenator chamber. Partial pressures above 400 mBars were obtained during perfusate oxygenation. Oxygen saturation and temperature were measured using a WTW OxiMeter 340i probe (WTW, Germany).

Before excising the heart, the Sonometric crystals were placed on the heart in the configuration shown on Figure A2 for the first surgical trial. The placement of the crystals was chosen to measure the vertical and horizontal displacements within the implant location as well as to obtain changes in area in healthy myocardial regions.

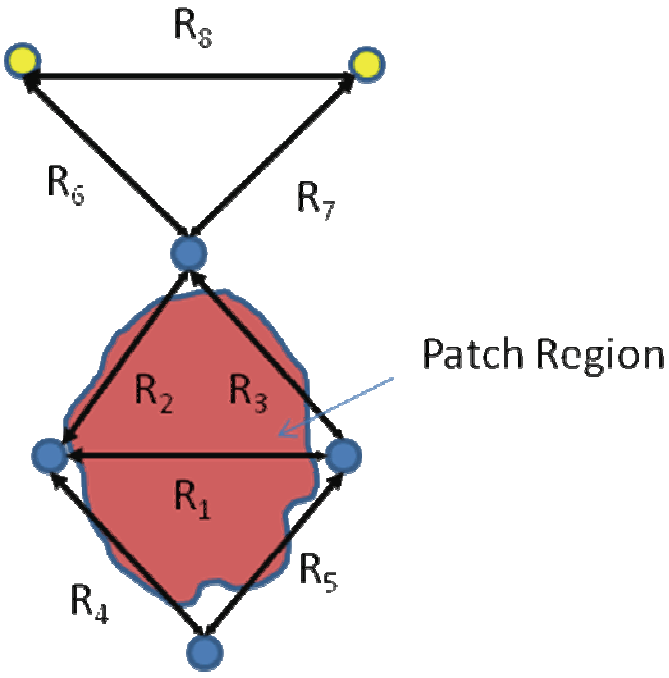

Figure A-2: Diagrammatic representation of the crystal placement.

Area changes can be determined based on the triangles created by the crystals as follow:

Triangle 1 = $R_1 + R_2 + R_3$

Triangle 2 = $R_1 + R_4 + R_5$

Triangle 3 = $R_6 + R_7 + R_8$

Based on the triangles mentioned above, the area can be calculated using Heron's formula as follow:

$$A_1 = \frac{\sqrt{2\left(R_1^2 \cdot R_2^2 + R_1^2 \cdot R_3^2 + R_3^2 \cdot R_2^2\right) - \left(R_1^2 + R_2^2 + R_3^2\right)}}{4} \tag{7}$$

$$A_2 = \frac{\sqrt{2\left(R_1^2 \cdot R_4^2 + R_1^2 \cdot R_5^2 + R_4^2 \cdot R_5^2\right) - \left(R_1^2 + R_4^2 + R_5^2\right)}}{4} \tag{8}$$

$$A_3 = \frac{\sqrt{2\left(R_8^2 \cdot R_6^2 + R_8^2 \cdot R_7^2 + R_7^2 \cdot R_8^2\right) - \left(R_8^2 + R_7^2 + R_6^2\right)}}{4} \tag{9}$$

where R_i (i as an indicator) represents the distances measured between crystals. Figure A2 shows a trial in which the crystals were placed on the epicardial surface.

As mentioned in Chapter 5, the dogs did not recover from anesthesia. However, the isolated heart system was tested on donor hearts obtained from the abattoir and from other studies after the animal had expired. Canine, calf, and porcine hearts were re-perfused using the methodologies described herein with relative success. A successful perfusion of a canine heart is shown in Figure A3. Porcine hearts were obtained from the abattoir immediately following euthanasia and placed on cold perfusate with heparin. After a transport time of approximately one hour, the hearts were placed on the isolated heart system and re-perfused. Contraction of the heart muscle was achieved but only on the right side of the heart. The left side of the heart showed no spontaneous contraction. Calf hearts were obtained from ongoing studies and procured after euthanizing the animal. There was no control over the anticoagulation therapy

and the hearts were harvested within 30 minutes of euthanasia. The hearts were placed on cold perfusate and transported to the isolated heart system. The calf heart began to spontaneously beat after raising the temperature to physiological levels but only on the right side of the heart. Canine heart were obtained from euthanized animals from the present study or from other ongoing studies and harvested within 30 minutes of euthanasia. Canine hearts that were harvested and perfused *in situ* immediately after harvesting showed good muscle contraction when placed on the isolated heart system. However, left ventricular function began to deteriorate and very little contraction was observed after 1 hour in the isolated heart system.

The most pressing limiting factor was the unpredictability of obtaining a donor heart and the conditions in which the hearts were obtained. There was very little control on the time, type of anti-coagulation, and the time available to extract the heart. Most of the hearts were procured from animals about to be euthanized or from other studies that required processing of tissue samples before the heart could be harvested. The time needed to set up the isolated heart system and prepare for un-expected availabilities of hearts made the conditions sub-optimal for the re-perfusion of the heart. Canine hearts in which we did have control over the procurement of the heart, the animal had just gone through an invasive procedure and the hearts either failed to "re-start" or began fibrillating once placed on the isolated heart system.

Future work will also focus on obtaining canine hearts in a more controlled fashion (control over anticoagulation and lower times between euthanasia and procurement). Controlling the anticoagulation and the time to harvest for each animal will allow for the recording of baseline heart contractility on ideal hearts in the isolated heart system. Also, measurements using the Sonometric crystals should be performed *in situ* prior to excising the heart and after

mounting in the isolated heart system. Comparisons between *in vivo* and *in vitro* results could be made and would help validate the results obtained in the isolated heart system.

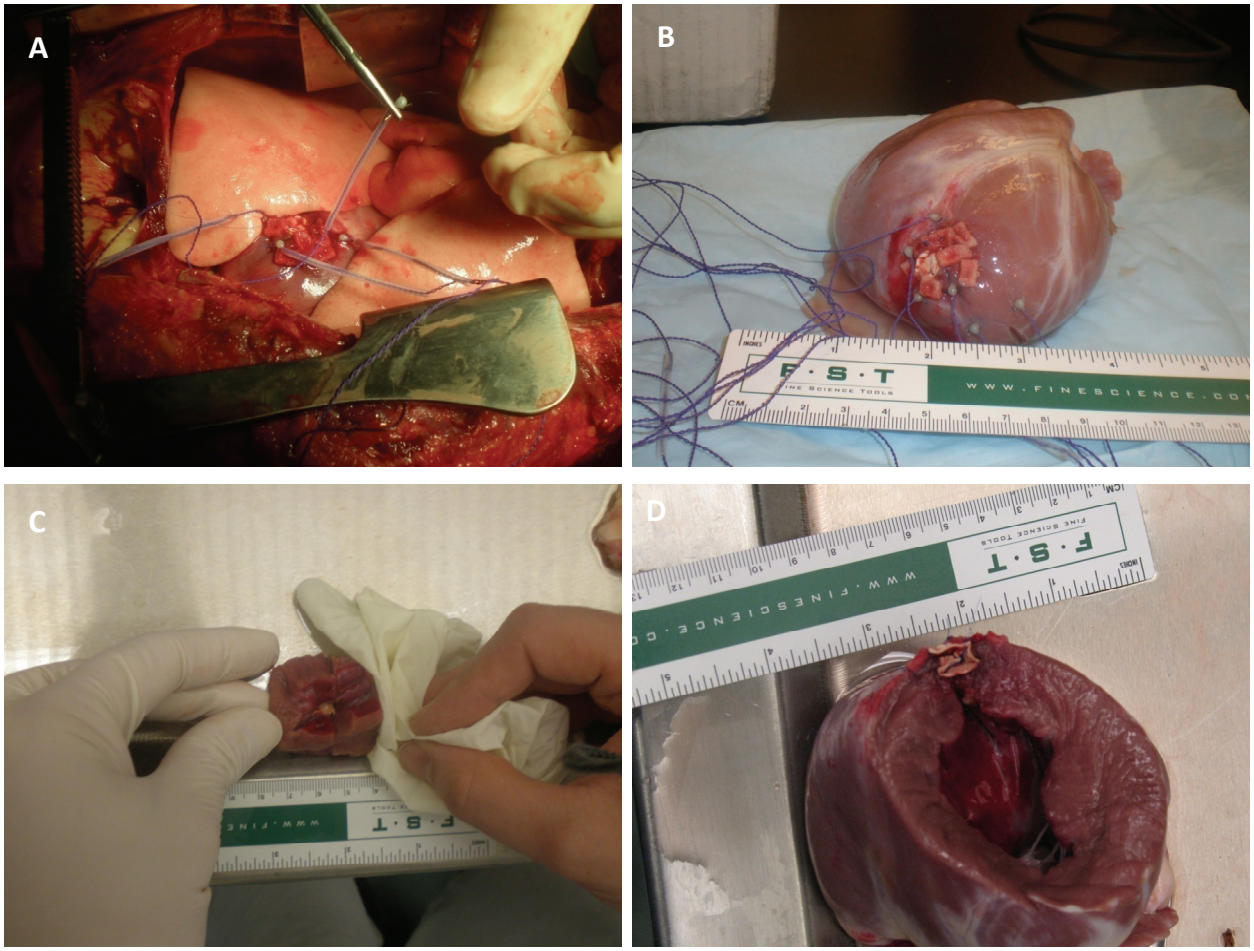

Figure A-3: (A) Placing Sonometric crystals on a canine heart; (B) Macroscopic view of patch with crystals; (C) Endocardial view of the PEUU cardiac patch; (D) Cross-sectional view of cardiac patch.

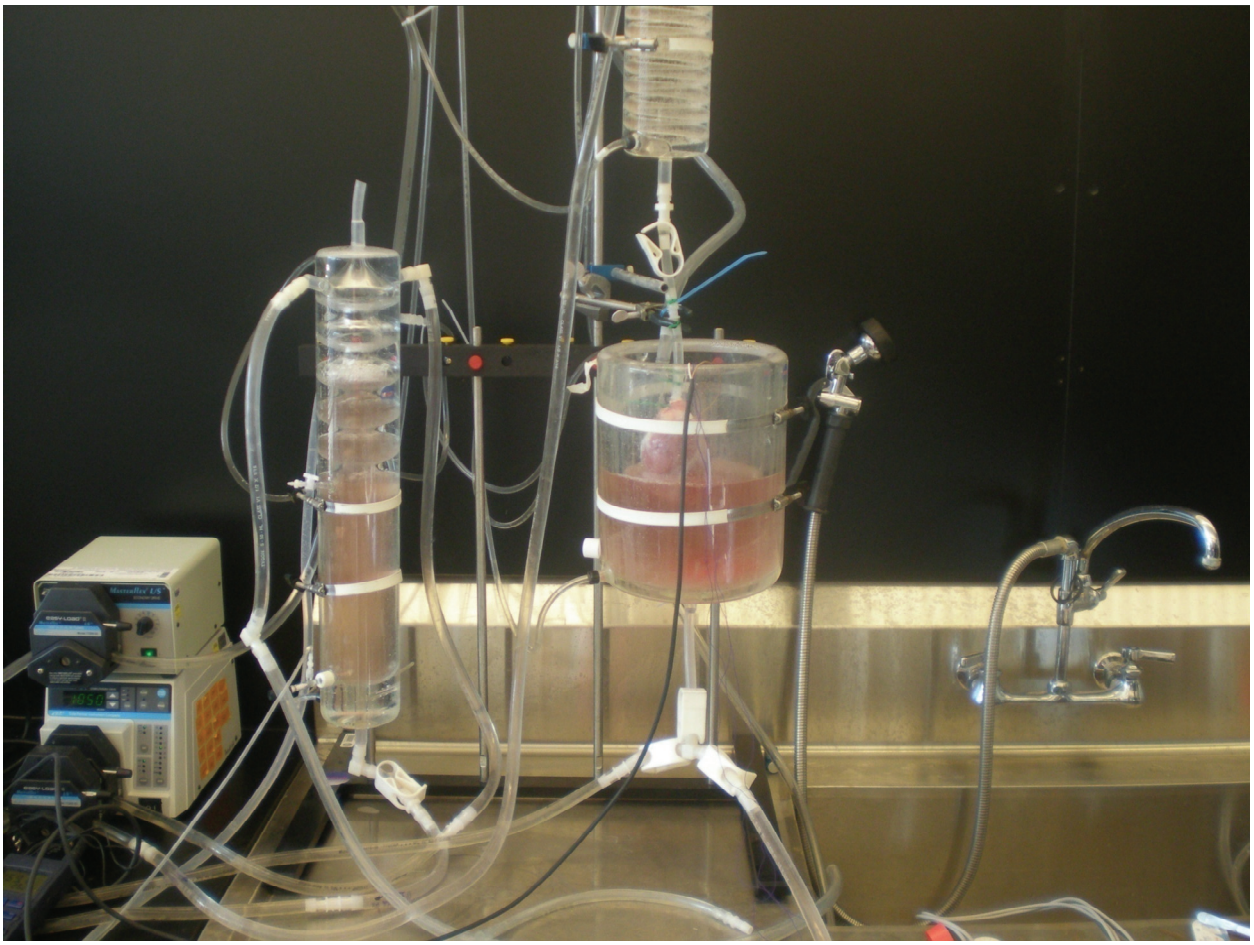

Figure A-4: Picture of the constant pressure isolated heart system.

BIBLIOGRAPHY

1. Dedecker, F., M. Grynberg, and F. Staerman, *[Small intestinal submucosa (SIS): prospects in urogenital surgery]*. Prog Urol, 2005. **15**(3): p. 405-10.

2. Wood, J.D., et al., *Use of a particulate extracellular matrix bioscaffold for treatment of acquired urinary incontinence in dogs.* J Am Vet Med Assoc, 2005. **226**(7): p. 1095-7.

3. Badylak, S., et al., *Resorbable bioscaffold for esophageal repair in a dog model.* J Pediatr Surg, 2000. **35**(7): p. 1097-103.

4. Badylak, S.F., *Regenerative medicine and developmental biology: the role of the extracellular matrix.* Anat Rec B New Anat, 2005. **287**(1): p. 36-41.

5. Badylak, S., et al., *Extracellular matrix for myocardial repair.* Heart Surg Forum, 2003. **6**(2): p. E20-6.

6. Badylak, S.F., et al., *The use of extracellular matrix as an inductive scaffold for the partial replacement of functional myocardium.* Cell Transplant, 2006. **15 Suppl 1**: p. S29-40.

7. Robinson, K.A., et al., *Extracellular matrix scaffold for cardiac repair.* Circulation, 2005. **112**(9 Suppl): p. I135-43.

8. Badylak, S., et al., *Naturally occurring extracellular matrix as a scaffold for musculoskeletal repair.* Clin Orthop Relat Res, 1999(367 Suppl): p. S333-43.

9. Badylak, S.F., et al., *The use of xenogeneic small intestinal submucosa as a biomaterial for Achilles tendon repair in a dog model.* J Biomed Mater Res, 1995. **29**(8): p. 977-85.

10. Zantop, T., et al., *Extracellular matrix scaffolds are repopulated by bone marrow-derived cells in a mouse model of achilles tendon reconstruction.* J Orthop Res, 2006. **24**(6): p. 1299-309.

11. Gilbert, T.W., T.L. Sellaro, and S.F. Badylak, *Decellularization of tissues and organs.* Biomaterials, 2006. **27**(19): p. 3675-83.

12. Badylak, S.F., *The extracellular matrix as a scaffold for tissue reconstruction.* Semin Cell Dev Biol, 2002. **13**(5): p. 377-83.

13. Li, F., et al., *Low-molecular-weight peptides derived from extracellular matrix as chemoattractants for primary endothelial cells.* Endothelium, 2004. **11**(3-4): p. 199-206.

14. Freytes, D.O., et al., *Preparation and rheological characterization of a gel form of the porcine urinary bladder matrix.* Biomaterials, 2008. **29**(11): p. 1630-7.

15. Brennan, E.P., et al., *Antibacterial activity within degradation products of biological scaffolds composed of extracellular matrix.* Tissue Eng, 2006. **12**(10): p. 2949-55.

16. Sarikaya, A., et al., *Antimicrobial activity associated with extracellular matrices.* Tissue Eng, 2002. **8**(1): p. 63-71.

17. Ratner, B.D., *Biomaterials science : an introduction to materials in medicine*. 2nd ed. 2004, Amsterdam ; Boston: Elsevier Academic Press. xii, 851.

18. Guan, J., J.J. Stankus, and W.R. Wagner, *Development of composite porous scaffolds based on collagen and biodegradable poly(ester urethane)urea.* Cell Transplant, 2006. **15 Suppl 1**: p. S17-27.

19. Guan, J. and W.R. Wagner, *Synthesis, characterization and cytocompatibility of polyurethaneurea elastomers with designed elastase sensitivity.* Biomacromolecules, 2005. **6**(5): p. 2833-42.

20. Guan, J., et al., *Preparation and characterization of highly porous, biodegradable polyurethane scaffolds for soft tissue applications.* Biomaterials, 2005. **26**(18): p. 3961-71.

21. Guan, J., et al., *Biodegradable poly(ether ester urethane)urea elastomers based on poly(ether ester) triblock copolymers and putrescine: synthesis, characterization and cytocompatibility.* Biomaterials, 2004. **25**(1): p. 85-96.

22. Guan, J., et al., *Synthesis, characterization, and cytocompatibility of elastomeric, biodegradable poly(ester-urethane)ureas based on poly(caprolactone) and putrescine.* J Biomed Mater Res, 2002. **61**(3): p. 493-503.

23. Stankus, J.J., J. Guan, and W.R. Wagner, *Fabrication of biodegradable elastomeric scaffolds with sub-micron morphologies.* J Biomed Mater Res A, 2004. **70**(4): p. 603-14.

24. Nieponice, A., et al., *Development of a tissue-engineered vascular graft combining a biodegradable scaffold, muscle-derived stem cells and a rotational vacuum seeding technique.* Biomaterials, 2008. **29**(7): p. 825-33.

25. Fujimoto, K.L., et al., *An elastic, biodegradable cardiac patch induces contractile smooth muscle and improves cardiac remodeling and function in subacute myocardial infarction.* J Am Coll Cardiol, 2007. **49**(23): p. 2292-300.

26. Soletti, L., et al., *A seeding device for tissue engineered tubular structures.* Biomaterials, 2006. **27**(28): p. 4863-70.

27. Courtney, T., et al., *Design and analysis of tissue engineering scaffolds that mimic soft tissue mechanical anisotropy.* Biomaterials, 2006. **27**(19): p. 3631-8.

28. Stankus, J.J., et al., *Microintegrating smooth muscle cells into a biodegradable, elastomeric fiber matrix.* Biomaterials, 2006. **27**(5): p. 735-44.

29. Stankus, J., et al., *Hybrid nanofibrous scaffolds from electrospinning of a synthetic biodegradable elastomer and urinary bladder matrix.* J. Biomater. Scie. Polymer Edn. **In Press**.

30. Badylak, S.F., *Xenogeneic extracellular matrix as a scaffold for tissue reconstruction.* Transpl Immunol, 2004. **12**(3-4): p. 367-77.

31. Badylak, S.F., et al., *In vivo remodeling: breakout session summary.* Ann N Y Acad Sci, 2002. **961**: p. 319-22.

32. Zern, M.A. and L.M. Reid, *Extracellular matrix: chemistry, biolgoy, and pathobiology with emphasis on the liver*. 1993, New York: Marcel Kekker, Inc.

33. Badylak, S.F., *The extracellular matrix as a biologic scaffold material.* Biomaterials, 2007. **28**(25): p. 3587-93.

34. Stein, G.S. and A.B. Pardee, *Cell cycle and growth control : biomolecular regulation and cancer*. 2nd ed. 2004, Hoboken, N.J.: Wiley-Liss. xiii, 800.

35. Davis, G.E., et al., *Regulation of tissue injury responses by the exposure of matricryptic sites within extracellular matrix molecules.* Am J Pathol, 2000. **156**(5): p. 1489-98.

36. van Hinsbergh, V.W., M.A. Engelse, and P.H. Quax, *Pericellular proteases in angiogenesis and vasculogenesis.* Arterioscler Thromb Vasc Biol, 2006. **26**(4): p. 716-28.

37. Humphrey, J.D., *Cardiovascular solid mechanics : cells, tissues, and organs*. 2002, New York: Springer. xvi, 757.

38. Bronzino, J.D., *The biomedical engineering handbook*. 2000, Boca Raton, FL: CRC Press. v. <1- >. cm.

39. Garrett, R. and C.M. Grisham, *Biochemistry*. 3rd ed. 2005, Belmont, CA: Thomson Brooks/Cole. 1 v. (various pagings).

40. Lodish, H.F., *Molecular cell biology*. 5th ed. 2004, New York: W.H. Freeman and Company. 1 v. (various pagings).

41. Quondamatteo, F., *Assembly, stability and integrity of basement membranes in vivo.* Histochem J, 2002. **34**(8-9): p. 369-81.

42. Hodde, J.P., et al., *Vascular endothelial growth factor in porcine-derived extracellular matrix.* Endothelium, 2001. **8**(1): p. 11-24.

43. Holtom, P.D., et al., *Porcine small intestine submucosa does not show antimicrobial properties.* Clin Orthop Relat Res, 2004(427): p. 18-21.

44. Badylak, S.F., et al., *Comparison of the resistance to infection of intestinal submucosa arterial autografts versus polytetrafluoroethylene arterial prostheses in a dog model.* J Vasc Surg, 1994. **19**(3): p. 465-72.

45. Badylak, S.F., et al., *Host protection against deliberate bacterial contamination of an extracellular matrix bioscaffold versus Dacron mesh in a dog model of orthopedic soft tissue repair.* J Biomed Mater Res B Appl Biomater, 2003. **67**(1): p. 648-54.

46. Shell, D.H.t., et al., *Comparison of small-intestinal submucosa and expanded polytetrafluoroethylene as a vascular conduit in the presence of gram-positive contamination.* Ann Surg, 2005. **241**(6): p. 995-1001; discussion 1001-4.

47. Jernigan, T.W., et al., *Small intestinal submucosa for vascular reconstruction in the presence of gastrointestinal contamination.* Ann Surg, 2004. **239**(5): p. 733-8; discussion 738-40.

48. Badylak, S., et al., *Naturally occurring extracellular matrix as a scaffold for musculoskeletal repair.* Clin Orthop, 1999(367 Suppl): p. S333-43.

49. Badylak, S., et al., *Strength over time of a resorbable bioscaffold for body wall repair in a dog model.* J Surg Res, 2001. **99**(2): p. 282-7.

50. Dejardin, L.M., et al., *Tissue-engineered rotator cuff tendon using porcine small intestine submucosa. Histologic and mechanical evaluation in dogs.* Am J Sports Med, 2001. **29**(2): p. 175-84.

51. Gu, Y. and K. Dai, *Substitution of porcine small intestinal submucosa for rabbit Achilles tendon, an experimental study.* Zhonghua Yi Xue Za Zhi, 2002. **82**(18): p. 1279-82.

52. Knapp, P.M., et al., *Biocompatibility of small-intestinal submucosa in urinary tract as augmentation cystoplasty graft and injectable suspension.* J Endourol, 1994. **8**(2): p. 125-30.

53. Kropp, B.P., et al., *Regenerative urinary bladder augmentation using small intestinal submucosa: urodynamic and histopathologic assessment in long-term canine bladder augmentations.* J Urol, 1996. **155**(6): p. 2098-104.

54. Lantz, G.C., et al., *Small intestinal submucosa as a small-diameter arterial graft in the dog.* J Invest Surg, 1990. **3**(3): p. 217-27.

55. Ueno, T., et al., *Clinical application of porcine small intestinal submucosa in the management of infected or potentially contaminated abdominal defects.* J Gastrointest Surg, 2004. **8**(1): p. 109-12.

56. Oelschlager, B.K., et al., *The use of small intestine submucosa in the repair of paraesophageal hernias: initial observations of a new technique.* Am J Surg, 2003. **186**(1): p. 4-8.

57. Napolitano, L., et al., *[Use of prosthetic materials in incisional hernias: our clinical experience]*. G Chir, 2004. **25**(4): p. 141-5.

58. Conklin, B.S., et al., *Development and evaluation of a novel decellularized vascular xenograft.* Med Eng Phys, 2002. **24**(3): p. 173-83.

59. Curtil, A., D.E. Pegg, and A. Wilson, *Freeze drying of cardiac valves in preparation for cellular repopulation.* Cryobiology, 1997. **34**(1): p. 13-22.

60. Lemer, M.L., D.C. Chaikin, and J.G. Blaivas, *Tissue strength analysis of autologous and cadaveric allografts for the pubovaginal sling.* Neurourol Urodyn, 1999. **18**(5): p. 497-503.

61. El-Kassaby, A.W., et al., *Urethral stricture repair with an off-the-shelf collagen matrix.* J Urol, 2003. **169**(1): p. 170-3; discussion 173.

62. Mostow, E.N., et al., *Effectiveness of an extracellular matrix graft (OASIS Wound Matrix) in the treatment of chronic leg ulcers: a randomized clinical trial.* J Vasc Surg, 2005. **41**(5): p. 837-43.

63. Khrupkin, V.I., et al., *[Application of viable cryopreserved alloderm transplants in the treatment of wound defects of soft tissues]*. Vestn Khir Im I I Grek, 2002. **161**(5): p. 55-9.

64. Ward, P.D., S.L. Thibeault, and S.D. Gray, *Hyaluronic acid: its role in voice.* J Voice, 2002. **16**(3): p. 303-9.

65. Huber, J.E., et al., *Extracellular matrix as a scaffold for laryngeal reconstruction.* Ann Otol Rhinol Laryngol, 2003. **112**(5): p. 428-33.

66. Ringel, R.L., et al., *The application of tissue engineering procedures to repair the larynx.* J Speech Lang Hear Res, 2006. **49**(1): p. 194-208.

67. Hahn, M.S., et al., *Collagen composite hydrogels for vocal fold lamina propria restoration.* Biomaterials, 2006. **27**(7): p. 1104-9.

68. Badylak, S.F., et al., *Esophageal reconstruction with ECM and muscle tissue in a dog model.* J Surg Res, 2005. **128**(1): p. 87-97.

69. Freytes, D.O., et al., *Biaxial strength of multilaminated extracellular matrix scaffolds.* Biomaterials, 2004. **25**(12): p. 2353-61.

70. Freytes, D.O., R.M. Stoner, and S.F. Badylak, *Uniaxial and biaxial properties of terminally sterilized porcine urinary bladder matrix scaffolds.* J Biomed Mater Res B Appl Biomater, 2008. **84**(2): p. 408-14.

71. Freytes, D.O., R.S. Tullius, and S.F. Badylak, *Effect of storage upon material properties of lyophilized porcine extracellular matrix derived from the urinary bladder.* J Biomed Mater Res B Appl Biomater, 2006. **78**(2): p. 327-33.

72. Freytes, D.O., et al., *Hydrated versus lyophilized forms of porcine extracellular matrix derived from the urinary bladder.* J Biomed Mater Res A, 2008.

73. Loo, S.C., C.P. Ooi, and Y.C. Boey, *Influence of electron-beam radiation on the hydrolytic degradation behaviour of poly(lactide-co-glycolide) (PLGA).* Biomaterials, 2005. **26**(18): p. 3809-17.

74. Prolo, D.J., P.W. Pedrotti, and D.H. White, *Ethylene oxide sterilization of bone, dura mater, and fascia lata for human transplantation.* Neurosurgery, 1980. **6**(5): p. 529-39.

75. Kearney, J.N., et al., *Evaluation of ethylene oxide sterilization of tissue implants.* J Hosp Infect, 1989. **13**(1): p. 71-80.

76. Kudryk, V.L., et al., *Toxic effect of ethylene-oxide-sterilized freeze-dried bone allograft on human gingival fibroblasts.* J Biomed Mater Res, 1992. **26**(11): p. 1477-88.

77. Bechtold, J.E., et al., *The effects of freeze-drying and ethylene oxide sterilization on the mechanical properties of human patellar tendon.* Am J Sports Med, 1994. **22**(4): p. 562-6.

78. Simonian, P.T., et al., *Effect of sterilization and storage treatments on screw pullout strength in human allograft bone.* Clin Orthop Relat Res, 1994(302): p. 290-6.

79. Pruss, A., et al., *Comparison of the efficacy of virus inactivation methods in allogeneic avital bone tissue transplants.* Cell Tissue Bank, 2001. **2**(4): p. 201-15.

80. Woo, L. and K.S. Purohit, *Advancements and opportunities in sterilisation.* Med Device Technol, 2002. **13**(2): p. 12-7.

81. Loo, J.S., C.P. Ooi, and F.Y. Boey, *Degradation of poly(lactide-co-glycolide) (PLGA) and poly(L-lactide) (PLLA) by electron beam radiation.* Biomaterials, 2005. **26**(12): p. 1359-67.

82. Burchardt, H., et al., *Freeze-dried allogeneic segmental cortical-bone grafts in dogs.* J Bone Joint Surg Am, 1978. **60**(8): p. 1082-90.

83. Cornu, O., et al., *Effect of freeze-drying and gamma irradiation on the mechanical properties of human cancellous bone.* J Orthop Res, 2000. **18**(3): p. 426-31.

84. Jackson, D.W., et al., *The effects of processing techniques on the mechanical properties of bone-anterior cruciate ligament-bone allografts. An experimental study in goats.* Am J Sports Med, 1988. **16**(2): p. 101-5.

85. Smith, C.W., I.S. Young, and J.N. Kearney, *Mechanical properties of tendons: changes with sterilization and preservation.* J Biomech Eng, 1996. **118**(1): p. 56-61.

86. Toritsuka, Y., et al., *Effect of freeze-drying or gamma-irradiation on remodeling of tendon allograft in a rat model.* J Orthop Res, 1997. **15**(2): p. 294-300.

87. Freytes, D.O., et al., *Analytically derived material properties of multilaminated extracellular matrix devices using the ball-burst test.* Biomaterials, 2005. **26**(27): p. 5518-31.

88. Valentin, J.E., et al., *Extracellular matrix bioscaffolds for orthopaedic applications. A comparative histologic study.* J Bone Joint Surg Am, 2006. **88**(12): p. 2673-86.

89. Buschow, K.H.J. and ScienceDirect (Online service), *Encyclopedia of materials science and technology*. 2001, Amsterdam ; New York: Elsevier. 11 v. (9913, xiv viii, 474).

90. Guan, J., J.J. Stankus, and W.R. Wagner, *Biodegradable elastomeric scaffolds with basic fibroblast growth factor release.* J Control Release, 2007. **120**(1-2): p. 70-8.

91. Webster, J.G., *Encyclopedia of medical devices and instrumentation*. 2nd ed. 2006, Hoboken, N.J.: Wiley-Interscience.

92. Tonnessen, T. and C.W. Knudsen, *Surgical left ventricular remodeling in heart failure.* Eur J Heart Fail, 2005. **7**(5): p. 704-9.

93. Kumar, V., et al. *Robbins and Cotran pathologic basis of disease*. 2005 [cited; 7th:[xv, 1525].

94. Lilly, L.S., *Pathophysiology of heart disease : a collaborative project of medical students and faculty*. 4th ed. 2007, Philadelphia: Wolters Kluwer/Lippincott Williams & Wilkins. xiii, 473.

95. Christman, K.L. and R.J. Lee, *Biomaterials for the treatment of myocardial infarction.* J Am Coll Cardiol, 2006. **48**(5): p. 907-13.

96. Jawad, H., et al., *Myocardial tissue engineering: a review.* J Tissue Eng Regen Med, 2007. **1**(5): p. 327-42.

97. Leor, J., Y. Amsalem, and S. Cohen, *Cells, scaffolds, and molecules for myocardial tissue engineering.* Pharmacol Ther, 2005. **105**(2): p. 151-63.

98. Dor, V., et al., *Left ventricular reconstruction by endoventricular circular patch plasty repair: a 17-year experience.* Semin Thorac Cardiovasc Surg, 2001. **13**(4): p. 435-47.

99. Dor, V., et al., *Endoventricular patch reconstruction of ischemic failing ventricle. a single center with 20 years experience. advantages of magnetic resonance imaging assessment.* Heart Fail Rev, 2004. **9**(4): p. 269-86.

100. Fujimoto, K.L., et al., *In vivo evaluation of a porous, elastic, biodegradable patch for reconstructive cardiac procedures.* Ann Thorac Surg, 2007. **83**(2): p. 648-54.

101. Ozawa, T., et al., *Optimal biomaterial for creation of autologous cardiac grafts.* Circulation, 2002. **106**(12 Suppl 1): p. I176-82.

102. Pego, A.P., et al., *Biodegradable elastomeric scaffolds for soft tissue engineering.* J Control Release, 2003. **87**(1-3): p. 69-79.

103. Pego, A.P., et al., *Preparation of degradable porous structures based on 1,3-trimethylene carbonate and D,L-lactide (co)polymers for heart tissue engineering.* Tissue Eng, 2003. **9**(5): p. 981-94.

104. Siepe, M., et al., *Construction of skeletal myoblast-based polyurethane scaffolds for myocardial repair.* Artif Organs, 2007. **31**(6): p. 425-33.

105. Siepe, M., et al., *Myoblast-seeded biodegradable scaffolds to prevent post-myocardial infarction evolution toward heart failure.* J Thorac Cardiovasc Surg, 2006. **132**(1): p. 124-31.

106. Kellar, R.S., et al., *Cardiac patch constructed from human fibroblasts attenuates reduction in cardiac function after acute infarct.* Tissue Eng, 2005. **11**(11-12): p. 1678-87.

107. Shin, M., et al., *Contractile cardiac grafts using a novel nanofibrous mesh.* Biomaterials, 2004. **25**(17): p. 3717-23.

108. Zong, X., et al., *Electrospun fine-textured scaffolds for heart tissue constructs.* Biomaterials, 2005. **26**(26): p. 5330-8.

109. Zimmermann, W.H., et al., *Cardiac grafting of engineered heart tissue in syngenic rats.* Circulation, 2002. **106**(12 Suppl 1): p. I151-7.

110. Zimmermann, W.H., I. Melnychenko, and T. Eschenhagen, *Engineered heart tissue for regeneration of diseased hearts.* Biomaterials, 2004. **25**(9): p. 1639-47.

111. Li, R.K., et al., *Survival and function of bioengineered cardiac grafts.* Circulation, 1999. **100**(19 Suppl): p. II63-9.

112. Badylak, S.F., *Regenerative medicine approach to heart valve replacement.* Circulation, 2005. **111**(21): p. 2715-6.

113. Kochupura, P.V., et al., *Tissue-engineered myocardial patch derived from extracellular matrix provides regional mechanical function.* Circulation, 2005. **112**(9 Suppl): p. I144-9.

114. Ota, T., et al., *Electromechanical characterization of a tissue-engineered myocardial patch derived from extracellular matrix.* J Thorac Cardiovasc Surg, 2007. **133**(4): p. 979-85.

115. Wei, H.J., et al., *Porous acellular bovine pericardia seeded with mesenchymal stem cells as a patch to repair a myocardial defect in a syngeneic rat model.* Biomaterials, 2006. **27**(31): p. 5409-19.

116. Chang, Y., et al., *Tissue regeneration observed in a basic fibroblast growth factor-loaded porous acellular bovine pericardium populated with mesenchymal stem cells.* J Thorac Cardiovasc Surg, 2007. **134**(1): p. 65-73, 73 e1-4.

117. Christman, K.L., et al., *Fibrin glue alone and skeletal myoblasts in a fibrin scaffold preserve cardiac function after myocardial infarction.* Tissue Eng, 2004. **10**(3-4): p. 403-9.

118. Ryu, J.H., et al., *Implantation of bone marrow mononuclear cells using injectable fibrin matrix enhances neovascularization in infarcted myocardium.* Biomaterials, 2005. **26**(3): p. 319-26.

119. Liu, J., et al., *Autologous stem cell transplantation for myocardial repair.* Am J Physiol Heart Circ Physiol, 2004. **287**(2): p. H501-11.

120. Huang, N.F., et al., *Injectable biopolymers enhance angiogenesis after myocardial infarction.* Tissue Eng, 2005. **11**(11-12): p. 1860-6.

121. Kofidis, T., et al., *Distinct cell-to-fiber junctions are critical for the establishment of cardiotypical phenotype in a 3D bioartificial environment.* Med Eng Phys, 2004. **26**(2): p. 157-63.

122. Guo, X.M., et al., *Creation of engineered cardiac tissue in vitro from mouse embryonic stem cells.* Circulation, 2006. **113**(18): p. 2229-37.

123. Dai, W., et al., *Thickening of the infarcted wall by collagen injection improves left ventricular function in rats: a novel approach to preserve cardiac function after myocardial infarction.* J Am Coll Cardiol, 2005. **46**(4): p. 714-9.

124. Xiang, Z., et al., *Collagen-GAG scaffolds grafted onto myocardial infarcts in a rat model: a delivery vehicle for mesenchymal stem cells.* Tissue Eng, 2006. **12**(9): p. 2467-78.

125. Iwakura, A., et al., *Intramyocardial sustained delivery of basic fibroblast growth factor improves angiogenesis and ventricular function in a rat infarct model.* Heart Vessels, 2003. **18**(2): p. 93-9.

126. Chang, Y., et al., *Tissue regeneration observed in a porous acellular bovine pericardium used to repair a myocardial defect in the right ventricle of a rat model.* J Thorac Cardiovasc Surg, 2005. **130**(3): p. 705-11.

127. Freytes, D.O., R.S. Tullius, and S.F. Badylak, *Effect of storage upon material properties of lyophilized porcine extracellular matrix derived from the urinary bladder.* J Biomed Mater Res B Appl Biomater, 2005.

128. Dor, V., *The endoventricular circular patch plasty ("Dor procedure") in ischemic akinetic dilated ventricles.* Heart Fail Rev, 2001. **6**(3): p. 187-93.

129. Voytik-Harbin, S.L., et al., *Small Intestinal Submucosa: A Tissue-Derived Extracellular Matrix That Promotes Tissue-Specific Growth and Differentiation of Cells in Vitro.* Tissue Eng, 1998. **4**(2): p. 157-174.

130. Bhattarai, N., et al., *Electrospun chitosan-based nanofibers and their cellular compatibility.* Biomaterials, 2005. **26**(31): p. 6176-84.

131. Duan, B., et al., *Electrospinning of chitosan solutions in acetic acid with poly(ethylene oxide).* J Biomater Sci Polym Ed, 2004. **15**(6): p. 797-811.

132. Jin, H.J., et al., *Electrospinning Bombyx mori silk with poly(ethylene oxide).* Biomacromolecules, 2002. **3**(6): p. 1233-9.

133. Huang, L., R.P. Apkarian, and E.L. Chaikof, *High-resolution analysis of engineered type I collagen nanofibers by electron microscopy.* Scanning, 2001. **23**(6): p. 372-5.

134. Wright, E.R., V.P. Conticello, and R.P. Apkarian, *Morphological characterization of elastin-mimetic block copolymers utilizing cryo- and cryoetch-HRSEM.* Microsc Microanal, 2003. **9**(3): p. 171-82.

135. Chandy, T., et al., *The development of porous alginate/elastin/PEG composite matrix for cardiovascular engineering.* J Biomater Appl, 2003. **17**(4): p. 287-301.

136. Clark, L.D., R.K. Clark, and E. Heber-Katz, *A new murine model for mammalian wound repair and regeneration.* Clin Immunol Immunopathol, 1998. **88**(1): p. 35-45.

137. Heber-Katz, E., et al., *Spallanzani's mouse: a model of restoration and regeneration.* Curr Top Microbiol Immunol, 2004. **280**: p. 165-89.

138. Reing, J.E., et al., *Degradation Products of Extracellular Matrix Affect Cell Migration and Proliferation.* Tissue Eng. **Submitted**.

139. Mankin, H.J. and L. Lippiello, *The glycosaminoglycans of normal and arthritic cartilage.* J Clin Invest, 1971. **50**(8): p. 1712-9.

140. Akalu, A., et al., *Inhibition of angiogenesis and tumor metastasis by targeting a matrix immobilized cryptic extracellular matrix epitope in laminin.* Cancer Res, 2007. **67**(9): p. 4353-63.

141. Brown, B., et al., *The basement membrane component of biologic scaffolds derived from extracellular matrix.* Tissue Eng, 2006. **12**(3): p. 519-26.

142. Kaspar, P. and M. Dvorak, *Involvement of phosphatidylserine externalization in the down-regulation of c-myb expression in differentiating C2C12 cells.* Differentiation, 2008. **76**(3): p. 245-52.

143. Rauch, C. and P.T. Loughna, *Inward relocation of exogenous phosphatidylserine triggered by IGF-1 in non-apoptotic C2C12 cells is concentration dependent.* Cell Biochem Funct, 2005. **23**(6): p. 383-8.

144. van den Eijnde, S.M., et al., *Transient expression of phosphatidylserine at cell-cell contact areas is required for myotube formation.* J Cell Sci, 2001. **114**(Pt 20): p. 3631-42.

145. Nieponice, A., T.W. Gilbert, and S.F. Badylak, *Reinforcement of esophageal anastomoses with an extracellular matrix scaffold in a canine model.* Ann Thorac Surg, 2006. **82**(6): p. 2050-8.

146. Reddy, G.K. and C.S. Enwemeka, *A simplified method for the analysis of hydroxyproline in biological tissues.* Clin Biochem, 1996. **29**(3): p. 225-9.

147. Gelman, R.A., B.R. Williams, and K.A. Piez, *Collagen fibril formation. Evidence for a multistep process.* J Biol Chem, 1979. **254**(1): p. 180-6.

148. Ray, J.L., et al., *Isolation of vascular smooth muscle cells from a single murine aorta.* Methods Cell Sci, 2001. **23**(4): p. 185-8.

149. Tobita, K., et al., *Engineered early embryonic cardiac tissue retains proliferative and contractile properties of developing embryonic myocardium.* Am J Physiol Heart Circ Physiol, 2006. **291**(4): p. H1829-37.

150. Chan, R.W. and I.R. Titze, *Viscosities of implantable biomaterials in vocal fold augmentation surgery.* Laryngoscope, 1998. **108**(5): p. 725-31.

151. Klemuk, S.A. and I.R. Titze, *Viscoelastic properties of three vocal-fold injectable biomaterials at low audio frequencies.* Laryngoscope, 2004. **114**(9): p. 1597-603.

152. Birk, D.E. and F.H. Silver, *Collagen fibrillogenesis in vitro: comparison of types I, II, and III.* Arch Biochem Biophys, 1984. **235**(1): p. 178-85.

153. Grant, D.S., et al., *The incubation of laminin, collagen IV, and heparan sulfate proteoglycan at 35 degrees C yields basement membrane-like structures.* J Cell Biol, 1989. **108**(4): p. 1567-74.

154. Birk, D.E., et al., *Collagen fibrillogenesis in vitro: interaction of types I and V collagen regulates fibril diameter.* J Cell Sci, 1990. **95 (Pt 4)**: p. 649-57.

155. Brightman, A.O., et al., *Time-lapse confocal reflection microscopy of collagen fibrillogenesis and extracellular matrix assembly in vitro.* Biopolymers, 2000. **54**(3): p. 222-34.

156. Pins, G.D., et al., *Self-assembly of collagen fibers. Influence of fibrillar alignment and decorin on mechanical properties.* Biophys J, 1997. **73**(4): p. 2164-72.

157. Rada, J.A., P.K. Cornuet, and J.R. Hassell, *Regulation of corneal collagen fibrillogenesis in vitro by corneal proteoglycan (lumican and decorin) core proteins.* Exp Eye Res, 1993. **56**(6): p. 635-48.

158. Salchert, K., et al., *Fibrillar collagen assembled in the presence of glycosaminoglycans to constitute bioartificial stem cell niches in vitro.* J Mater Sci Mater Med, 2005. **16**(6): p. 581-5.

159. Ghosh, K., et al., *Cell adaptation to a physiologically relevant ECM mimic with different viscoelastic properties.* Biomaterials, 2007. **28**(4): p. 671-9.

160. Chan, R.W. and I.R. Titze, *Hyaluronic acid (with fibronectin) as a bioimplant for the vocal fold mucosa.* Laryngoscope, 1999. **109**(7 Pt 1): p. 1142-9.

161. Brown, D., et al., *Analysis of oxygen transport in a diffusion-limited model of engineered heart tissue.* Biotechnol Bioeng, 2006.

162. Davis, B.H., et al., *An In Vitro System to Evaluate the Effects of Ischemia on Survival of Cells Used for Cell Therapy.* Ann Biomed Eng, 2007.

163. Badylak, S.F., *Extracellular matrix scaffolds*, in *Encyclopedia of Biomaterials and Biomedical Engineering*. 2004, Marcel Dekker: New York.

164. Badylak, S.F., *Xenogeneic extracellular matrix as a scaffold for tissue reconstruction.* Transpl. Immunol., 2004. **12**: p. 367-377.

165. Freytes, D.O., et al., *Biaxial strength of multilaminated extracellular matrix scaffolds.* Biomaterials, 2004. **25**: p. 2353-2361.

166. Badylak, S.F., *The extracellular matrix as a scaffold for tissue reconstruction.* Cell Dev Biol, 2002. **13**: p. 377-383.

167. Sarikaya, A., et al., *Antimicrobial activity associated with extracellular matrices.* Tiss Eng, 2002. **8**: p. 63-71.

168. Li, W.J., et al., *Electrospun nanofibrous structure: a novel scaffold for tissue engineering.* J Biomed Mater Res, 2002. **60**: p. 613-621.

169. Stankus, J., J. Guan, and W.R. Wagner, *Fabrication of biodegradable elastomeric scaffolds with sub-micron morphologies.* J Biomed Mater Res, 2004. **70A**: p. 603-614.

170. Guan, J., et al., *Synthesis, characterization, and cytocompatibility of elastomeric, biodegradable poly(ester-urethane)ureas based on poly(caprolactone) and putrescine.* J Biomed Mater Res, 2002. **61**: p. 493-503.

171. Gilbert, T.W., et al., *Production and characterization of ECM powder: implications for tissue engineering applications.* Biomaterials, 2005. **26**(12): p. 1431-5.

172. Badylak, S., *Small intestinal submucosa (SIS): A biomaterial conductive to smart tissue remodeling.*, in *Tissue Engineering: Current Perspectives*, E. Bell, Editor. 1993, Burkhauser Publishers: Cambridge, MA. p. 179-189.

173. Delfino, J.G., et al., *Determination of transmural, endocardial, and epicardial radial strain and strain rate from phase contrast MR velocity data.* J Magn Reson Imaging, 2008. **27**(3): p. 522-528.

174. Anderson, C.F. and D.M. Mosser, *A novel phenotype for an activated macrophage: the type 2 activated macrophage.* J Leukoc Biol, 2002. **72**(1): p. 101-6.

175. Gordon, S. and P.R. Taylor, *Monocyte and macrophage heterogeneity.* Nat Rev Immunol, 2005. **5**(12): p. 953-64.

176. Mantovani, A., A. Sica, and M. Locati, *Macrophage polarization comes of age.* Immunity, 2005. **23**(4): p. 344-6.

177. Webb, A.R., J. Yang, and G.A. Ameer, *Biodegradable polyester elastomers in tissue engineering.* Expert Opin Biol Ther, 2004. **4**(6): p. 801-12.

178. Garlotta, D.A., *A literature review of poly(lactic acid).* J Polym Environ, 2001. **9**(2): p. 149-57.

179. Ramsay B.A., Langlade V., and Carreau P.J., *Biodegradability and mechanical properites of poly-(beta-hydroxybutyrate-co-beta-hydroxyvalerate) startch blends.* Appl Environ Microbiol, 1993. **59**(4): p. 2744-79.

180. Chen, Q.Z., et al., *Characterisation of a soft elastomer poly(glycerol sebacate) designed to match the mechanical properties of myocardial tissue.* Biomaterials, 2008. **29**(1): p. 47-57.

181. Sellaro, T.L., et al., *Maintenance of hepatic sinusoidal endothelial cell phenotype in vitro using organ-specific extracellular matrix scaffolds.* Tissue Eng, 2007. **13**(9): p. 2301-10.